UNIVERSIDADE FEDERAL DO RIO GRANDE DO SUL

Programa de Pós-Graduação em Engenharia de Minas, Metalúrgica e Materiais – PPGE3M

Área de concentração: Tecnologia Mineral, Ambiental e Metalurgia Extrativa

DIANA RAMOS LIMA

SÍNTESE E CARACTERIZAÇÃO DE MATERIAIS CARBONADOS ATIVADOS A PARTIR DE RESÍDUOS VEGETAIS DE CASTANHA DO PARÁ E SERRAGEM DE MADEIRA E SUA UTILIZAÇÃO COMO ADSORVENTES NA REMOÇÃO DE CONTAMINANTES EMERGENTES

PORTO ALEGRE

2022

DIANA RAMOS LIMA

SÍNTESE E CARACTERIZAÇÃO DE MATERIAIS CARBONADOS ATIVADOS A PARTIR DE RESÍDUOS VEGETAIS DE CASTANHA DO PARÁ E SERRAGEM DE MADEIRA E SUA UTILIZAÇÃO COMO ADSORVENTES NA REMOÇÃO DE CONTAMINANTES EMERGENTES

Tese de doutorado submetido ao Programa de Pós-Graduação em Engenharia de Minas, Metalúrgica e Materiais como parte dos requisitos para obtenção do título de Doutor em Engenharia.

Orientador: Prof. Titular Dr. Éder C. Lima

PORTO ALEGRE
2022

CIP - Catalogação na Publicação

Lima, Diana Ramos
SÍNTESE E CARACTERIZAÇÃO DE MATERIAIS CARBONADOS ATIVADOS A PARTIR DE RESÍDUOS VEGETAIS DE CASTANHA DO PARÁ E SERRAGEM DE MADEIRA E SUA UTILIZAÇÃO COMO ADSORVENTES NA REMOÇÃO DE CONTAMINANTES EMERGENTES / Diana Ramos Lima. -- 2022.
91 f.
Orientador: Éder Claúdio Lima.

Tese (Doutorado) -- Universidade Federal do Rio Grande do Sul, Escola de Engenharia, Programa de Pós-Graduação em Engenharia de Minas, Metalúrgica e de Materiais, Porto Alegre, BR-RS, 2022.

1. Engenharia. 2. Materiais. 3. Adsorção. 4. Carvão Ativado. 5. Biocarbono. I. Claúdio Lima, Éder, orient. II. Título.

Elaborada pelo Sistema de Geração Automática de Ficha Catalográfica da UFRGS com os dados fornecidos pelo(a) autor(a).

ATA Nº 615

ATA DE DEFESA DE TESE

Ao primeiro dia do mês de julho de 2022, às catorze horas, em Ambiente Virtual pela Universidade Federal do Rio Grande do Sul, realizou-se a defesa da Tese de Doutorado de **M. Sc. Diana Ramos Lima**, intitulada **"Síntese e Caracterização de Materiais Carbonados Ativados a Partir de Resíduos Vegetais de Castanha do Pará e Serragem de Madeira e sua Utilização como Adsorventes na Remoção de Contaminantes Emergentes"**. A Comissão Examinadora, presidida pelo orientador da candidata, Prof. Dr. Éder Cláudio Lima (PPGE3M/UFRGS), constituiu-se dos seguintes membros: Prof. Dr. Irineu Antonio Schadach de Brum (PPGE3M/UFRGS), Profa. Dra. Mariliz Gutterres Soares (DEQUI/UFRGS) e Prof. Dr. Fernando Machado Machado (UFPel). Após a apresentação da candidata pelo Presidente da Comissão, a mesma expôs seu trabalho de tese, sendo, logo a seguir, arguida pelos membros da Comissão Examinadora. A candidata prestou esclarecimentos sobre sua tese, respondendo às perguntas formuladas. Às 17 horas e 08 minutos, a Comissão Examinadora procedeu ao julgamento do trabalho. Consultados individualmente, os membros da Comissão Examinadora justificaram e emitiram os seguintes pareceres: Prof. Dr. Irineu Antonio Schadach de Brum Aprovada, Profa. Dra. Mariliz Gutterres Soares Aprovada e Prof. Dr. Fernando Machado Machado Aprovada. Desta forma e de acordo com o regimento interno do PPGE3M a tese foi aprovada e considerada adequada para a concessão do título de **"Doutora em Engenharia – Área de Concentração: Tecnologia Mineral, Ambiental e Metalurgia Extrativa".** A candidata deve efetuar as correções indicadas pelos examinadores dentro do prazo regimental. O professor Éder Cláudio Lima agradeceu aos membros da comissão Examinadora pela presença e colaboração recebida, quando foi lida a presente Ata, que vai assinada por todos os membros da Comissão Examinadora, orientador e aluna.

gov.br Documento assinado digitalmente
FERNANDO MACHADO MACHADO
Data: 04/07/2022 19:43:26-0300
Verifique em https://verificador.iti.br

gov.br Documento assinado digitalmente
IRINEU ANTONIO SCHADACH DE BRUM
Data: 04/07/2022 16:37:06-0300
Verifique em https://verificador.iti.br

Prof. Dr. Éder Cláudio Lima

Prof. Dr. Irineu Antonio Schadach de Brum

Profa. Dra. Mariliz Gutterres Soares

Prof. Dr. Fernando Machado Machado

gov.br Documento assinado digitalmente
MARILIZ GUTTERRES SOARES
Data: 06/07/2022 16:42:39-0300
Verifique em https://verificador.iti.br

M. Sc. Diana Ramos Lima

DIANA RAMOS LIMA:02777679037
Assinado de forma digital por DIANA RAMOS LIMA:02777679037

gov.br Documento assinado digitalmente
EDER CLAUDIO LIMA
Data: 01/07/2022 14:17:03-0300
Verifique em https://verificador.iti.br

ESTRUTURA DA TESE

Esta tese foi estruturada na forma de artigos científicos, de acordo com a Resolução N˚ 093/2007, de 12/06/2007 da Assembleia de Pós-Graduação da Universidade do Rio Grande do Sul (UFRGS), em seu Art. 3º e 5°, que estabelece diretrizes para a publicação e redação de Teses de Doutorado, Dissertações de Mestrado e Conclusão de Cursos de Especialização no formato de artigos em língua estrangeira. A tese está estruturada com os tópicos: i) Introdução; ii) Objetivos; iii) Fundamentação teórica e Revisão da Literatura; iii) Artigos formatados conforme periódico; iv) conclusão; v) Referências bibliográficas.

Produção Científica de Diana Ramos Lima no Grupo Latama (2018-2022)

1- **LIMA, DIANA R.**; Lima, Eder C.; Thue, Pascal S.; Dias, Silvio L.P.; Machado, Fernando M.; Seliem, Moaaz K.; Sher, Farooq; Dos Reis, Glaydson S.; Saeb, Mohammad Reza; Rinklebe, Jörg. Comparison of Acidic Leaching Using a Conventional and Ultrasound-Assisted Method for Preparation of Magnetic-Activated Biochar. JOURNAL OF ENVIRONMENTAL CHEMICAL ENGINEERING. , V.9, P.105865, 2021.

2. **LIMA, DIANA R.**; Hosseini-Bandegharaei, Ahmad; Thue, Pascal S; Lima, Eder C.; De Albuquerque, Ytallo R.T.; Dos Reis, Glaydson S.; Umpierres, Cibele S.; Dias, Silvio L.P.; Tran, Hai Nguyen. Efficient Acetaminophen Removal From Water And Hospital Effluents Treatment By Activated Carbons Derived From Brazil Nutshells. COLLOIDS AND SURFACES A-PHYSICOCHEMICAL AND ENGINEERING ASPECTS. , V.583, P.123966, 2019.

3. **LIMA, DIANA R.**; Gomes, Adriano A.; Lima, Eder C.; Umpierres, Cibele S.; Thue, Pascal S.; Panzenhagen, José C.P.; Dotto, Guilherme L.; El-Chaghaby, Ghadir A.; De Alencar, Wagner S. Evaluation Of Efficiency And Selectivity In The Sorption Process Assisted By Chemometric Approaches: Removal Of Emerging Contaminants From Water. SPECTROCHIMICA ACTA PART A-MOLECULAR AND BIOMOLECULAR SPECTROSCOPY. , V.218, P.366 - 373, 2019.

4. **LIMA, DIANA RAMOS**; Lima, Eder C.; Umpierres, Cibele S.; Thue, Pascal Silas; El-Chaghaby, Ghadir A.; Da Silva, Raphaelle Sanches; Pavan, Flavio A.; Dias, Silvio L. P.; Biron, Camille. Removal Of Amoxicillin From Simulated Hospital Effluents By Adsorption Using Activated Carbons Prepared From Capsules Of Cashew Of Para. Environmental Science And Pollution Research. , V.26, P.1 - 13, 2019.

Colaboração Científica de Diana Ramos Lima no Grupo Latama (2018-2022)

1. Sellaoui, Lotfi; Dhaouadi, Fatma; Taamalli, Sonia; Alzahrani, Hanan Yahya Saeed; Louis, Florent; Bakali, Abderrahman El; Erto, Alessandro; Lamine, Abdelmottaleb Ben; **Lima, Diana Ramos**; Lima, Eder Claudio; Chen, Zhuqi. Application Of A Multilayer Physical Model For The Critical Analysis Of The Adsorption Of Nicotinamide And Propranolol On Magnetic-Activated Carbon. Environmental Science And Pollution Research. , V.30, P.S11356-021-1848 - , 2022.

2. Thue, Pascal S.; **Lima, Diana Ramos**; Lima, Eder C.; Teixeira, Roberta A.; Dos Reis, Glaydson S.; Dias, Silvio L.P.; Machado, Fernando M. Comparative Studies Of Physicochemical And Adsorptive Properties Of Biochar Materials From Biomass Using Different Zinc Salts As Activating Agents. JOURNAL OF ENVIRONMENTAL CHEMICAL ENGINEERING. , V.10, P.107632 - , 2022.

3. Sellaoui, Lotfi; Yazidi, Amira; Taamalli, Sonia; Bonilla-Petriciolet, Adrián; Louis, Florent; El Bakali, Abderrahman; Badawi, Michael; Lima, Eder C.; **Lima, Diana R.**; Chen, Zhuqi. Adsorption Of 3-Aminophenol And Resorcinol On Avocado Seed Activated Carbon: Mathematical Modelling, Thermodynamic Study And Description Of Adsorbent Performance. JOURNAL OF MOLECULAR LIQUIDS. , V.342, P.116952 - , 2021.

4. Della-Flora, Alexandre; Wilde, Marcelo L.; **Lima, Diana**; Lima, Eder C.; Sirtori, Carla. Combination Of Tertiary Solar Photo-Fenton And Adsorption Processes In The Treatment Of Hospital Wastewater: The Removal Of Pharmaceuticals And Their Transformation Products. JOURNAL OF ENVIRONMENTAL CHEMICAL ENGINEERING. , V.9, P.105666 - , 2021.

5. Thue, Pascal S.; **Lima, Diana R.**; Naushad, Mu; Lima, Eder C.; De Albuquerque, Ytallo R. T.; Dias, Silvio L. P.; Cunha, Mariene R.; Dotto, Guilherme L.; De Brum, Irineu A. S. High Removal Of Emerging Contaminants From Wastewater By Activated Carbons Derived From The Shell Of Cashew Of Para. Carbon Letters. , V.31, P.13 - 28, 2021.

6. Rodrigues, Daniel Lucas Costa; Machado, Fernando Machado; Osório, Alice Gonçalves; De Azevedo, Cristiane Ferraz; Lima, Eder Claudio; Da Silva, Raphaelle S.; **Lima, Diana Ramos**; Gonçalves, Fernanda Medeiros. Adsorption Of Amoxicillin Onto High Surface Area-Activated Carbons Based On Olive Biomass: Kinetic And Equilibrium Studies. Environmental Science And Pollution Research. , V...., P.... - , 2020.

7. Della-Flora, Alexandre; Wilde, Marcelo L.; Thue, Pascal S.; **Lima, Diana**; Lima, Eder C.; Sirtori, Carla Combination Of Solar Photo-Fenton And Adsorption Process For Removal Of The Anticancer Drug Flutamide And Its Transformation Products From

Hospital Wastewater. JOURNAL OF HAZARDOUS MATERIALS. , V.396, P.122699 - , 2020.

8. Caicedo, Diana Fernanda; Dos Reis, Glaydson Simoes; Lima, Eder Claudio; De Brum, Irineu A.S.; Thue, Pascal Silas; Cazacliu, Bogdan Grigore; **Lima, Diana Ramos**; Dos Santos, Arthur Hoffmann; Dotto, Guilherme Luiz.Efficient Adsorbent Based On Construction And Demolition Wastes Functionalized With 3-Aminopropyltriethoxysilane (APTES) For The Removal Ciprofloxacin From Hospital Synthetic Effluents. JOURNAL OF ENVIRONMENTAL CHEMICAL ENGINEERING. , V.8, P.103875 - , 2020.

9. Thue, Pascal S.; Umpierres, Cibele S.; Lima, Eder C.; **Lima, Diana R.**; Machado, Fernando M.; Dos Reis, Glaydson S.; Da Silva, Raphaelle S.; Pavan, Flavio A.; Tran, Hai Nguyen. Single-Step Pyrolysis For Producing Magnetic Activated Carbon From Tucumã (Astrocaryum Aculeatum) Seed And Nickel(II) Chloride And Zinc(II) Chloride. Application For Removal Of Nicotinamide And Propanolol. JOURNAL OF HAZARDOUS MATERIALS. , V.398, P.122903 - , 2020.

10. Kasperiski, Fernando M.; Lima, Eder C.; Umpierres, Cibele S.; Dos Reis, Glaydson S.; Thue, Pascal Silas; **Lima, Diana Ramos**; Dias, Silvio L.P.; Saucier, Caroline; Da Costa, Janaina B. Production Of Porous Activated Carbons From Caesalpinia Ferrea Seed Pod Wastes: Highly Efficient Removal Of Captopril From Aqueous Solutions. JOURNAL OF CLEANER PRODUCTION. , V.197, P.919 - 929, 2018.

11- Umpierres, C. S.; Lima, D. R.; Dias, Silvio L. P.; Thue, Pascal S; Lima, Eder C. 'Carvão Ativado Magnético, Processo De Obtenção De Carvão Ativado Magnético E Usos De Carvão Ativado Magnético', 2019. Categoria: Produto E Processo. Instituição Onde Foi Depositada: INPI - Instituto Nacional Da Propriedade Industrial. País: Brasil. Natureza: Patente De Invenção. Número Do Registro: BR10201901854. Data De Depósito: 03/09/2019. Depositante/Titular: LIMA, EDER C.

12-Roberta A. Teixeira ; **LIMA, É. C.** ; BENETTI, A. D. ; THUE, PASCAL S. ; CUNHA, MARIENE R. ; CIMIRRO, NILTON F. G. M. ; Mohammad Hadi Dehghani ; REIS, G. S.; DOTTO, GUILHERME L. Preparation of hybrids of wood sawdust with 3-aminopropyl-triethoxysilane. Application as an adsorbent to remove Reactive Blue 4 dye from wastewater effluents.. Journal of the Taiwan Institute of Chemical Engineers JCR, v. 125, p. 141-152, 2021.

Dedico essa Tese e todos os meus anos de estudo aos meus irmãos (Felipe, Isis, Agnes, Rovena, Yan, Yuri, Micael, Suliê, Islani, Ravel) eles são a ponte com meu passado e os pilares para o meu futuro.

AGRADECIMENTOS

Agradeço primeiramente aos meus pais Carlos Ênio Jorge Lima e Eliane Albrecht Ramos por me proporcionarem a oportunidade de estar nesse “mundo véio louco” e ainda por me ensinar a viver nele.

Agradeço ao prof. Éder Cláudio Lima pela oportunidade de realizar o doutorado no LATAMA, grupo de pesquisa consolidado e visionário, pelas inúmeras oportunidades de crescer como pesquisadora e pelo enriquecimento na formação profissional.

Agradeço aos amigos e colegas do LATAMA: Pascal Thue, Roberta Ârleu, Cibele Umpierres, Raphaelle Sanches, Ytallo Albuquerque vocês foram essenciais e fizeram toda diferença no dia a dia do laboratório, nas conversas de corredor, nos almoços do RU e em toda a caminhada. Vocês contribuíram com conhecimento, motivação, compreensão e amizade. A construção de uma tese é mais fácil quando rodeada de pessoas especiais como vocês.

Agradeço aos amigos de longa data Gabriel, Giani e Lauren que nesses 4 anos foram saudade presente, luz no fim túnel, conversa jogada fora, com certeza foram esses intervalos acadêmicos que me mantiveram enxergando perspectiva.

Agradeço a Sizenando Braga “meu broto” pelos anos de companhia, de compreensão e abraços silenciosos quando o amanhã parecia não existir.

Agradeço a oportunidade de ter acesso a Universidades Federais, ensino público e de qualidade, em especial a UNIPAMPA, a UFSM e UFRGS, minhas escolas formadoras.

Aos professores e funcionários do PPGE3M.

A CAPES pela concessão de bolsa de doutorado.

E a todos aqueles que contribuíram de alguma forma para que mais essa etapa fosse concluída

RESUMO

A presente tese investigou metodologias para o preparo de carvões ativados, usando como precursores carbonáceos os resíduos da Castanha do Para (*Bertholletia excelsa)* e da serragem do Sapelli *(Entandrophragma cylindricum)* bem como a aplicação desses carvões como adsorventes em efluentes contendo contaminantes de preocupação emergente. A tese é apresentada no formato de 3 artigos, já publicados em periódicos internacionais com classificação Capes A1 e B1. As metodologias de preparo dos carvões tiveram dois enfoques: i) a melhoria das propriedades texturais (área superficial e volume de poros); ii) atribuição de caraterísticas magnéticas sem perder potencialidade como adsorvente. Na primeira investigação usando os resíduos da Castanha do Pará (CCP) buscou-se entender o efeito da temperatura de pirolise na preparação do carvão ativado, sendo preparado pastas na proporção de 1:1 (CCP: $ZnCl_2$) e a pirolise realizada nas temperaturas de 600°C e 700°C, denominados respectivamente CCP600 e CCP700. Na segunda investigação, também usando os resíduos da Castanha do Pará (CCP) a pesquisa focou os estudos na influência da quantidade de Cloreto de Zinco na preparação dos carvões, sendo produzido carvões na proporção 1:1 (CCP : $ZnCl_2$) e na proporção 1:1.5 (CCP : $ZnCl_2$), denominados respectivamente BNS1.0 e BNS1.5, ambos pirolisadas 600°C. Na terceira investigação a serragem de Sapelli foi usada como precursor dos carvões ativados e os estudos foram direcionados para o preparo de materiais magnéticos, onde apurou-se misturas de Sapelli com Cloreto de níquel ($NiCl_2$) - (1:1), bem como a mistura Sapelli: Cloreto de Zinco ($ZnCl_2$): Cloreto de Níquel ($NiCl_2$) – (1:1:1), ambas as pastas foram pirolisadas a 700°C. Nesse estudo ainda se investigou duas formas de eliminação dos inorgânicos do carvão ativado, a lixiviação com ácido clorídrico (0.1M) sob refluxo e a lixiviação assistida por ultrassom (US- 15 min, 600 W), obtendo-se quatro compósitos: SNiAL, SNiUS, SNiZnAL, SNiZnUS. Todos os carvões foram caracterizados por análise elementar de CHN/O, a razão hidrofóbica/hidrofílica, FTIR, TGA, titulação modificada de Bohem, BET/BJH e para a última investigação caracterizou-se os carvões quanto a magnetização usando o VSM. Essas análises mostram que os adsorventes têm diferentes grupos polares, o que confere uma superfície hidrofílica. Quanto às propriedades texturais o CCP600 e CCP700 apresentaram área superficial e volume total de poros de 1457 $m^2.g^{-1}$ e 0.275 $cm^3.g^{-1}$ e 1419 $m2.g^{-1}$ e 0.285 $cm^3.g^{-1}$ respectivamente, o BNS 1:0 e o BNS 1:1,5

apresentaram 1457 $m^2.g^{-1}$ e 0.5486 $cm^3.g^{-1}$; 1640 $m^2.g^{-1}$ e 0.7947 $cm^3.g^{-1}$; enquanto SNiAL, SNiUS, SNiZnAL, SNiZnUS apresentaram área superficial e volume total de poros de 384 $m^2.g^{-1}$ e 0,136 $cm^3.g^{-1}$; 396 $m^2.g^{-1}$ e 0,147 $cm^3\ g^{-1}$; 1628 $m^2.g^{-1}$ e 0,660 $cm^3\ g^{-1}$; 1212 $m^2.g^{-1}$ e 0,497 $cm^3.g^{-1}$, respectivamente. No que tange ao magnetismo os carvões ativados atingiram saturação de magnetização (Ms) de 6.86 (emu/g) para SNiZnAL; 10.81 (emu/g) para SNiZnUS; 15.00 (emu/g) para SNiAL e 12.59 (emu/g) para SNiUS. As metodologias propostas possibilitaram inferir que variação de 100°C na pirólise dos precursores não causou modificações significativas nas propriedades texturais dos carvões bem como possibilitou validar que o cloreto de zinco favorece o incremento das propriedades texturais, ademais foi possível identificar que o processo de lixiviação via ultrassom pode ser usado a favor da manutenção das propriedades magnéticas do carvão. Os ensaios de adsorção possibilitaram atestar a eficiência dos carvões produzidos como adsorvente de contaminantes emergentes de diferentes classes.

Palavras chaves: Carvão ativado. Biocarbono. Biocarbono ativado magnético. Lixiviação. Adsorção. Contaminantes emergentes.

ABSTRACT

The thesis investigated methodologies for preparing activated carbons, using the residues of Brazil Nut (*Bertholletia excelsa*) and Sapelli sawdust (*Entandrophragma cylindricum*) as carbon precursors. The application of these carbon materials as adsorbents for treating effluents containing contaminants of emerging concern. The thesis is presented in the format of 3 papers already published in international journals with CAPES classifications A1 and B1. The preparation methodologies of carbons had two approaches: i) the improvement of textural properties (surface area and pore volume); ii) attribution of magnetic characteristics without losing the potentiality of being utilized as adsorbent. In the first investigation using the residues of Brazil Nut (CCP) we sought to understand the effect of pyrolysis temperature on the preparation of activated carbon, being prepared pastes in the proportion of 1:1 (CCP: $ZnCl_2$) and pyrolysis performed at temperatures of 600°C and 700°C, respectively called CCP600 and CCP700. In the second investigation, also using the residues of Brazil Nut (CCP), the research focused the studies on the influence of the amount of zinc chloride in the preparation of carbons, being produced activated carbons in the proportion 1:1 (CCP: $ZnCl_2$) and the proportion 1:1.5 (CCP: $ZnCl_2$), respectively BNS1.0 and BNS1.5, both pyrolyzed 600°C. In the third investigation, Sapelli sawdust was used as a precursor of activated carbons, and studies were directed to the preparation of magnetic materials, where Sapelli mixtures with nickel chloride ($NiCl_2$) - (1:1), as well as the Sapelli mixture: Zinc Chloride ($ZnCl_2$): Nickel Chloride ($NiCl_2$) – (1:1:1), both pastes were pyrolyzed at 700°C. In this study, two forms of elimination of inorganics from activated carbon were investigated, leaching with 0.1M hydrochloric acid under reflux and ultrasound-assisted leaching (US- 15 min, 600 W), obtaining four composites: SNiAL, SNiUS, SNiZnAL, SNiZnUS. All activated carbons were characterized by elemental analysis of CHN/O, hydrophobic/hydrophilic ratio, FTIR, TGA, modified titration of Bohem, BET/BJH, and in the last investigation, the carbon materials were characterized by magnetization using VSM. These analyses show that adsorbents have different polar groups, which confers a hydrophilic surface. As for the textural properties, CCP600 and CCP700 presented surface area and total pore volume of 1457 m^2. g^{-1} and 0.275 $cm^3.g^{-1}$and 1419 $m^2.g^{-1}$and 0.285 $cm^3.g^{-1}$, respectively, BNS 1:0 and BNS 1:1.5 presented 1457 m^2. $g^{-1}$and 0.5486 $cm^3.g^{-1}$; 1640 m^2. g^{-1} and 0.7947 $cm^3.g^{-1}$; while SNiAL, SNiUS, SNiZnAL, SNiZnUS presented surface area and total

pore volume of 384 $m^2.g^{-1}$ and 0.136 $cm^3.g^{-1}$; 396 $m^2.g^{-1}$ and 0.147 $cm^3.g^{-1}$; 1628 $m^2.g^{-1}$ and 0.660 $cm^3.g^{-1}$; 1212 m^2. $g^{-1}$and 0.497. $cm^3.g^{-1}$, respectively. When it comes to magnetism, carbon reached magnetization saturation (Ms) of 6.86 (emu/g) for SNiZnAL; 10.81 (emu/g) for SNiZnUS; 15.00 (emu/g) for SNiAL and 12.59 (emu/g) for SNiUS. The proposed methodologies made it possible to infer that a variation of 100°C in the pyrolysis of the precursors did not cause significant changes in the textural properties of the carbon materials, as well as to validate that zinc chloride favors the increase of textural properties, in addition, it was possible to identify that the leaching process via ultrasound can be used in favor of maintaining the magnetic properties of coal. The adsorption tests made it possible to attest to the efficiency of the coals produced as adsorbents of emerging contaminants of different classes.

Keywords: Activated carbon. Biochar. Magnetic activated biochar. Leaching. Adsorption. Emerging Contaminants.

LISTA DE FIGURAS

LISTA DE TABELAS

ABREVIATURAS

CCP-Capsulas de Castanha do Pará

BNS- *Brazil nut shells*

CE-Contaminantes emergentes

BET - Brunauer, Emmett e Teller

BJH - Barrett, Joyner e Halenda

SEM - *Scanning electron microscopy*

EDS - Espectroscopia por dispersão de raios X

UV-VIS - Ultravioleta-Visível

Q_{max} – quantidade máxima de adsorvato adsorvido pelo material

ΔG° – variação da energia de Gibbs padrão

ΔH° – variação de entalpia padrão

ΔS° – variação de entropia padrão

MEV-Microscopia eletrônica de varredura;

DRX- Difração de raios-X;

FTIR- Espectroscopia no infravermelho por transformada de Fourier;

CHN-Análise Elementar de carbono, hidrogênio e nitrogênio

pH_{pcz} – pH no ponto de carga zero;

COP- Conferência das Partes

POP-Poluentes Orgânicos Persistentes

khz-quilohertz

LISTA DE SÍMBOLOS

T: Temperatura (°C/ K);

t: Tempo (min);

te: Tempo de equilíbrio;

Q_{max}: Capacidade máxima de adsorção calculada pelo modelo (mg g^{-1});

q: quantidade adsorvida do adsorvato por grama do adsorvente (mg.g^{-1});

C_o e C_f :são as concentrações iniciais e finais da solução do adsorvato, (mg.L^{-1});

V: Volume de solução do adsorvato colocado em contato com o adsorvente (L);

m: e a massa do adsorvente (g);

q_e: quantidade de adsorbato retida no adsorvente no equilíbrio (mg g^{-1});

C_e: concentração atingida no equilíbrio (mg L^{-1});

n_F: expoente de Freundlich;

K_F: constante isotérmica de Freundlich (mg g^{-1}(mg L^{-1}) $^{-1/n}$);

K_L: constante de Langmuir (L mg^{-1});

K_g: constante de equilíbrio de Liu (L. mg^{-1});

n_L: é um expoente adimensional da equação de Liu;

R: é a constante universal dos gases (8,314 J K^{-1} mol^{-1});

K_e^0 (adimensional): é a constante de equilíbrio termodinâmico

q_t: é a quantidade de adsorção fixada no tempo (mg.g^{-1});

k_f: é a constante da taxa pseudo-primeira-ordem (min^{-1});

k_s : é a constante da taxa pseudo-segunda-ordem (g mg^{-1} min^{-1});

k_{AV}: é a constante cinética de Avrami (min^{-1});

n: é a ordem de adsorção fracionária.

SUMÁRIO

1 INTRODUÇÃO

A poluição ambiental está diretamente relacionada com desenvolvimento industrial devido à eliminação de efluentes e ou rejeitos tóxicos, resistentes à degradação e a tratamentos convencionais, proveniente de subprodutos gerados pelas indústrias (RODRIGUEZ *et al.*, 2017; TRÖGER *et al.*, 2021).

Os efluentes líquidos contendo corantes, fármacos, agrotóxicos e outros precursores da indústria química são gerados em diferentes setores industriais, em quantidades crescentes e recebem tratamentos e destinações diversificadas (ERTÜRK e SAÇAN, 2013; SOPHIA e LIMA, 2018; TRÖGER *et al*.., 2021). A constituição química e os efeitos dessas substâncias no ecossistema são monitorados por uma rede de colaboração entre diversos centros de pesquisa e organizações da Europa (*Network of Reference Laboratories, Research Centres and Related Organisations For Monitoring of Emerging Environmental Substances*), com a finalidade de identificar possíveis substâncias que não são normalmente controladas no ambiente, mas que tem potencial para causar efeitos adversos ecológicos e (ou) sobre a saúde humana, sendo estes efeitos conhecidos ou suspeitos. Essa rede monitora os efeitos no ecossistema de mais 111.000 substâncias. A lista é apresentada com os produtos classificados em: plastificantes, aditivos alimentares, aditivos combustíveis, composto intermediários da indústria, produtos para cuidados pessoais, compostos farmacêuticos, hormônios, pesticidas, retardadores de chama, surfactantes e outros produtos químicos.

O tratamento eficaz desses resíduos é uma questão emergente, uma vez que esses contaminantes são compostos de moléculas que não são facilmente biodegradadas ou hidrolisadas sendo consideradas moléculas estáveis e recalcitrantes (KASPERISKI *et al.*, 2018; SOPHIA e LIMA, 2018; GADELHA *et al.*, 2019; TRÖGER *et al*., 2021).

Dessa forma a busca por novos métodos eficazes de tratamento de efluentes é intensa, visando diminuir ou eliminar a toxicidade desses contaminantes no ecossistema. Agências de proteção ambiental como *United States Environmental Protection Agency (USEPA*); *United States Geological Surveya (USGS*) e pactos firmados entre as nações como o acordo de Estocolmo e a agenda para atingir os Objetivos de Desenvolvimento Sustentável (ODS), reconhecem que os contaminantes emergentes têm propriedades tóxicas, são resistentes à degradação, bioacumulam-

se, são transportados pelo ar, pela água e pelas espécies migratórias através das fronteiras internacionais e depositados distantes do local de sua liberação, onde se acumulam em ecossistemas terrestres e aquáticos.

Pesquisas apontam a emergente preocupação com esses compostos podendo citar os trabalhos de: ARLOS *et al.*, 2018; LI *et al.*., 2021; PREDIERI *et al.*, 2020; TETZLAFF *et al.*, 2021; TRÖGER *et al.*, 2021; Sophia e Lima, 2016; Silva *et al*. 2018, Cunha *et al.*, 2020; Thue *et al.*,2022 entre outros. As pesquisas ilustram o uso de diferentes tecnologias no tratamento desses contaminantes, entre elas: oxidação avançada, membrana de separação, adsorção, biossorção, nanofiltração, fenton, fotocatálise, troca iônica e outros. O custo médio dessas tecnologias por m^3 de efluente a ser tratada após o tratamento convencional é estimado em valores que variam de US$ 0.5 até US$ 1.2 (DWI, 2007, TRÖGER *et al.*, 2021; LI *et al.*, 2021).

O levantamento bibliográfico indicou que a adsorção tem se mostrado como uma das técnicas mais utilizadas, devido ao seu baixo custo, baixa necessidade de energia, alta eficiência na remoção de contaminantes emergentes e a não formação de produtos de transformação (ÁLVAREZ-TORRELLAS *et al.*, 2016; BACCAR *et al.*, 2012; GISI *et al.*, 2016; THUE *et al.*, 2016, 2017), bem como também é citada em muitos estudos como uma operação versátil no que tange ao uso de adsorventes e adsorvatos (KOTTUPARAMBIL *et al.*, 2014; LARA-VÁSQUEZ, SOLACHE e GUTIÉRREZ, 2016; LIMA, ADEBAYO, MACHADO, 2015; TAKDASTAN *et al.*,2016). A adsorção tem seu conceito amplamente difundido e descreve o fenômeno no qual moléculas (adsorvatos) que estão presentes em um fluido (gasoso ou líquido) concentram-se sobre uma superfície sólida (adsorvente).

Os autores Kumar *et al. (*2009); Umpierres *et al. (*2017); Rodriguez-Narvaez *et al.* (2017); Nilsen *et al. (*2019) enfatizam que o carvão ativado (CA) comercial é o adsorvente mais utilizado para a remoção de compostos orgânicos de efluentes industriais devido a suas propriedades de texturas. Além disso, um levantamento do Instituto Nacional de Tecnologia (INT, 2017) indica que os principais consumidores de adsorventes, no Brasil, são as empresas de abastecimento de água potável, empresa de fármacos, transporte de gases, dentre outras, com inúmeras formas de utilização (INT, 2017). No entanto, apesar das vantagens, o carvão ativado comercial ainda tem seu uso restrito, pelo custo e por sua produção comercial ser inferior a demanda. Dados de mercado disponíveis na *Fortune Business insights* indicam que o mercado global de carvão ativado foi de US$ 2.96 bilhões em 2020 e está projetado para crescer US$

4.50 bilhões até 2028. CRINI *et al.* (2019) apontam que o CA é requerido principalmente por indústrias que investem no sistema terciário de tratamento de efluentes e setores da saúde. Por conseguinte, os pesquisadores estão voltados a buscar fontes alternativas de preparação e reaproveitamento de carvão ativado (INT, 2017) assim o uso de resíduos agroindustriais como precursor de carbono no desenvolvimento de carvão ativado aumentou consideravelmente nos últimos anos, sendo possível citar trabalhos de Hu *et al.* (2017); Silva *et al.* (2018); Zhu *et al.* (2018); Cunha *et al.* (2020); Cimirro *et al.* (2020) Wang *et al.* (2022); entre outros. Aliado a demanda por carvão ativado, os setores industriais também estão buscando formas de separação do adsorvente após adsorção do adsorvato e sua regeneração pelo maior número de ciclos possíveis.

Propostas de metodologias de impregnação química e tratamentos de superfícies para aplicação de funcionalidades e ou incremento de propriedades adsorventes ao carvão ativado tem ganhado destaque. O *Spacenet* no ano de 2022 registra 499 patentes acerca de produção de carvões ativos magnéticos, sendo que 265 dessas foram depositadas nos últimos 5 anos (2017-2022). Quando se relaciona os termos "*leaching" and "ultrasound" or Ultrasound-assited" and "magnetic activated carbon"* a busca não retorna resultados.

Considerando o exposto, este trabalho de tese teve como objetivo geral a investigação de metodologias potencialmente inovadoras para o preparo de carvões ativados e compósitos magnéticos, tendo como precursores resíduos agroindustriais da Castanha do Pará (*Bertholletia excelsa)* e do Sapelli *(Entandrophragma cylindricum)* e sua aplicação como adsorvente em contaminantes de preocupação emergente.

2 OBJETIVOS

Este trabalho de tese teve como objetivo geral a investigação de metodologias potencialmente inovadoras para o preparo de carvões ativados e compósitos magnéticos, tendo como precursores resíduos agroindustriais da Castanha do Pará (*Bertholletia excelsa)* e da serragem do Sapelli *(Entandrophragma cylindricum)* e sua aplicação como adsorvente em contaminantes de preocupação emergente.

Objetivos específicos

- Investigar modificações das biomassas com os sais Cloreto de Zinco ($ZnCl_2$) e Cloreto de Níquel ($NiCl_2$);
- Estudar os parâmetros e efeitos da carbonização, dos resíduos modificados, em forno tubular vertical, visando obter carvão ativado com alta área superficial;
- Averiguar formas de lixiviação dos sais inorgânicos impregnados na etapa de modificação dos resíduos;
- Caracterizar físico-quimicamente os adsorventes produzidos;
- Estudar a aplicação dos carvões ativados na adsorção de efluentes líquidos simulados contendo contaminantes emergentes;
- Construir curvas cinéticas de adsorção em diferentes concentrações de contaminantes emergentes e ajustar a modelos da literatura;
- Construir curvas de equilíbrio experimentais e ajustar a modelos da literatura;
- Verificar os mecanismos de adsorção através do estudo termodinâmico,dados de cinética e equilíbrio.

3 FUNDAMENTAÇÃO TEÓRICA E REVISÃO LITERATURA

Neste capítulo será abordado um panorama geral sobre os efluentes que contenham em solução os contaminantes emergentes bem como a descrição e detalhamento da operação unitária adsorção, usando carvões ativados provenientes de resíduos agroindustriais, como técnica de tratamento desses contaminantes. Ademais serão apresentadas formas de potencializar as características de superfície desse carvão.

3.1 CONTAMINANTES EMERGENTES

Segundo a agência Norte-Americana *United States Geological Surveya (USGS*), um contaminante emergente (CE) pode ser definido como:

> "uma substância química de ocorrência natural ou antrópica, ou qualquer micro-organismo que não é normalmente controlado no ambiente, mas que tem potencial para entrar no ambiente e causar efeitos adversos ecológicos e (ou) sobre a saúde humana, sendo estes efeitos conhecidos ou suspeitos*". (USGS, tradução livre).*

Ademais, a agência de Proteção Ambiental dos Estados Unidos *United States Environmental Protection Agency (USEPA*) define esses contaminantes como:

> "Poluentes que, atualmente, não são incluídos em programas de monitoramento e que podem se tornar candidatos para legislações futuras dependendo de pesquisas sobre a toxicidade, efeitos sobre a saúde, percepção pelo público e dados sobre sua ocorrência em vários ambientes" (USEPA, tradução livre).

Com o crescimento das pesquisas científicas e possíveis evidências do perigo destes contaminantes, que não devem ser considerados novas substâncias e sim substâncias naturais ou sintéticas que não são comumente monitoradas no meio ambiente e que têm efeitos indesejáveis conhecidos ou suspeitos sobre os seres humanos e o ecossistema, começaram a serem elaboradas regulações embasadas no princípio da precaução, para tentar conhecer estes contaminantes e estudar seus efeitos.

Em 2005, uma rede de colaboração entre diversos centros de pesquisa e organizações da Europa, foi criada com a finalidade de identificar possíveis

substâncias e/ou poluentes emergentes que possam ter impactos negativos no meio ambiente e na saúde humana, a rede intitula-se: *Network of Reference Laboratories, Research Centres and Related Organisations For Monitoring of Emerging Environmental Substances (*NORMAN*)*, popularmente conhecida como projeto NORMAN. Esse projeto tem por missão atualizar periodicamente a lista de contaminantes reconhecidamente perigosos ao ecossistema, a atualização principia de uma lista prévia denominada NORMAN *Suspect List* que contempla, no corrente ano, mais de 111.000 substâncias. A lista é apresentada seguindo classificação exposta na Quadro 1:

Quadro 1- Categorias de CE

Substâncias per e polifluoroalquil	Produtos químicos de contato com alimentos	Biocidas
Produtos químicos para água potável	Aditivos alimentares	Substâncias do ambiente interno
Retardadores de chama	Produtos de cuidados pessoais	Toxinas naturais
Produtos químicos industriais	Produtos fitofarmacêuticos	
Metais e seus compostos	Metabólitos humanos	
Compostos de fumaça	Neurotoxinas humanas	
Surfactantes	Drogas de abuso	

Fonte: NORMAN SusDat

O Brasil segue regulamentação acordada na negociação internacional da Convenção de Estocolmo com texto aprovado por meio do Decreto Legislativo nº 204, de 7 de maio de 2004, com emendas aprovadas durante COP 7 e COP 8, realizada em maio de 2015 e maio de 2017, respectivamente. Nessa regulamentação são reconhecidos apenas 22 poluentes denominados, nesse documento, de Poluentes Orgânicos Persistentes (POP's).

A convenção de Estocolmo reconhece que os POP's têm propriedades tóxicas, são resistentes à degradação, bioacumulam-se, são transportados pelo ar, pela água e pelas espécies migratórias através das fronteiras internacionais e depositados

distantes do local de sua liberação, onde se acumulam em ecossistemas terrestres e aquáticos. A Figura 1 realça as principais fontes, rotas e disposição desses poluentes.

Figura 1- Fontes e rotas de disposição de CE no ecossistema

Fonte: Adaptado de Sophia e Lima (2018) e Ahmed *et al.* (2019)

Os processos de atenuação natural e de tratamento convencional de águas, que contenham esses poluentes, não são capazes de diminuir ou eliminar a toxicidade desses contaminantes no ecossistema. As pesquisas atuais ilustram o uso de diferentes tecnologias no tratamento desses contaminantes, entre elas: oxidação avançada, membrana de separação, adsorção, biossorção, nanofiltração, Fenton, fotocatálise, troca iônica e outros. O Custo médio dessas tecnologias por m^3 de efluente a ser tratada após o tratamento convencional é estimado em valores que variam de US$ 0.5 até US$ 1.2, (DWI, 2007, TRÖGER *et al.*, 2021; LI *et al*., 2021).

O levantamento bibliográfico indicou que a adsorção tem se mostrado como uma das técnicas mais utilizadas, devido ao seu baixo custo, baixa necessidade de energia, alta eficiência na remoção de contaminantes emergentes e a não formação de produtos de transformação (ÁLVAREZ-TORRELLAS *et al.*, 2016; BACCAR *et al.*, 2012; GISI, De *et al.*, 2016; THUE *et al.*, 2016, 2017), bem como também é citada em muitos estudos como uma operação versátil no que tange ao uso de adsorventes

e adsorvatos (KOTTUPARAMBIL *et al.*, 2014; LARA-VÁSQUEZ, SOLACHE e GUTIÉRREZ, 2016; LIMA, ADEBAYO, MACHADO, 2015; TAKDASTAN *et al.*, 2016).

3.2 ADSORÇÃO

O conceito amplamente conhecido de adsorção foi proposto em 1984 por Rutheven, onde o mesmo descreve a adsorção como uma operação unitária que envolve o contato entre um sólido e um fluido, originando uma transferência de massa da fase fluida para a superfície do sólido. Para Gomide (1988) a adsorção descreve o fenômeno no qual moléculas que estão presentes em um fluido (gasoso ou líquido) concentram-se sobre uma superfície sólida e ainda denomina que a substância que acumula na interface é chamada de adsorvato, enquanto o sólido é chamado de adsorvente.

Weber e Smith (1986); Rudzinski e Plazinski (2007); Çeçen e Aktas (2011); Lima *et al.*(2021) salientam que de um modo geral, o processo de adsorção ocorre seguindo as etapas ilustradas na Figura 2.

Figura 2- Mecanismos envolvidos no transporte do adsorvato até o adsorvente

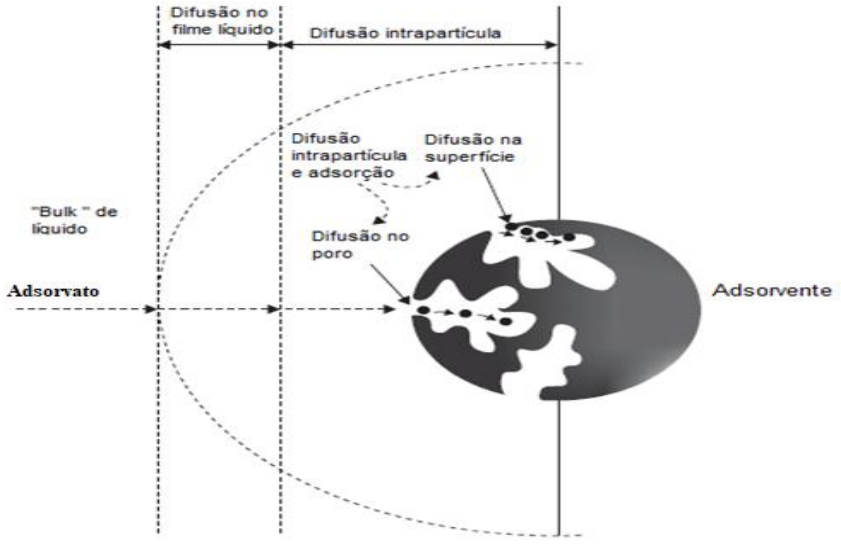

Fonte: adaptado de Çeçen e Aktas (2011)

Onde, as etapas podem ser descritas como:

i) Transporte do contaminante (adsorvato) da fase aquosa para o filme que forma a camada limite (interface sólido-líquido);

ii) Transporte do adsorvato através da camada limite até a superfície das partículas do adsorvente, essa etapa ocorre por difusão e a força motriz é a diferença de concentração;

iii) Difusão do adsorvato na superfície e nos poros do adsorvente (difusão intrapartícula);

iv) Interação física e/ou química entre adsorbato e adsorvente (adsorção).

Çeçen e Aktas (2011); Lima *et al.* (2021) destacam que os adsorvatos permanecem adsorvidos na superfície do adsorvente pela ação de interações a nível molecular e essas interações são as mesmas independente se ocorrem na superfície ou nos poros do adsorvente.

ZHANG *et al.* (2019); Doke e Khan (2013) indicam que o fenômeno de adsorção é termodinamicamente explicado pela existência de forças de atração perpendiculares ao plano da superfície da fase sólida. A intensidade dessas forças depende da natureza do sólido, principalmente das características da superfície e do tipo das moléculas adsorvidas. Segundo Atkins e De Paula (2008), dependendo da força das ligações entre as moléculas que estão sendo adsorvidas e o material sólido, podem-se diferenciar dois tipos principais de interação, a adsorção física (fisiossorção) e a adsorção química (quimiossorção). A Tabela 1 realça as características de cada interação, sendo relevante enfatizar que sob condições favoráveis ambos os processos podem ocorrer simultaneamente ou alternativamente.

Tabela 1- Características gerais da natureza das interações adsorvato-adsorvente

Característica	Fisiosorção	Químiosorção
Natureza da Interação	Ligações de Van der Waals, interações π-π, dipolo-dipolo, ligações de hidrogênio e interações eletrostáticas; (05-80) kJ Mol^{-1}.	Ligações covalente (200-800) kJ Mol^{-1} e Ligação iônica com formação de uma rede cristalina; (200-400) kJ Mol^{-1}.
Dependência com aumenta Temperatura	Desfavorece interações de natureza física.	Favorece interações de natureza química.
Cobertura do adsorvente	Monocamada ou multicamadas.	Monocamadas.

Fonte:Adaptado Çeçen e Aktas (2011); Bergmann *et al.* (2015).

Lima *et al.* (2015); Gisi *et al.* (2016) relatam que as propriedades dos adsorvatos e adsorventes são bastante específicas e dependem de seus constituintes.

Considerando os adsorventes, é amplamente reconhecido pelos pesquisadores (DĄBROWSKI 2001; MACHADO *et al.*, 2015; CRINI *et al.*, 2019; CHENG *et al.,*2021) que as propriedades de textura, como área de superfície, volume de poros e diâmetro médio de poros são os principais fatores para determinar a capacidade de adsorção.

A cerca do adsorbato as características que mais influenciam o processo de adsorção são: peso molecular, os arranjos espaciais de átomos e grupos da molécula, grau de solubilidade e polaridade da molécula, pH e temperatura no qual essas moléculas são solubilizadas (ÇEÇEN e AKTAS, 2011).

Ademais, Dąbrowski (2001); Machado *et al.* (2015); Gisi *et al.* (2016); Umpierres *et al.* (2019), enfatizam que a busca atual deve ser por metodologias que potencializam as características do adsorvente bem como desenvolvam os sítios de superfície de adsorção ou ligações pendentes das estruturas que também podem desempenhar um papel importante no processo de adsorção ao investir em aumentar a afinidade entre adsorbato e adsorvente.

A quantidade de adsorvato, que pode ser adsorvida por um adsorvente em função da temperatura e concentração do adsorvato pode ser descrita por uma isoterma de adsorção, enquanto que relação entre o tempo necessário para que esse sistema adsorvato/adsorvente entre em equilíbrio é descrito por modelos cinéticos. A quantidade adsorvida do adsorvato (q) na fase sólida e a sua porcentagem de remoção do efluente aquoso são dadas pelas Equações 1 e 2:

$$q=\frac{(C_o-C_f)}{m}.V \quad (1)$$

$$\%\ remoção = 100.\frac{C_0-C_f}{C_0} \quad (2)$$

Nas quais, *q* é a quantidade adsorvida do adsorvato por grama do adsorvente ($mg.g^{-1}$); C_o *e* C_f são as concentrações iniciais e finais da solução do adsorvato, ($mg.L^{-1}$); *V* e o volume em litros de solução do adsorvato colocado em contato com o adsorvente (L); *m* e a massa do adsorvente em gramas (g).

3.2.1 Isotermas de adsorção

Alleoni *et al.* (1998); Tommes *et al.* (2015) enfatizam que as isotermas expressam a relação existente entre a quantidade de adsorvato removido da fase aquosa e a quantidade de adsorvato remanescente na solução a uma temperatura constante. Ademais, esses autores ainda salientam que as isotermas são comumente descritas por modelos matemáticos (físicos, empíricos, semi-empíricos).

O formato da isoterma está relacionado com o tipo de porosidade do sólido, como explica Muttakin *et al*. (2018). No caso de adsorventes porosos, a superfície pode ser subdividida em uma superfície externa e uma superfície interna, sendo essas definidas no caso geral como: a superfície externa é a superfície fora dos poros, enquanto a superfície interna é a superfície de todas as paredes dos poros. Com essas considerações, desde 1985 considera-se a classificação de tamanho de poros elaborado pela IUPAC, sendo elas:

(i) poros com larguras superiores a cerca de 50 nm são chamados macroporos;
(ii) poros de larguras entre 2 nm e 50 nm são chamados mesoporos;
(iii) poros com larguras não superiores a 2 nm são chamados microporos.

As isotermas foram classificadas a partir de 1985 pela *International Union of Pure and Applied Chemistry* (IUPAC) segundo *reporting* publicado por Sing (1985) e recentemente atualizadas em Thommes *et al.* (2015), onde foram adicionadas as curvas de histerese associada a cada isoterma. A classificação das isotermas conforme IUPAC é apresentada na Figura 3.

Figura 3- Classificação das isotermas conforme recomendação IUPAC 1985 (a) e 2015 (b)

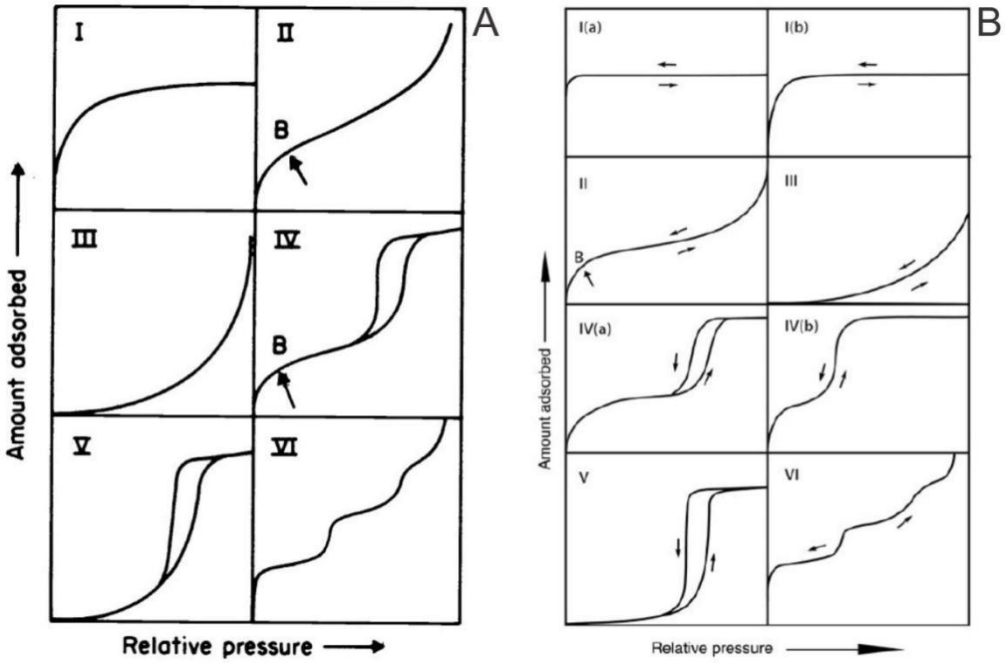

Fonte: (a) Sing (1985); (b) Thommes *et al.* (2015)

Thommes *et al*. (2015) elucidam quais as características de cada agrupamento de isotermas, sendo: a isoterma reversível do Tipo I ocorre comumente em sólidos microporosos como, carvão ativado, zeólitas, e em alguns óxidos porosos. É conhecida como isoterma de Langmuir, e baseia-se na aproximação gradual da adsorção limite que corresponde à monocamada completa. A isoterma reversível do Tipo II é obtida em adsorventes não-porosos ou macroporosos, e não apresenta restrição quanto à adsorção em monocamada. As isotermas reversíveis do Tipo III são raras, a adsorção inicial é lenta em virtude das forças de adsorção pouco intensas. A característica das isotermas de adsorção do Tipo IV e V é a condensação capilar, comum em materiais mesoporosos.

A literatura evidencia diversos modelos disponíveis de isotermas para analisar os dados experimentais e para descrever o equilíbrio de adsorção, incluindo, Langmuir, Freundlich, BET, Toth, Temkin, Redlich-Peterson, Sips, Liu Frumkin, Harkins-Jura, Halsey, Henderson e Dubinin-Radushkevich entre outros. Lima *et al.*(2015) enfatizam que os parâmetros dos modelos das isotermas de adsorção fornecem informações úteis sobre as propriedades da superfície, mecanismo de adsorção e interação entre o adsorvente e o adsorvato.

O modelo de isoterma de Langmuir (1918) assume que um adsorvente possui sítios específicos, homogêneos e energeticamente idênticos de adsorção, e prevê o recobrimento da monocamada na superfície externa do adsorvente. Dessa forma, quando uma molécula atinge determinado sítio, nenhuma adsorção adicional pode ocorrer naquele local. Tendo o adsorvente, segundo esse modelo, uma capacidade finita de adsorver determinada substância, a Equação 3 descreve essa isoterma.

A isoterma de Freundlich é caracterizada por uma equação empírica, aplicável a sistemas caracterizados por heterogeneidade. Freundlich (1906) propôs que não há limite para a capacidade de adsorção, pois a quantidade adsorvida tende ao infinito, ou seja, não prevê a saturação. A isoterma de Freundlich é descrita pela Equação 4.

O modelo Liu é uma combinação matemática de Langmuir e modelos isotérmicos de Freundlich. O modelo Liu tem três parâmetros, considerando os sítios de adsorção como sítios energeticamente diferentes e ocorrência de saturação da superfície, a Equação 5 descreve esse modelo. Os modelos previamente descritos estão sumarizados a seguir:

Langmuir $$q_e = \frac{Q_{\max} \cdot K_L \cdot C_e}{1 + K_L \cdot C_e} \quad (3)$$

Freundlich $$q_e = K_F \cdot C_e^{1/n_F} \quad (4)$$

Liu $$q_e = \frac{Q_{\max} \cdot (K_g \cdot C_e)^{n_L}}{1 + (K_g \cdot C_e)^{n_L}} \quad (5)$$

Onde, q_e=quantidade de adsorbato retida no adsorvente no equilíbrio (mg g^{-1}); C_e= concentração atingida no equilíbrio (mg L^{-1}); n_F = expoente de Freundlich; Q_{max} = capacidade máxima de adsorção (mg g^{-1}) K_F constante isotérmica de Freundlich (mg g^{-1}(mg $L^{-1})^{-1/n}$); K_L =constante de Langmuir (L mg^{-1}); K_g é a constante de equilíbrio de Liu (L. mg^{-1}); n_L é um expoente adimensional da equação de Liu.

3.2.2 Termodinâmica

Segundo Geankoplis (1993) e Lima *et al.* (2015; 2021) os parâmetros termodinâmicos fornecem informações essenciais para o entendimento do processo de adsorção. Utilizando os dados dos modelos de isotermas de adsorção é possível

determinar os parâmetros termodinâmicos: Variação de entropia *(ΔS^0)*, aponta o grau de desordem do sistema após a adsorção; Variação de entalpia (ΔH^0), indica através do sinal se o processo de adsorção é endotérmico ou exotérmico e através da magnitude do valor do $\Delta H°_{ads}$ a natureza da interação entre o adsorvente e o adsorvato na condição de equilíbrio; Variação de energia de livre de Gibbs (ΔG^0), descreve se a ocorrência da adsorção é espontânea. Lima *et al.* (2019) descrevem como determinar os parâmetros termodinâmicos usando a equação de Van't Hoof. Esses autores relacionam a constante de equilíbrio (K_e) de forma correta desde a sua determinação usando dados das isotermas de equilíbrio a várias temperaturas, ajustadas a modelos não lineares. As equações 6,7, 8 e 9 representam os parâmetros termodinâmicos.

$$\Delta G^0 = \Delta H^0 - T\Delta S^0 \quad (6)$$

$$\Delta G^0 = -RTLn(K_e) \quad (7)$$

$$K_e^0 = \frac{(1000.K_g.peso\ molecular\ adsorvato.concentração\ padrão\ do\ adsorvato)}{coeficiente\ de\ atividade\ do\ adsorvato} \quad (8)$$

A combinação das equações leva a equação 9

$$LnK_e = \frac{\Delta S°}{R} - \frac{\Delta H°}{R} x \frac{1}{T} \quad (9)$$

Onde R é a constante universal dos gases (8,314 J K^{-1} mol^{-1}); T é a temperatura absoluta (Kelvin); K_e^0 (adimensional) é a constante de equilíbrio termodinâmico, calculada de acordo com equação 8.

3.2.3 Cinética

A cinética de adsorção descreve a taxa com que um determinado poluente (adsorvato) é removido de uma solução por ação do adsorvente. Ho e Mckay (1998); Rudzinski e Plazinski (2007); Lima *et al.* (2015) relatam que a taxa de adsorção é dependente das características físico-químicas do adsorvato (natureza, massa molecular, solubilidade, estrutura química entre outros), do adsorvente (natureza, estrutura dos poros) e da solução (pH, temperatura e concentração). Lima *et al.* (2015;

2021) explicam que conhecer a cinética de adsorção possibilita: i) determinar o tempo de residência necessário para completar o processo de adsorção; ii) projetar e avaliar o adsorvente em todo o processo; iii) avaliar a natureza das etapas determinantes da velocidade; bem como iv) favorece no planejamento e regeneração do adsorvente. Todos os processos cinéticos de adsorção estão diretamente ligados com as interações entre adsorvente-adsorvato e dependendo da afinidade entre esses, a taxa de adsorção inicial pode ser muito rápida (TRAN *et al*. 2017).

A cinética de adsorção é descrita pelos mecanismos de transporte do adsorvato até o adsorvente, conforme ilustrado anteriormente na Figura 2 e descritos como: transporte do adsorvato do seio da solução; difusão através do filme que circunda as partículas sorventes; difusão nos poros do sorvente; sorção e dessorção na superfície sólida (ÇEÇEN E AKTAS, 2011). A velocidade de adsorção e a quantidade adsorvida dependem de um ou mais dos estágios indicados, O'Neill *et al.* (1999).

Os modelos cinéticos avaliam os mecanismos de adsorção, descrevem a ordem e as etapas de controle da taxa de adsorção, que incluem o transporte de massa e os processos cinéticos baseados em reações químicas. Muitos modelos de cinética foram desenvolvidos com o objetivo de encontrar as constantes intrínsecas da cinética de adsorção.

A fim de estudar o passo determinante na velocidade de adsorção, diversos modelos cinéticos são empregados, entre eles destacam-se as equações propostas por Lagergren (1898) e as equações propostas por Blanachard *et al*.(1984) também chamadas de pseudo-primeira ordem e a equação de pseudo-segunda ordem, respectivamente, que segundo Lima *et al.* (2015; 2021) descrevem o processo de adsorção baseado em reações químicas. Ademais autores como Qiu *et al.* (2009); Vaghetti *et al.* (2009) indicam que modelos cinéticos empíricos podem descrever dados cinéticos, tais como o modelo Avrami. A equação de Avrami é uma função exponencial adaptada da modelagem de decomposição térmica. O modelo cinético de Avrami considera as variações possíveis de concentração inicial, tempo de adsorção bem como ordens cinéticas fracionárias, mantendo uma correlação entre dados experimentais e dados calculados.

As equações 10, 11 e 12 descrevem os modelos cinéticos citados e suas respectivas equações não linearizadas.

Pseudo primeira ordem	$\frac{dq}{dt} = k_f \cdot (q_e - q_t)$	$q_t = q_e \cdot \left[1 - \exp\left(-k_f \cdot t\right)\right]$ (equação não linear)	(10)
Pseudo-segunda ordem	$\frac{dq_t}{dt} = k_s \cdot (q_e - q_t)^2$	$q_t = \frac{k_s \cdot q_e^2 \cdot t}{1 + q_e \cdot k_s \cdot t}$ (equação não linear)	(11)
Avrami		$q_t = q_e \cdot \left\{1 - \exp\left[-\left(k_{AV} \cdot t\right)\right]^n\right\}$	(12)

onde o q_t é a quantidade de adsorção fixada no tempo t ($mg.g^{-1}$), q_e é a capacidade de adsorção no equilíbrio ($mg.g^{-1}$), k_f é a constante da taxa pseudo-primeira-ordem (min^{-1}), k_s é a constante da taxa pseudo-segunda-ordem ($g\ mg^{-1}\ min^{-1}$), k_{AV} é a constante de Avrami cinética (min^{-1}), e n é a ordem de adsorção fracionária, que está relacionada com o mecanismo de adsorção, t é tempo de contato adsorvente/adsorvato em minutos.

3.3 CARVÃO ATIVADO

O carvão ativado é um material carbonáceo, poroso de alta área superficial, constituído majoritariamente por carbono (Hung *et al.,* 2006). O carvão ativado é registrado sob o número CAS 7440-44-0.

Diferentes estudos na última década vêm apontando o carvão ativado como o material adsorvente que apresenta propriedades texturais com maior potencialidade para coletar seletivamente gases, líquidos ou impurezas no interior dos seus poros (RAND; APPLEYARD; YARDIM, 2012;). O que os qualifica com um excelente poder de clarificação, desodorização e purificação de líquidos ou gases (Gupta *et al*., 2009; Bergman e Machado, 2015; Yang, 2015).

Os carvões ativados podem ser preparados a partir de precursores de origem vegetal, animal e sintética, (Yang, 2015; Thue *et al.* 2019).

MENÉNDEZ-DÍAZ e MARTÍN-GULLÓN (2006) enfatizam que os materiais denominados carbonáceos têm como característica serem encontrado majoritariamente em três formas alotrópicas: diamante, grafeno e fulereno, bem como é o tipo de hibridização dos átomos de carbono que favorecem a formação das formas alotrópicas. Rand; Appleyard; Yardim (2012) realçam que, em escala atômica, a

maioria dos carbonos exibe a forma alotrópica do grafite, ou seja, uma estrutura baseada em hibridização sp^2 (estrutura 2D). A estrutura de um carvão ativo é formada por camadas de átomos de carbono dispostas de forma desordenada, mas com certo paralelismo, conforme ilustrado Figura 4.

Figura 4- Arranjo hexagonal Grafeno e o carvão ativado como rede defeituosa do grafeno e sua microestrutura porosa

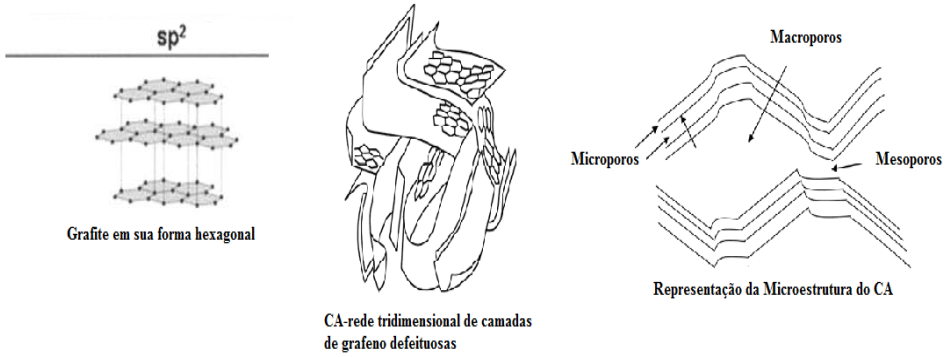

Fonte: adaptado de *Mendndez- Gullon (2006)*

A escolha do material precursor do carvão ativado pode evidenciar a presença ou ausência de grupos de superfície, formados por heteroátomos, que podem se ligar aos átomos de carbono nas extremidades e dão origem a carvões com propriedades químicas diferentes. Os heteroátomos frequentemente presentes na estrutura do carvão ativado são: oxigênio, nitrogênio e enxofre (ÇEÇEN E AKTAS , 2011). A quantidade e as formas químicas desses heteroátomos dependem da origem do carbono, das etapas de sua preparação e condições de tratamento (HUNG *et al.,*2006; LÁSZLÓ, 2006).

A ativação do carvão pode ser realizada via duas rotas, ativação física e ativação química, em ambas as rotas calor é transferido para o precursor carbonáceo. O tratamento térmico, bem como as técnicas de impregnação ou dopagem, são frequentemente usadas para melhorar o desempenho de carbonos porosos. Menéndez e Martín (2006); Çeçen e Aktas, (2011); Thue *et al.* (2022) sumarizam as etapas de ativação:

- Ativação física: Geralmente consiste em duas etapas consecutivas. O primeiro passo é a carbonização térmica da matéria-prima, onde ocorre a desvolatilização, realizada em temperaturas médias ou altas (450°C- 900°C),

para produzir um carvão rico em carbono. A segunda etapa é a ativação, onde o carvão restante é parcialmente gaseificado com um agente oxidante.

- Ativação Química: A matéria-prima carbonácea primeiramente é impregnada com um agente químico, a proporção e o tipo de reagente químico versus matéria-prima são objeto de muitos estudos. Sophia e Lima (2018); Thue *et al*. (2022) indicam que os agentes químicos mais utilizados são o KOH, $ZnCl_2$, $FeCl_3$, H_3PO_4, e, na sequência essa mistura é carbonizada em atmosfera inerte. O produto deve ser lavado para eliminar qualquer excesso de agente químico após a carbonização.

A eficácia dos carvões ativados como adsorventes para a variedade de poluentes está bem documentada. Ademais, é amplamente reconhecido para a remoção eficiente de compostos orgânicos, metais e outros poluentes inorgânicos.

A busca das pesquisas da atualidade está focada em ampliar os precursores com potencialidade para tornar-se carvões ativados (CUNHA *et al.* 2020; CIMIRRO *et al.* 2020, THUE *et al.,* 2021; WANG *et al.,* 2022), aumentar a eficiência da superfície de carvões já estabelecidos bem como propor metodologias que facilitem a separação do carvão após adsorção (SAUCIER *et al*., 2017; THUE *et al.,* 2022; UMPIERRES *et al.,* 2020; LIMA *et al.,* 2022).

As estratégias visam contribuir com uma crescente demanda, dados de mercado disponíveis na *Fortune Business insights* (2021) indicam que o mercado global de carvão ativado foi de US $2.96 bilhões em 2020 e está projetado para crescer US $4.50 bilhões até 2028.

3.3.1 Castanha do Pará e serragem do Sapelli como carvão ativado

Materiais residuais derivados de biomassa agrícola têm sido amplamente investigados como material adsorvente para remediação de águas residuais devido à sua relação custo-benefício, disponibilidade, composição química única e natureza renovável (CUNHA *et al.* 2020; CIMIRRO *et al.* 2020, THUE *et al.,* 2021; WANG *et al.,* 2022).

O carvão ativado produzido a partir de biomassa de resíduos agrícolas possui baixo teor de cinzas e dureza razoável (BAGOTIA *et al*., 2021), portanto, a conversão de resíduos agrícolas em adsorventes de baixo custo é uma alternativa promissora para solucionar problemas ambientais e também reduzir os custos de preparação. O

potencial dos resíduos agroindústrias como carvão ativado está associado com sua constituição lignocelulosica (OKOLIE *et al*., 2021).

- A Castanha do Pará/Brasil (*Bertholletia excelsa*) ocorre nas florestas da Bacia Amazônica, principalmente no Brasil, Venezuela, Colômbia, Bolívia e Peru. A Figura 5 mostra como a castanha do Pará é encontrada na natureza, onde a parte comestível da castanha do Brasil é o endosperma de suas sementes. Cada semente é protegida por uma casca dura (tegumento). Todas as sementes são envoltas por um pericarpo globular lenhoso seco muito duro (TORRES *et al*., 2021; JANNAT *et al*., 2021).

Figura 5- Apresentação da Castanha do Pará

Fonte:Emprapa

Apenas a parte comestível (sementes) é comercializada no mercado, tanto a casca da semente quanto o pericarpo são considerados resíduos (TORRES *et al*., 2021).

A composição química, rica nas frações lignocelulósicas, da Castanha do Pará segundo estudos de Leandro *et al*. (2019) e Petrechen, Arduin, Ambrósio (2019) é o que tornam os resíduos da castanha adequados para o desenvolvimento de carbono ativado de alta qualidade

Dados do IBGE indicam que o Estado do Amazonas é o maior produtor e que no ano de 2020 o País produziu mais de 33 mil toneladas de castanha onde cerca de 80% em peso da produção é de casca e demais resíduos, Souza (2019) indica que majoritariamente esses resíduos sólidos são utilizados como combustível.

- O Sapelli (*Entandrophragma cylindricum)* é uma madeira de cor vermelha e altamente exigida por sua durabilidade, originária da África e encontrada principalmente em Camarões, Costa do Marfim e Congo. Tem como característica ser uma madeira muito forte e, portanto, amplamente utilizada para vários fins e em

particular na fabricação de pequenas pontes. Esta madeira é composta por 98% de componentes vegetais como celulose, hemicelulose, lignina e pectina. Estudos de Thue *et al.* (2016; 2017) indicam que a análise elementar dessa madeira evidencia que 46.16% de sua constituição é carbono e 37 % é oxigênio. Os principais resíduos de processamento de madeira são as lascas e serragem de biomassa, (THUE *et al*., 2017).

3.3.2 Biocarbono ativado magnético

O aumento crescente dos custos de diferentes processos de tratamento de águas e/ou gases que utilizam carvões ativados associados às dificuldades operacionais de recuperação e a reutilização desses materiais em grande escala tem estimulado a pesquisa por novos protocolos e métodos de preparação desses materiais (RAND; APPLEYARD; YARDIM, 2012; CRINI *et al.,* 2020).

Os materiais com características adsorventes e magnéticas têm sido uma alternativa buscada pelos pesquisadores para agregar valor a esses carvões (WAN; BI; SUN, 2016; CAZETA *et al.,* 2016; WANG *et al.* 2020; SAUCIER *et al.*, 2017).

As pesquisas indicam que em comparação com os carvões convencionais, os biocarbonos com propriedades magnéticas geralmente são mais adequados para aplicações de adsorção, pois permitem que sejam facilmente removidos, com aplicação de um campo magnético de baixa intensidade, das soluções juntamente com os poluentes que absorveram.

A busca por inovações relacionando os termos "*magnetic activated biochar*" no S*pacenet* indicou o registro de 499 patentes sendo que mais de 50% dessas inovações foram registradas nos últimos 5 anos (2017-2022), evidenciando a crescente demanda por metodologias de produção desses carvões. A Tabela 2 indica algumas dessas inovações.

Tabela 2- Recorte patentes sobre carvões magnéticos

Registro	Nome da invenção	Ano da invenção
CN113332955A	Magnetic activated carbon as well as preparation method, regeneration method and application thereof	2021

CN108479703A	Preparation method of magnetic activated carbon for efficiently removing 17beta-estradiol in water	2018
CN107774232A	A kind of magnetic active carbon mixture of the ball containing charcoal and preparation method thereof	2017
EP3290109A1	Magnetised Activated Carbon and Method For Its Preparation	2016
JP2017217622A	Production Method of Magnetic Carbonized Product And Sludge Carbonization Apparatus	2017
BR102018068130-3 A2	Carvão Ativado Adsorvente e de Alta Magnetização, Processo de Obtenção e Uso do Carvão Ativado Adsorvente e de Alta Magnetização.	2020
BR102019018546-5 A2	Carvão Ativado Magnético, Processo de Obtenção De Carvão Ativado Magnético e Usos de Carvão Ativado Magnético.	2021

Fonte: autora 2022

Embora prevaleça a denominação de carvão ativado magnético, segundo Lima *et al.* (2022) o termo mais adequado seria biocarbono ativado magnético ou compósitos de carbono magnético. O carvão ativado tem como característica o baixíssimo teor de cinzas (<5%) e se ele for magnético esse teor de cinzas será entre 20-50%. A cerca dessa nomenclatura, "*magnetic biochars*", o *Spacenet* identifica apenas 13 patentes depositadas, sendo que as últimas 10 inovações foram registradas entre 2018-2022.

As pesquisas citadas na Tabela 1 indicam que carvões ativados e com propriedades magnéticas são preparados principalmente via 3 rotas:

i) Co-precipitação do material magnético com carvão ativado;

ii) Impregnação do carvão ativado com um sal de ferro, cobalto ou níquel e posterior aquecimento em temperaturas mais altas formando o material magnético que é impregnado na matriz de carbono;

iii) Impregnação da biomassa com sal de ferro, cobalto ou níquel e posterior pirólise, onde a carbonização, ativação e magnetização ocorrem em uma única etapa.

Segundo Thue *et al.* (2020) e Saucier *et al*. (2017) um dos maiores desafios é produzir materiais que acumulem um elevado magnetismo em conjunto com uma alta área superficial assim como produzir um material com o menor número de etapas possíveis.

3.4 MODIFICAÇÃO SONOQUÍMICA DE MATERIAIS

A sonoquímica é um ramo da ciência na qual as moléculas sofrem uma reação química ou efeitos mecânicos devido à aplicação da radiação de ultrassom (20 kHz–10 MHz) (SUSLICK *et. al*., 1991).

Segundo os autores Mason e Peters (2002); Tao e Sun (2015), o ultrassom é transmitido através de ondas mecânicas acústicas, que necessitam de um meio para se propagarem, as quais possuem frequência acima de 20 kHz. Quando aplicadas em líquidos, as ondas de ultrassom consistem em uma sucessão cíclica de fases de expansão e compressão transmitidas por vibração mecânica (TANG 2003). Os ciclos de compressão exercem uma pressão positiva e juntam as moléculas do líquido, enquanto os ciclos de expansão (rarefação) exercem uma pressão negativa e separam as moléculas (VAJNHANDL E MARECHAL 2005).

Wu (2013) aponta que as ondas ultrassônicas são classificadas dependendo da sua frequência e intensidade. Alta frequência (2 a 20 MHz) e baixa intensidade (<1 Wcm^{-2}) compõem ultrassons de baixa energia, que não são destrutivos e podem ser empregada na área de alimentos, principalmente, em técnicas analíticas para promover informações sobre propriedades físico-químicas, composição, estrutura e estado físico de alimentos. Já o ultrassom de alta energia possui baixa frequência (20 a 100 kHz) e desenvolve níveis de intensidade mais altos (10 a 1000 Wcm^{-2}), com energia suficiente para romper ligações intermoleculares, capazes de modificar algumas propriedades físicas e favorecer reações químicas.

Yao (2016) e Wu (2013) enfatizam que se a intensidade do ultrassom for suficiente para superar a resistência à tração do meio, ocorre um ponto em que as forças intermoleculares não são capazes de manter a estrutura molecular unida, produzindo pequenas cavidades (microbolhas), esse fenômeno denomina-se cavitação acústica. A cavitação é o principal evento da sonoquímica e apresenta como fases a criação, crescimento e colapso violento de bolhas que se formam no líquido induzido pelas flutuações de pressão o qual o meio está exposto (GEDANKEN, 2004;

COLMENARES e CHATEL, 2017). A Figura 6 ilustra esse fenômeno, onde as zonas de compressão (maior pressão) são representadas visualmente por uma crista de onda e a rarefação (menor pressão) por um vale, bem como evidência que a alternância dessas ondas favorece com que uma bolha de gás presa em um líquido se expanda quando o líquido circundante experimenta pressão negativa da onda sonora.

Figura 6- Descrição esquemática do crescimento de uma bolha em um campo acústico

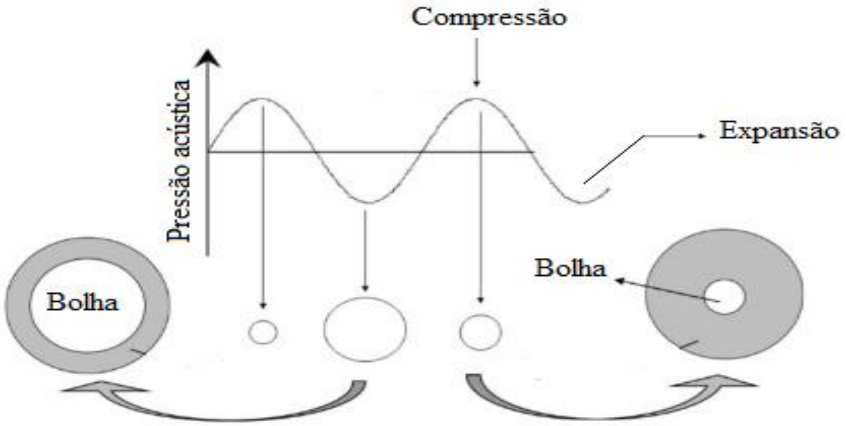

Fonte: Adaptado de Colmenares e Chatel, 2017.

As aplicações de ondas acústicas em diferentes processos da indústria têm sido amplamente pesquisadas, entre elas estão: ambientais e tecnologia de remediação (biológica e química) disponíveis em Goskonda; Catallo; Junk, (2002); Cao *et al.* (2020); De Andrade; Augusti; De Lima (2021); produção de nanomateriais, proposto por Gedanken (2004); Kamali *et al.* (2021); LI *et al.* (2021), extração aprimorada, cristalização e novos métodos em polímeros e eletroquímica, metodologias investigadas por Wen (2018); Kumar; Srivastav; Sharanagat (2021) e biotecnologia proposto por Hiremath *et al.* (2020).

Na engenharia de materiais, a área de partículas assistida por ultrassom (US) estudada por Zhang; He; Jing (2010); Chang *et al.* (2017); Li *et al.* (2021) entre outros, está sendo explorada para produzir partículas com tamanho, cristalinidade, morfologia e propriedades de superfície alteradas, considerando que em um sistema sólido-líquido heterogêneo, o colapso da bolha de cavitação terá efeitos mecânicos significativos. Segundo Mason e Peters (2002); Acisli *et al.*(2016) quando os líquidos que contêm sólidos são irradiados com ultrassom, a cavitação ocorre perto de uma superfície sólida, o colapso da bolha não é esférico e ocorrem jatos de alta velocidade

de líquido na superfície. Estes jatos e ondas de choque associadas podem causar modificações superficiais substanciais e expor superfícies, pois a irradiação ultrassônica das suspensões de líquido-pó acarreta em colisões entre partículas em alta velocidade e assim as colisões resultantes são capazes de induzir mudanças na morfologia superficial, na composição e na reatividade do material.

4 RESULTADOS

As metodologias, resultados e discussões deste trabalho estão apresentados na forma de três artigos, publicados nas revistas *Environmental Science and Pollution Research; Colloids and Surfaces A: Physicochemical and Engineering Aspects e Journal of Environmental Chemical Engineerin*g, publicados entre os anos 2019 e 2021.

4.1 ARTIGO 1

LIMA, DIANA RAMOS; Lima, Eder C.; Umpierres, Cibele S.; Thue, Pascal Silas; El-Chaghaby, Ghadir A.; Da Silva, Raphaelle Sanches; Pavan, Flavio A.; Dias, Silvio L. P.; Biron, Camille. Removal of Amoxicillin From Simulated Hospital Effluents By Adsorption Using Activated Carbons Prepared From Capsules Of Cashew Of Para. **Environmental Science And Pollution Research**.V.26, P.1 - 13, 2019.

4.2 ARTIGO 2

LIMA, DIANA R.; Hosseini-Bandegharaei, Ahmad; Thue, Pascal S; Lima, Eder C.; De Albuquerque, Ytallo R.T.; Dos Reis, Glaydson S.; Umpierres, Cibele S.; Dias, Silvio L.P.; Tran, Hai Nguyen. Efficient Acetaminophen Removal From Water And Hospital Effluents Treatment By Activated Carbons Derived From Brazil Nutshells. **Colloids and Surfaces A-Physicochemical and Engineering Aspects**. V.583, P.123966 , 2019.

4.3 ARTIGO 3

LIMA, DIANA R.; Lima, Eder C.; Thue, Pascal S.; Dias, Silvio L.P.; Machado, Fernando M.; Seliem, Moaaz K.; Sher, Farooq; Dos Reis, Glaydson S.; Saeb, Mohammad Reza; Rinklebe, Jörg. Comparison of Acidic Leaching Using a Conventional and Ultrasound-Assisted Method for Preparation of Magnetic-Activated Biochar. **Journal Of Environmental Chemical Engineering**.V.9, P.105865, 2021.

Os artigos estão estruturados de acordo com a formatação do periódico o qual foi submetido.

Environmental Science and Pollution Research (2019) 26:16396–16408
https://doi.org/10.1007/s11356-019-04994-6

RESEARCH ARTICLE

Removal of amoxicillin from simulated hospital effluents by adsorption using activated carbons prepared from capsules of cashew of Para

Diana Ramos Lima[1] · Eder C. Lima[1,2,3] · Cibele S. Umpierres[3] · Pascal Silas Thue[3] · Ghadir A. El-Chaghaby[4] · Raphaelle Sanches da Silva[2] · Flavio A. Pavan[5] · Silvio L. P. Dias[2,3] · Camille Biron[1]

Received: 25 January 2019 / Accepted: 26 March 2019 / Published online: 13 April 2019

Abstract

High-surface-area activated carbons were prepared from an agroindustrial residue, *Bertholletia excelsa* capsules known as capsules of Para cashew (CCP), that were utilized for removing amoxicillin from aqueous effluents. The activated carbons were prepared with the proportion of CCP:$ZnCl_2$ 1:1, and this mixture was pyrolyzed at 600 (CCP-600) and 700 °C (CCP700). The CCP.600 and CCP.700 were characterized by CHN/O elemental analysis, the hydrophobic/hydrophilic ratio, FTIR, TGA, Boehm titration, total pore volume, and surface area. These analyses show that the adsorbents have different polar groups, which confers a hydrophilic surface. The adsorbents presented surface area and total pore volume of 1457 $m^2\ g^{-1}$ and 0.275 $cm^3\ g^{-1}$ (CCP.600) and 1419 $m^2\ g^{-1}$ and 0.285 $cm^3\ g^{-1}$ (CCP.700). The chemical and physical properties of the adsorbents were very close, indicating that the pyrolysis temperature of 600 and 700 °C does not bring relevant differences in the physical and chemical properties of these adsorbents. The adsorption data of kinetics and equilibrium were successfully adjusted to Avrami fractional-order and Liu isotherm model. The use of the adsorbents for treatment of simulated hospital effluents, containing different organic and inorganic compounds, showed excellent removals (up to 98.04% for CCP.600 and 98.60% CCP.700).

Keywords Adsorption · *Bertholletia excelsa* capsules · Activated carbon · Amoxicillin, emerging contaminant

Introduction

The release of pharmaceuticals to natural waters is one of the significant environmental concerns in the last days (Sophia et al. 2016; Sophia and Lima 2018), because these compounds could threaten the water resources (Abazari et al. 2019). These releases come from the pharmaceutical industries, excretions of humans and livestock animals, and also hospital effluents (Sophia et al. 2016; Abazari et al. 2019). Among the pharmaceuticals, the antibiotic class is used with high frequency, and they could generate microbial resistance even in small amounts found in the waters (Bondarczuk and Piotrowska-Seget 2019; Qiu et al. 2019).

The municipal wastewater treatment plants are not always able to remove antibiotics and other emerging contaminants (Krzeminski et al. 2019) altogether. In this way, tertiary water treatments methods are required (McConnell et al. 2018; Le et al. 2018; Moreira et al. 2015). The methods for treatment of water contaminated with antibiotics are removed by using membrane bioreactor systems (Le et al. 2018), photocatalytic methods (Moreira et al. 2015; Li and Shi 2016; Lu et al. 2019),

Responsible editor: Tito Roberto Cadaval Jr

Electronic supplementary material The online version of this article (https://doi.org/10.1007/s11356-019-04994-6) contains supplementary material, which is available to authorized users.

✉ Eder C. Lima
eder.lima@ufrgs.br

[1] Graduate program in Metallurgical, Mine and Materials Engineering (PPGE3M). School of Engineering, Federal University of Rio Grande do Sul (UFRGS), Av. Bento Gonçalves, Porto Alegre, RS 9500, Brazil

[2] Institute of Chemistry, Federal University of Rio Grande do Sul (UFRGS), Av. Bento Gonçalves 9500, P.O. Box 15003, Porto Alegre, RS 91501-970, Brazil

[3] Graduate program in Science of Materials (PGCIMAT). Institute of Chemistry, Federal University of Rio Grande do Sul (UFRGS), Av. Bento Gonçalves, Porto Alegre, RS 9500, Brazil

[4] RCFF-Agricultural Research Center, Giza, Egypt

[5] Federal University of Pampa (UNIPAMPA), Bagé, RS, Brazil

catalytic ozonation (Moreira et al. 2015; Lu et al. 2019), plasma reactors (Tang et al. 2018), combined process of activated sludge followed by ozonization (Wang et al. 2018), and adsorption (Li et al. 2017; Takdastan et al. 2016; Saucier et al. 2017). Among all of these treatment methods for removal of antibiotics from aqueous effluents, the adsorption method is one of the preferable methods because of its simplicity of operation, low-initial implementation costs, and high efficiency for removal of pharmaceuticals from aqueous effluents (Babaei et al. 2016; Cunha et al. 2018; Kasperiski et al. 2018; Thue et al. 2017a).

Activated carbons are one of the most effective adsorbents for removal of pharmaceuticals from aqueous solution due to its textural properties (high surface area and pore volumes) (Thue et al. 2017a, b; Leite et al. 2017, 2018; Umpierres et al. 2018). Furthermore, activated carbons have excellent mechanical strength and thermal stability (Kasperiski et al. 2018; Cunha et al. 2018), which has the possibility of being used as adsorbent at high temperatures. The production of activated carbon needs carbon precursors that are usually the agricultural wastes, such as rice husk, peach stones, date palm, lotus stalk, rice straw, almond shell, macadamia nutshell, walnut shells, tea waste, sugar beet pulp, peanut hulls, woodchips, olive stones, and bamboo waste (Silva et al. 2018).

Amoxicillin is an antibiotic of in the beta-lactam family that is used to treat a wide variety of bacterial infections. This pharmaceutical is a penicillin-type antibiotic, whose action mechanism is stopping the growth of bacteria. It may be used for skin infections, pneumonia, strep throat, middle ear infection, urinary tract infections, and other uses. Amoxicillin is listed on the World Health Organization's List of Essential Medicines, as one of the most effective and safe medicines needed in a health system (Roy 2012; WHO 2015).

In this work, the *Bertholletia excelsa* capsules known as capsules of Para cashew (CCP) (or Brazil nut) was used as a carbon source for preparation of activated carbons. The CCP activated carbons were used for the removal of the amoxicillin from the aqueous effluent. Then, this work allies the necessity of removal of antibiotics from contaminated effluents and the need for the use of agricultural residue for preparation of activated carbons. Up to our best knowledge, this is the first report of the use of CCP as a precursor to prepare activated carbons.

The Brazil nut tree is the only species in the monotypic genus *Bertholletia*. It is an indigenous tree from Bolivia, Colombia, Guianas, Peru, Venezuela, and Brazil. It appears in vast forests on the margin of the Orinoco, Amazonas, Tapajós, and Negro rivers (Kosikova 2018). The fruit takes about 14 months for maturing, and it is a large woody capsule of 10–15 cm in diameter, seeming a coconut exocarp in size and weights up to 2 kg. It is a woody shell of 8–12-mm thick, which have from 8 to 24 triangular seeds presenting a size of 4–5 cm (the "Brazil nuts" or cashew of Pará) distributed, such as the buds of an orange. The weight of the woody capsule is about 10–15 times higher than the cashew. In 2014, the global production of cashew of Pará was 95,000 tons (Kosikova 2018). Considering the number of wastes generated, at least 950,000 tons of capsule is produced annually. This work adds value to the capsule of Para cashew (Brazil nut) producing efficient activated carbon that presents potentiality of being used for the treatment of hospital effluents.

Materials and methods

Preparation of the adsorbents

The activated carbons were prepared using 100.0 g of milled capsules of cashew of Pará (CCP) and mechanically mixed with 40-mL $ZnCl_2$ solution (containing 100-g $ZnCl_2$), forming a homogeneous paste material (Leite et al. 2017). This material was dried at 80 °C in a greenhouse for 2 h. Then the dried material was placed in a quartz reactor of a vertical convective furnace. The furnace was heated from 25 up to 600 °C (CCP.600) or 700 °C (CCP.700) under the N_2 flow (200 mL min^{-1}) at a rate of 10 °C min^{-1}. Afterward, the furnace was cooled-down, under an N_2 flow until the temperature attained values lower than 200 °C.

Subsequently, to extract zinc compounds from the pyrolyzed samples, they were refluxed with HCl solution (Thue et al. 2016).

Characterization of the adsorbents

The quantitative amounts of the total acidity and basicity groups of CCP.600 and CCP.700 were acquired by using a modified Boehm-titration procedure (Oickle et al. 2010; Goertzen et al. 2010). Fourier-transform infrared spectroscopy (FTIR) was performed using a Bruker FTIR spectrophotometer (Alpha model). This technique was used to obtain the qualitative identification of the functional groups present on the surface of the adsorbents. The FTIR spectra were obtained from 4000 to 400 cm^{-1} (resolution of 4 cm^{-1}; Prola et al. 2013).

The pH_{pzc} of the adsorbents were obtained according to the procedure previously described (Prola et al. 2013).

The hydrophobicity/hydrophilicity ratio (HI) was obtained as previously described (Kasperiski et al. 2018; Leite et al. 2017; Umpierres et al. 2018).

The N_2 adsorption and desorption isotherms were performed using a TriStar II 3020 Micrometrics instrument that was used to obtain the textural characterization of the CCP.600 and CCP.700 adsorbents. The solid samples were firstly dried for 12 h at 120 °C in an internal oven of the apparatus, and then the surface analyzer was run at − 196 °C for obtaining the N_2 isotherms of adsorption and desorption

(dos Reis et al. 2016a, b). The pore size distribution was calculated by the DFT method using the nitrogen adsorption branch (Jagiello and Thommes 2004). The surface areas were calculated using the BET method (Thommes et al. 2015). The textural surface of activated carbons was investigated by scanning electron microscopy (SEM) (Jeol, JSM-6610LV, Japan) (Souza et al. 2018).

Adsorption studies and evaluation of nonlinear models

Batch contact adsorption procedure was performed using amoxicillin as adsorbate and CCP.600 and CCP.700 as adsorbents.

Measurements of amoxicillin were performed in triplicate using standard conditions (Lima et al. 1998a, b, 1999, 2000, 2002).

The statistical evaluation of the nonlinear models was performed using $R^2_{adjusted}$, the standard deviation of the residues (SD), and the Bayesian information criterion (BIC) (Lima et al. 2015; Schwarz 1978). For further details, please see Supplementary material.

Kinetic of adsorption

Pseudo-first-order, pseudo-second-order, and Avrami fractional-order models were used to fit the kinetic data (for further details see Supplementary material; Lima et al. 2015).

Isotherms of adsorption

The Langmuir, Freundlich, and Liu isotherm modes were used for the equilibrium data. Further details are seen in Supplementary material (Lima et al. 2015).

Thermodynamics of adsorption

The thermodynamic data were evaluated using the correct thermodynamic equilibrium constant as earlier reported (Kasperiski et al. 2018; Lima et al. 2019). For further details, see Supplementary material.

Synthetic effluents

Two synthetic hospital effluents containing six pharmaceuticals, two sugars, four organic compounds, and eight inorganic salts typically found in hospital effluents were prepared (Table 1). The synthetic effluents were used to evaluate the performance of CCP.600 and CCP.700 as adsorbents for the treatment of effluents and evaluate the performance of the adsorbents for potential application in real situations.

Table 1 The chemical composition of the synthetic hospital effluents

Pharmaceuticals	Concentration (mg L^{-1})	
	Effluent 1	Effluent 2
Amoxicillin	30.0	60.0
Paracetamol	20.0	40.0
Sodium diclofenac	20.0	40.0
Tetracycline	20.0	40.0
Propranolol hydrochloride	20.0	40.0
Enalapril maleate	20.0	40.0
Sugars		
Glucose	30.0	50.0
Saccharose	30.0	50.0
Organics		
Humic acid	10.0	20.0
Sodium dodecyl sulphate	5.0	10.0
Citric acid	10.0	20.0
Urea	10.0	20.0
Inorganic components		
Sodium chloride	50.0	70.0
Sodium sulphate	10.0	20.0
Sodium carbonate	10.0	20.0
Ammonium phosphate	20.0	30.0
Ammonium chloride	20.0	30.0
Magnesium chloride	10.0	20.0
Potassium nitrate	10.0	20.0
Calcium nitrate	10.0	20.0
pH*	7.0	7.0

Results and discussion

Characterization of the activated carbons

The isotherm curves of adsorption/desorption of nitrogen for both CCP.600 and CCP.700 materials could be classified by IUPAC (Thommes et al. 2015) as isotherm of type I(b) (see Fig. 1). This type of isotherm is distinctive of microporous materials, with pore size having the width diameter ranging from 1 nm (microporous) to a broader scales of pores (up to 3 nm at mesopore scale). The pore size distribution of CCP.600 obtained by DFT method (Jagiello and Thommes 2004) presents a maximum peak at 1 nm, then a second peak around 1.25 nm, the third peak around 1.6–1.75 m, and a fourth broader peak 2.0–3.0 nm, showing that CCP.600 presents besides the fraction of micropores a small fraction of mesopores. The CCP.700 presents pores wider when compared with CCP.600 adsorbent, since it does not present pores around 1 nm or lower, presents a peak around 1.25 nm, another peak 1.6–1.75 nm, and a wider peak 2.0–3.0 nm. By this figure, it is possible to verify that the pore size distribution of CCP.700 material is slightly higher than CCP.600. This observation is confirmed in Table 2.

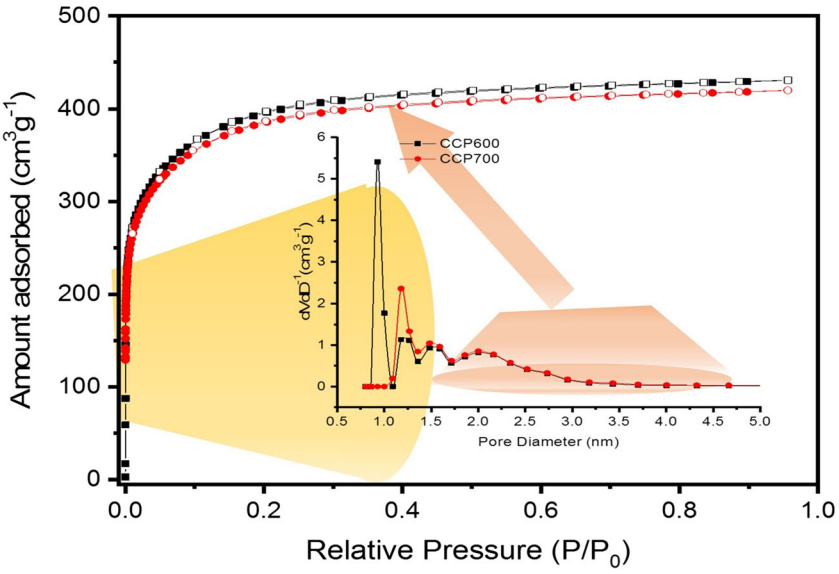

Fig. 1 The isotherms of nitrogen for CCP.600 and CCP.700. Inset pore size distributions for CCP.600 and CCP.700 samples

The total amount of N_2 adsorbed by CCP.600 and CCP.700 are 419.8 and 419.5 $cm^3\ g^{-1}$, respectively, again showing that both carbon materials present very similar textural properties. Indicating that the pyrolysis of capsules of cashew of Pará carried out at 600 and 700 °C does not bring relevant differences in the produced activated carbons. The BET surface area of CCP.600 is slightly higher than CCP.700 (2.7%). However, the BJH total pore volume of CCP.700 is 3.6% higher than CCP.600. Also, the mesopore volume of CCP.700 is 23.1% higher than CCP.600. Another feature is that the BJH desorption cumulative surface area of pores of CCP.700 is 5.4% higher than CCP.600.

Moreover, it was observed that both activated carbons presented $S_{BET} > 1400\ m^2\ g^{-1}$ and total pore volumes > 0.27 $cm^3\ g^{-1}$. The surface area and total pore volume of CCP.600 and CCP.700 adsorbents are higher than other activated carbons reported previously in the literature (Li et al. 2011; Khadhri et al. 2019; Suo et al. 2019; Hoppen et al. 2019; Puchana-Rosero et al. 2016; Zhu et al. 2018).

Based on the results of Fig. 1 and Table 2, it could be cited that both activated carbon materials are predominantly microporous materials, and the surface area of CCP.600 is slightly higher than CCP.700. However, the pore volume of CCP.700 is slightly higher than CCP.600. However, these differences are not remarkable, since the percentual differences obtained by these textural characteristics are within the experimental error of the nitrogen adsorption-desorption curves, and therefore it is not expected that these materials will present relevant differences as an adsorbent for removal of pharmaceuticals from aqueous solutions. This statement will be confirmed in the application of these activated carbons shown in the next sections.

The functional groups present on CCP.600 and CCP.700 were identified using FTIR analysis. These results are essential to identify potential functional groups present on the activated carbon that could affect the adsorption of amoxicillin. The FTIR spectra of CCP.600 and CCP.700 are shown in Fig. 2. It is important to highlight that both activate carbons presented a very similar FTIR spectra (see Fig. 2). Following the dashed lines, the differences in the bands are about ≤ 4 cm^{-1} that are within the error of these analyses.

The broadband at 3340 cm^{-1} is attributed to O—H stretch of hydroxyl groups (Leite et al. 2017; Prola et al. 2013). The two peaks at 2918 (asymmetric) and 2852 cm^{-1} (symmetric) are attributed to C—H stretch (Prola et al. 2013). The bands at 1628 cm^{-1} were attributed to the O=C stretch of carboxylic acids (dos Reis et al. 2016a). The small bands at 1425 cm^{-1} are attributed to ring modes of aromatics (Kasperiski et al. 2018; Prola et al. 2013). The vibrational bands at 1375 and 1319 cm^{-1} are attributed to the bending of C—H bonds or C—N stretch of amines or amides (Kasperiski et al. 2018; Cunha et al. 2018). The bands at 1109 and 1057 cm^{-1} are attributed to C—O stretch (Kasperiski et al. 2018). The vibrational bands at 804 cm^{-1} can be attributed to out of plane C—H bends (Prola et al. 2013).

Table 2 The textural properties of the activated carbons

Sample	BET surface area ($m^2\ g^{-1}$)	BJH total pore volume ($cm^3\ g^{-1}$)	Mesopore volume ($cm^3\ g^{-1}$)	BJH desorption cumulative surface area of pores ($m^2\ g^{-1}$)
CCP.600	1457 ± 10	0.275 ± 0.001	0.078 ± 0.001	463
CCP.700	1419 ± 10	0.285 ± 0.001	0.096 ± 0.001	488

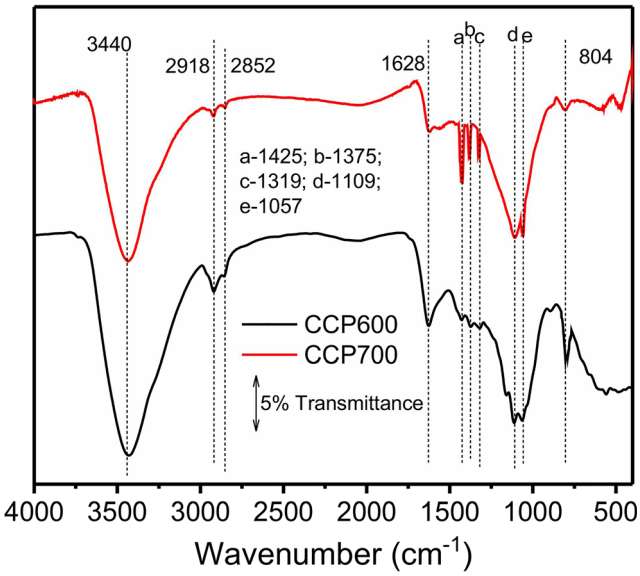

Fig. 2 FTIR spectra of CCP.600 and CCP.700 activated carbons

FTIR spectra provide qualitative information about the functional groups present on the carbon adsorbents. On the other hand, the Boehm titration provides quantitative information (mmol g^{-1}) of the acidic and basic groups present on the surface of the solid sample (Oickle et al. 2010; Goertzen et al. 2010). The total acidity and basicity of the CCP.600 and CCP.700 were measured (see Table 3). The CCP.600 adsorbent presents a small amount of total acidic groups (3.01%) higher than CCP.700; on the other hand, the total basicity of CCP.700 is also slightly higher (1.34%) than CCP.600.

The total ratio acidity divided by total basicity of CCP.600 and CCP.700 was 1.591 and 1.524, respectively, indicating that CCP.600 presents a more acidic surface than CCP.700. These results are confirmed by the pH_{pzc} of the adsorbents, where CCP.600 and CCP.700 presented the values of 6.46 and 6.90, respectively (see Table 3 and Supplementary Fig. 2).

The sum of the number of acid groups plus basic groups of CCP.600 and CCP.700 was 0.5734 and 0.5661 mmol g^{-1}, respectively. These values are in agreement with the hydrophobic-hydrophilic balance (HI) values of both activated carbons, as early observed (Kasperiski et al. 2018; Leite et al. 2018; Thue et al. 2017b). HI is the quantity of *n*-heptane vapors uptake by the solid surface divided by the water vapors adsorbed by the solid surface (dos Reis et al. 2016b; Umpierres et al. 2018). The HI of CCP.600 and CCP.700 was 0.8151 and 0.9395, respectively (see Table 3). Therefore, CCP.600 is more hydrophilic than CCP.700. The activated carbons with a higher amount of functional polar groups (acidic and basic) generate a surface that has higher affinity to water (dos Reis et al. 2016b; Leite et al. 2018).

Although there are differences of polarity in the surface of CCP.600 and CCP.700, both activated carbons are hydrophilic, because the HI ratio obtained was lower 1 (see Table 3). In order to have a scale of comparison of HI values, at the author's laboratory, nanoparticles of TiO_2 were prepared, which were functionalized with trimethoxy propyl silane that are known by its superhydrophobic characteristics (Ramanathan and Weibel 2012). These materials presented HI values higher than 36. Also, in previous studies reported in the literature (dos Reis et al. 2016b), nanocomposites of polysiloxane and sewage sludge pyrolyzed presented HI values ranging from 3 to 12. Based on these values, it is possible to state that CCP.600 and CCP.700 present hydrophilic characteristics, and CCP.600 is more hydrophilic than CCP.700.

The thermogravimetric curves of CCP.600 and CCP.700 activated carbons were obtained under a nitrogen atmosphere from room temperature until 800 °C and under synthetic air from 800 up to 1000 °C using a rate of 10 °C min^{-1} (see Fig. 3). The use of an oxidizing atmosphere for temperatures higher than 800 °C is to acquire the ash contents of the samples in the TGA analysis (Cunha et al. 2018). Moreover, the pyrolysis of activated carbon can be explored up to 800 °C , because N_2 is used as purge gas (room temperature up to 800 °C).

Figure 3a, b presented the TGA curves of the CCP.600 and CCP.700 activated carbons, respectively. The thermal behavior of CCP.600 is approximately the same as CCP.700. Five weight losses were observed in Fig. 3a, and four weight losses were observed in Fig. 3b. The difference is that CCP.600 presents more moisture than CCP.700. For CCP.600, there is a weight loss of 11.90% from 17.8 to 81.0 °C corresponding to the loss of adsorbed water that it is not observed in CCP.700. On the other hand, both activated carbons were thermally stable up to 516.4 (CCP.600) and 555.2 °C (CCP.700). This loss from 22.6 to 555.2 °C (CCP.700) and 81 to 516.4 °C (CCP.600) corresponds to a loss of any water present in the interstitials of the activated carbons (Cunha et al. 2018; Leite

Table 3 The elemental analysis and chemical surface properties of activated carbons

Sample	C (%)	H (%)	N (%)	Ashes(%)[a]	O(%)[b]	pH_{pzc}	Total acidity (mmol g^{-1})	Total basicity (mmol g^{-1})	HI[C]
CCP.600	77.10	2.99	1.38	0.28	18.25	6.46	0.3520	0.2213	0.8151
CCP.700	79.56	1.25	1.55	0.58	17.06	6.90	0.3418	0.2243	0.9395

[a] Obtained by TGA using synthetic air from 800 to 1000 °C

[b] Obtained by %O = 100% − (%C + %H + %N + %ashes)

[c] HI—the amount of adsorbed of vapor of n-heptane (mg g^{-1}) divided by amount adsorbed of vapor water (mg g^{-1})

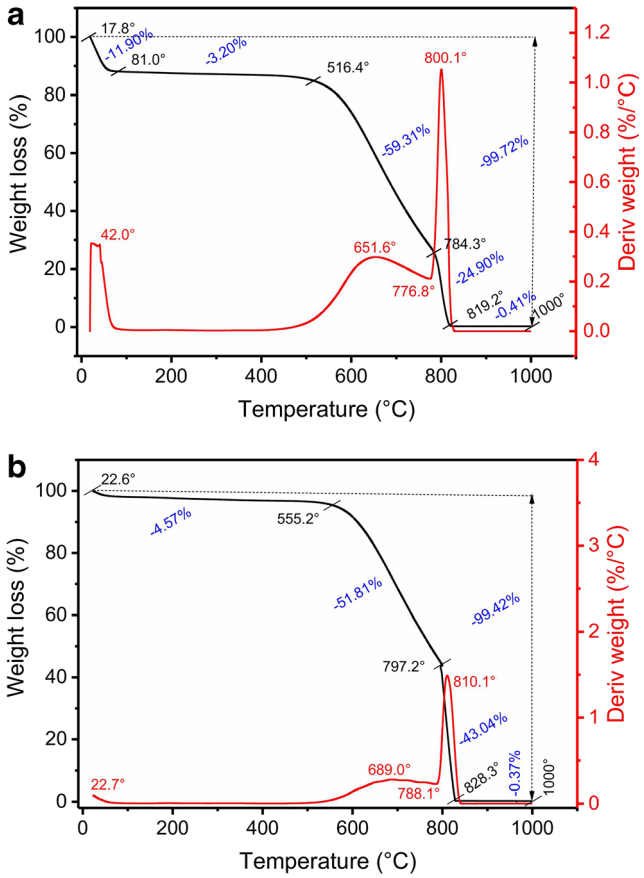

Fig. 3 Thermogravimetric curves (TA) and differential thermal curves (DTA) for **a** CCP.600 and **b** CCP.700

et al. 2017). The third stage (CCP.600) and second (CCP.700) stage presented the highest loss of mass, and temperature ranges from 516.4 to 784.3 °C (CCP.600) and 555.2 to 797.2 °C (CCP700) were observed; this stage is ascribed to the decomposition of the carbonaceous matrix of the samples. The weight loss would remain practically constant if the atmosphere of N_2 was continued up to 1000 °C. However, at 800 °C, the flow of gas was changed from N_2 to synthetic air to oxidize the carbonaceous matrix entirely in the presence of air. Therefore, the content of ashes could be obtained by using a TGA analysis using two atmospheres (inert and oxidizing) during a run. The total weight loss of CCP.600 and CCP.700 was 99.72 and 99.42%, respectively (see Fig. 3), indicating that the ash contents of the activated carbons were 0.28 (CCP.600) and 0.58% (CCP.700).

Elemental analysis (C H N/O) for CCP.600 and CCP.700 is given in Table 3. The CCP.600 and CCP.700 present high carbon percentage that justifies the use of capsules of Para cashew (*B. excelsa* capsules) as a carbon source for production of activated carbons. The percentage of nitrogen agreed with the total basicity of the samples, and the oxygen content is also compatible with the total acidity of the samples.

The textural surface of CCP.600 and CCP.700 was investigated by SEM (see Fig. 4). The particles of both activated carbons are irregular pieces of carbon, with the high extension of rugosity and several holes on its surface that allows the passage of solvent during the adsorption process. By these images, it could be seen that the textural surface of both carbon materials is not entirely different; the fact that explains that both activated carbons present similar behavior as an adsorbent.

After performing the characterization of CCP.600 and CCP.700 (the results of Tables 2 and 3 and Figs. 1 to 3), it is possible to make the statement that both activated carbons present similar surface area and pore volume (Fig. 1, Table 2); same functional groups (Fig. 2); close amount of acidic and basic groups (Table 3); close hydrophobicity/hydrophilicity behavior (Table 3); close pHpzc (Table 3, Supplementary Fig. 2); close thermal stability; and close contents of ashes (Fig. 3, Table 3). Therefore, although some differences in sorption capacity could present CCP.600 and CCP.700, these differences will not be so significant. Therefore, utilizing a proportion of $ZnCl_2$:CCP of 1:1, the temperature of pyrolysis does not provoke remarkable differences on the physical and chemical properties of the obtained activated carbons, and therefore, remarkable differences of these materials are not expected as an adsorbent for removal of pharmaceuticals from aqueous solutions. The next sections will prove this statement.

Adsorption kinetics

One of the criteria of adsorption efficiency is the rate of adsorption. The knowledge of the kinetics of adsorption helps to establish the mechanism of adsorption (Lima et al. 2015).

Hereto, the kinetic of adsorption data of amoxicillin on CCP.600 and CCP.700 was fitted by nonlinear models of Avrami-fractional model, pseudo-first-order, and pseudo-second-order kinetic models. The kinetic curves and the values of the parameters of these equations are shown in Fig. 5 and Table 4.

The fitting of the models was statistically evaluated by the adjusted determination coefficient (R^2_{Adj}), as well as by the root of mean square error (SD) (Cunha et al. 2018; Leite et al. 2017). Ideally, for any fitting of an adsorption model, the R^2_{Adj} values should be closer to 1.00, and the SD values should be the lowest possible values. In this situation, the experimental and theoretical values of sorption capacity (q) present practically the same value. Therefore, based on these statistical parameters, the Avrami-fractional kinetic of adsorption model was the model that was better fitted by the experimental data, to describe the kinetics of adsorption of amoxicillin on the CCP.600 and CCP.700 adsorbents (Table 4). The R^2_{Adj} values of the Avrami fractional-order kinetic model were the closest to 1.000 (0.9997 to 0.9999), and its SD values were the minimum values (0.7516 to 1.217 mg g^{-1}) of all the tested kinetic models used for both activated carbons (Table 4). Therefore,

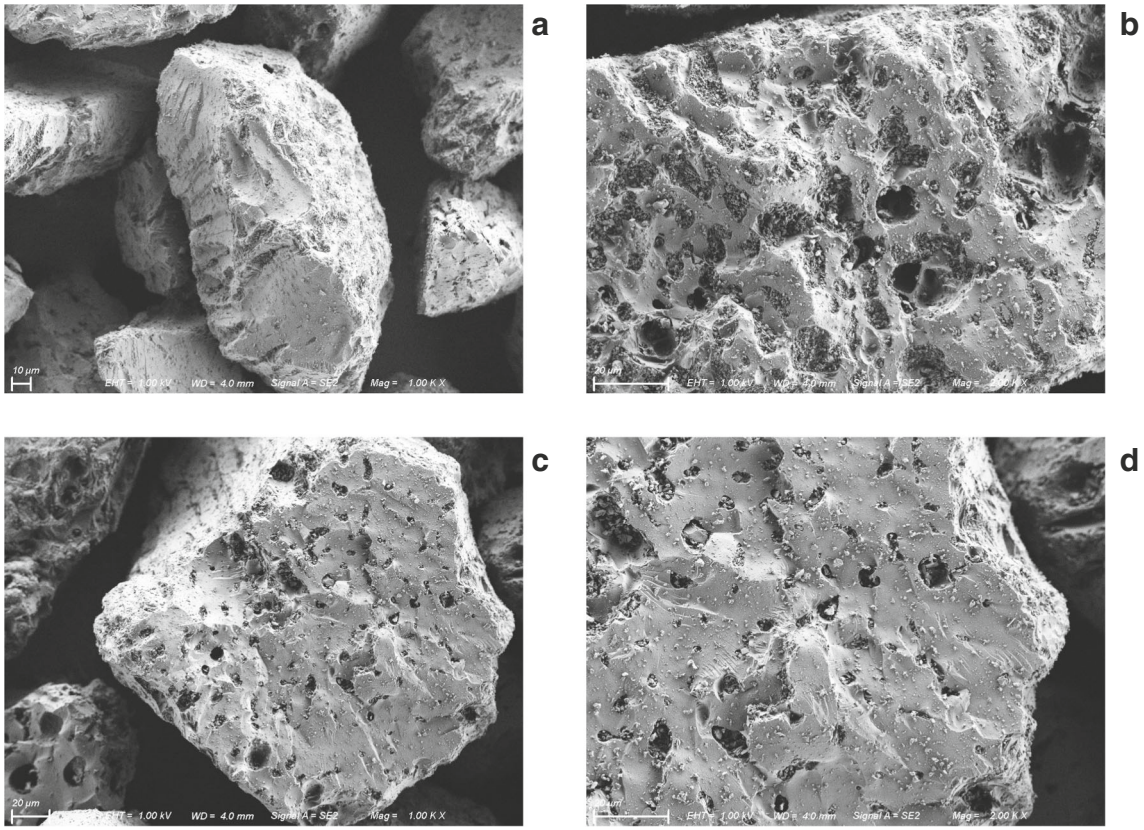

Fig. 4 SEM images of CCP.600 and magnification of ×1000 (**a**); CCP.600 and magnification of ×2000 (**b**); CCP.700 and magnification of ×1000 (**c**); and CCP.700 and magnification of ×2000 (**d**)

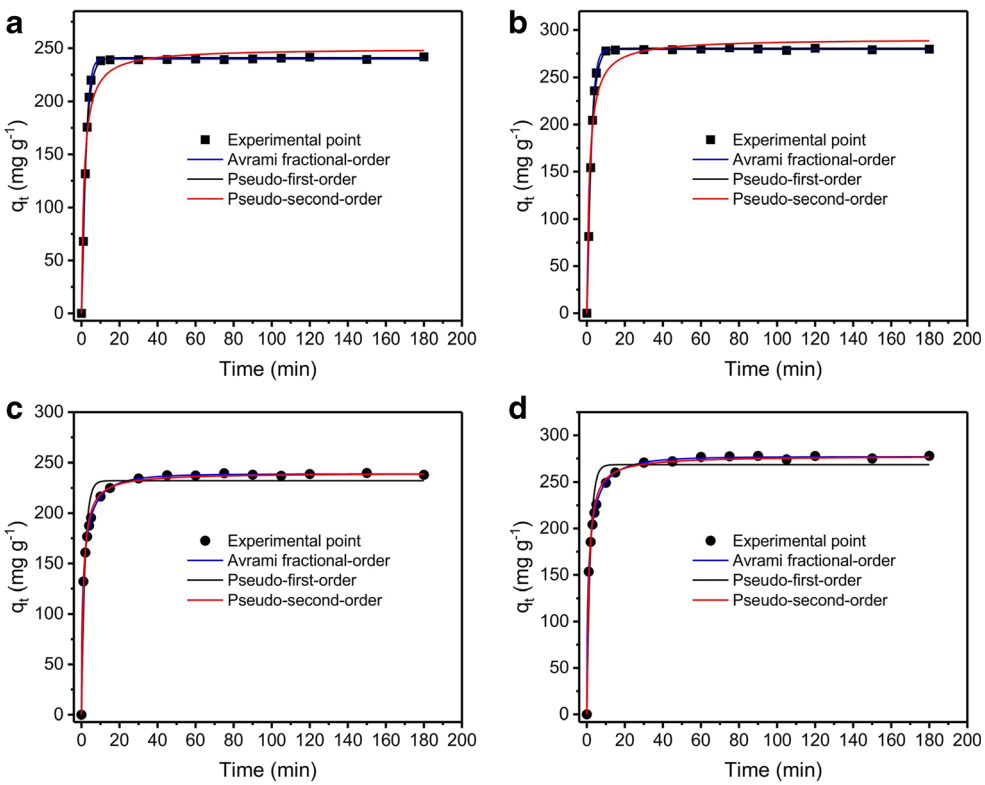

Fig. 5 Kinetic adsorption curves of amoxicillin onto activated carbon. **a** C_o 400.0-mg L^{-1} amoxicillin onto CCP.600; **b** C_o 600.0-mg L^{-1} amoxicillin onto CCP600; **c** C_o 400.0-mg L^{-1} amoxicillin onto CCP700; and **d** C_o 600.0-mg L^{-1} amoxicillin onto CCP700. The pH was fixed at 7.0, the adsorbent dosage of 1.5 g L^{-1}, and the temperature of 25 °C

Table 4 The kinetic parameters of adsorption of amoxicillin onto CCP.600 and CCP.700 adsorbents. Conditions initial pH of pharmaceutical solution 7.0, initial concentrations of 400.0 and 600.0 mg L^{-1}, and an adsorbent dosage of 1.5 g L^{-1}. All values of parameters are expressed with four significant digits

	CCP.600		CCP.700	
C_0 (mg L^{-1})	400.0	600.0	400.0	600.0
Avami fractional-order				
q_e (mg g^{-1})	239.9	279.5	238.9	276.9
k_{AV} (min^{-1})	0.4162	0.4166	0.6299	0.6286
n_{AV}	1.250	1.212	0.467	0.4575
$t_{1/2}$ (min)	1.792	1.774	0.725	0.7140
$t_{0.95}$ (min)	5.778	5.938	16.61	17.51
R^2 adjusted	0.9998	0.9999	0.9999	0.9997
SD (mg g^{-1})	0.8917	0.7516	0.7130	1.217
BIC	4.134	− 1.674	− 3.467	14.71
Pseudo-first order				
q_e (mg g^{-1})	240.9	280.6	232.2	268.7
k_1 (min^{-1})	0.4195	0.4195	0.5549	0.5537
$t_{1/2}$ (min)	1.652	1.652	1.249	1.252
$t_{0.95}$ (min)	7.140	7.142	5.399	5.411
R^2_{adj}	0.9946	0.9961	0.9521	0.9500
SD (mg g^{-1})	5.198	5.165	13.47	15.94
BIC	62.41	62.20	94.80	100.5
Pseudo-second order				
q_e (mg g^{-1})	249.8	290.8	240.0	277.9
k_2 (g mg^{-1} min^{-1})	0.002813	0.002426	0.004281	0.003677
$t_{1/2}$(min)	1.423	1.418	0.9732	0.9786
$t_{0.95}$ (min)	27.04	26.93	18.49	18.59
R^2_{adj}	0.9566	0.9596	0.9961	0.9956
SD (mg g^{-1})	14.77	16.54	3.827	4.741
BIC	97.93	101.8	52.00	59.28

sorption capacities at any time ($q_{t\ model}$) foreseen by the Avrami fractional kinetic model are very close to the sorption capacities at any time ($q_{t\ experimental}$) experimentally measured.

Another essential statistical parameter that is used to make a comparison among different adsorption models is the BIC (Schwarz et al., 1978). In Table 4, it is shown that the Avrami fractional-order model has the lowest BIC values when compared with the other kinetic models. Also, the BIC difference (ΔBIC) between pseudo-first-order and Avrami fractional-order model and between pseudo-second-order and Avrami fractional kinetic model was at least 44. According to the BIC, when $\Delta BIC \geq 10$, the kinetic model that has the lowest value of BIC is indeed the best-adjusted model (Schwarz 1978; see Supplementary material). Therefore, based on all statistical parameters evaluated, the best kinetic adsorption model for describing the adsorption of amoxicillin onto CCP.600 and CCP.700 activated carbon is the Avrami fractional-order model.

Considering that different kinetic adsorption models present different rate constants (k) that have different units, it is complicated to compare different values of k directly. In this way, it is necessary to define a parameter of time to facilitate the comparison of the kinetic results. The $t_{1/2}$ is the time to the adsorbent took to attain 50% of the saturation of the kinetic curve, and $t_{0.95}$ is the time that the adsorbent took to attain 95% of the saturation of the kinetic curve using a fixed initial concentration of the adsorbate (Saucier et al. 2017; Kasperiski et al. 2018; Leite et al. 2017; Saucier et al. 2017). The interpolation at the fitted kinetic curve was used to obtain the values of $t_{1/2}$ and $t_{0.95}$. It is considered that the best kinetic of adsorption model was the Avrami fractional-order model; only the values of $t_{1/2}$ and $t_{0.95}$ of this kinetic model present physical meaning (Table 4).

It is important to highlight that the kinetics of adsorption of amoxicillin onto CCP.700 was faster than CCP.600 to attain 50% of the saturation ($t_{1/2}$); however, to attain the 95% of saturation ($t_{0.95}$), the CCP.600 was faster than CCP.700 (Table 4).

For farther adsorption experiments, the contact time between the adsorbent and adsorbate was fixed at 30 min. It is necessary to use a contact time higher than the value of $t_{0.95}$ to guarantee that the pair adsorbent/adsorbate will attain the equilibrium.

Isotherms of adsorption

Adsorption isotherms define the amount of pollutants that are retained to surface of an adsorbent at a fixed temperature when the system attains the equilibrium. Adsorption isotherms are fundamental to optimize and know the use of an adsorbent (Lima et al. 2015). Also, the study of isotherms can help to elucidate the mechanism of adsorption between the adsorbent and adsorbate (Prola et al. 2013). The Langmuir, Freundlich, and Liu isotherm models were used to evaluate the equilibrium data.

The isotherms of adsorption of the antibiotic amoxicillin onto CCP.600 and CCP.700 adsorbents were carried out using the experimental conditions, temperatures fixed in the interval of 10 to 45 °C, pH of amoxicillin solution fixed at 7.0, the adsorbent dosage of 1.50 g L^{-1}, and contact time between sorbing specie and adsorbents of 30 min. Figure 6 shows the isotherms at 45 °C. In Table 5, the parameters of the six isotherms obtained from 10° to 45 °C are presented.

The fittings of the isotherm models of the adsorption of amoxicillin onto CCP.600 and CCP.700 activated carbons were statistically evaluated by the R^2_{Adj} and SD values, which are presented in Table 5. Based on these statistical parameters, Liu isotherm was the isotherm that was better fitted to the experimental data for both adsorbents. The Liu model exhibited the lowest SD and R^2_{Adj} values closer to 1.00 for CCP.600 and CCP.700 activated carbons. This result indicates that the

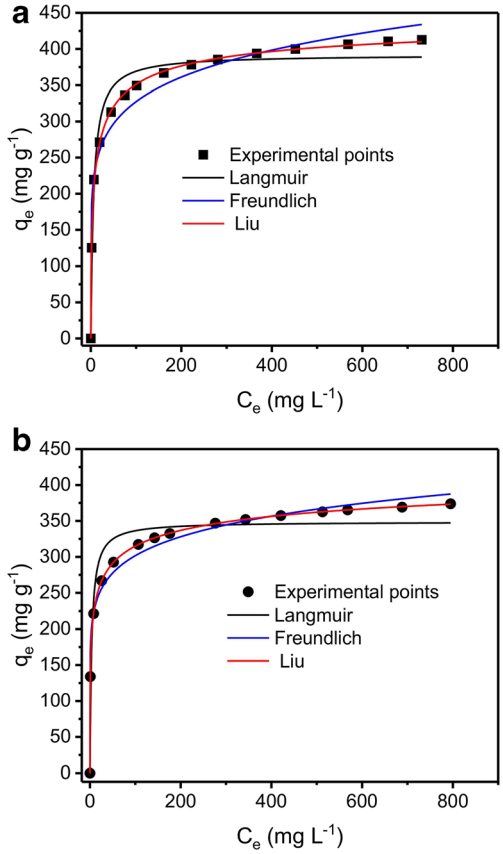

Fig. 6 Adsorption isotherms of amoxicillin onto **a** CCP.600 and **b** CCP.700. The pH was fixed at 7.0, the adsorbent dosage of 1.5 g L^{-1}, the temperature of 45 °C, and contact time of 30 min

sorption capacities (q) obtained experimentally are closer to the sorption capacities (q) found by the Liu isotherm model (Prola et al. 2013; Saucier et al. 2017). The BIC was carried out to complement the statistical evaluation of the model. For CCP.600, the ΔBIC between the Langmuir and Liu model was ≥ 22.6, and the ΔBIC between the Freundlich and Liu model was ≥ 43.4. For the CCP.700 activated carbon, the ΔBIC of Langmuir and Liu model was ≥ 87.7, and the ΔBIC between Freundlich and Liu model was ≥ 88.7. Therefore, based on the BIC values analysis, the Liu model also was the best equilibrium model fitted by the experimental data, since all the differences of BIC values are much higher than 10 (Schwarz 1978).

Regarding the maximum sorption capacities based on the Liu model, the values obtained by CCP.700 are slightly higher than (0.55 to 1.49%) the maximum sorption capacities obtained with CCP.600. However, this difference is not remarkable, as it was expected based on the characterization data discussed in the previous sections. Both activated carbons present similar surface area, total pore volumes, similar amounts of functional groups, and practically the same functional groups and similar hydrophilicity behavior. Therefore, remarkable differences in sorption capacity are not expected. The preparation of activated carbons by chemical activation using the zinc chloride as an activating agent at the proportion in weight of 1:1 with capsules of cashew of Para and using pyrolysis at 600 and 700 °C leads to CCP.600 and CCP.700. These two materials do not have remarkable physical chemical differences, and they also not have remarkable differences in the performance for removal of the antibiotic amoxicillin from waters.

Thermodynamic of adsorption and the mechanism of adsorption

The thermodynamic parameters of adsorption, Gibbs free energy (ΔG°), enthalpy (ΔH°), and entropy (ΔS°) are essential to have a notion about the interaction of the sorbing specie and adsorbent. Please see Supplementary material for the calculations of these parameters (Lima et al. 2019) and Table 6 to see the values of the thermodynamic parameters.

When the values of ΔG° is negative, it indicates that the process of the adsorption is spontaneous. All the values of ΔG° at the different temperatures (283–318 K) were negative being the process of adsorption of amoxicillin favorable and spontaneous (Cunha et al. 2018; Kasperiski et al.,2018).

The ΔH° of adsorption of amoxicillin into CCP.600 and CCP.700 was negative. Therefore, the process of adsorption process is exothermic for amoxicillin uptaking using both adsorbents. ΔH° ≤ 25 kJ mol^{-1} is compatible with physical adsorption (Lima et al. 2015). ΔS° values reported in Table 6 are positives that imply one increasing of randomness when the adsorption process takes place (Kasperiski et al. 2018).

The values of ΔH° of adsorption is compatible with physical adsorption. The mechanisms of interaction of the antibiotic amoxicillin onto CCP.600 and CCP.700 activated carbons should occur by (Saucier et al. 2017; Thue et al. 2017a):

- π-π interactions (π bonds of the activated carbon with π bonds of antibiotic);
- donor-acceptor complex formation between the surface carbonyl groups (electron donors) and the aromatic ring of the antibiotic acting as the acceptor;
- hydrogen bonds between the OH and NH groups of the amoxicillin and the OH and NH groups of the activated carbons.

This proposal of the mechanism of interaction of amoxicillin onto CCP.600 and CCP.700 activated carbons is compatible with the polar groups that exist in the surface of the activated carbons (see Fig. 2 and Table 3) and the antibiotic (see Supplementary Fig. 1).

The application of activated carbons for the removal of pharmaceuticals in simulated hospital effluents

According to the results of isotherms of adsorption, it was observed that both CCP.600 and CCP.700 activated carbons

Table 5 Langmuir, Freundlich, and Liu isotherm parameters for the adsorption of amoxicillin onto CCP600 and CCP700 adsorbents. Conditions, initial pH 7.0, contact time of adsorbent, and adsorbate was adjusted at 30 min

Langmuir	10 °C	20 °C	25 °C	30 °C	40 °C	45 °C
CCP.600						
Q_{max} (mg g^{-1})	236.4	298.0	289.2	334.8	386.6	392.1
K_L (L mg^{-1})	0.8730	0.2747	0.3018	0.2301	0.1379	0.1612
R^2_{adj}	0.9538	0.9830	0.9515	0.9679	0.9881	0.9670
SD (mg g^{-1})	15.08	11.16	19.21	17.37	12.79	21.72
BIC	87.37	78.34	94.64	91.61	82.43	98.32
Freundlich						
K_F (mg g^{-1} (mg $L^{-1})^{-1/nF}$)	131.0	171.9	144.5	167.6	165.5	170.5
n_F	10.14	11.22	8.323	8.599	7.135	7.059
R^2_{adj}	0.9731	0.8881	0.9694	0.9775	0.9487	0.9649
SD (mg g^{-1})	11.51	28.63	15.28	14.56	26.56	22.39
BIC	79.28	106.6	87.77	86.32	104.4	99.24
Liu						
Q_{max} (mg g^{-1})	274.9	292.1	335.9	383.3	412.2	451.0
K_g (L mg^{-1})	0.3361	0.2457	0.2074	0.1730	0.1212	0.1096
n_L	0.3917	2.176	0.4460	0.4705	0.6738	0.5255
R^2_{adj}	0.9990	0.9966	0.9999	0.9998	0.9999	0.9982
SD (mg g^{-1})	2.251	5.000	0.3858	1.217	0.2850	5.012
BIC	31.83	55.77	− 21.09	13.37	− 30.17	55.84
CCP.700						
Q_{max} (mg g^{-1})	258.9	233.4	292.0	303.8	388.4	348.9
K_L (L mg^{-1})	0.2967	0.6574	0.2947	0.3524	0.1319	0.2681
R^2_{adj}	0.9861	0.9320	0.9668	0.9094	0.9843	0.9192
SD (mg g^{-1})	8.533	17.80	15.43	27.59	13.97	29.74
BIC	70.30	92.35	88.07	105.5	85.10	107.7
Freundlich						
K_F (mg g^{-1} (mg $L^{-1})^{-1/nF}$)	149.1	132.07	152.8	158.9	180.0	173.1
n_F	11.05	10.29	9.322	9.096	7.867	8.286
R^2_{adj}	0.9703	0.9881	0.9814	0.9841	0.9619	0.9846
SD (mg g^{-1})	12.48	7.435	11.57	11.57	21.80	12.98
BIC	81.71	66.16	79.43	79.43	98.43	82.88
Liu						
Q_{max} (mg g^{-1})	276.4	295.5	340.9	387.8	418.8	454.7
K_g (L mg^{-1})	0.3232	0.2449	0.1983	0.1699	0.1258	0.1076
n_L	0.5598	0.3097	0.4183	0.3209	0.6311	0.3424
R^2_{adj}	0.9999	0.9999	0.9999	0.9999	0.9999	0.9999
SD (mg g^{-1})	0.4357	0.2634	0.5724	0.3796	0.3786	0.4163
BIC	− 17.44	− 32.54	− 9.255	− 21.57	− 21.65	− 18.81

showed to be potential adsorbents for the treatment of effluents contaminated with amoxicillin. However, in a real situation, other compounds are presented in a hospital effluent. In this work, two simulated hospital effluents (see Table 1) were prepared, which were composed of six pharmaceuticals, two sugars, and others four organics and eight inorganic salts that are usually present in hospital effluents (Kasperiski et al. 2018).

The treatment of these two synthetic hospital effluents is necessary to assess the potential use of CCP.600 and CCP.700 adsorbents for real wastewater treatment.

Considering that absorbance is an additive property, the area under the absorption bands corresponds to the sum of compounds that absorb UV-Vis radiation (Skoog et al. 2007). The UV-Vis spectra of the two effluents before and after the treatment with CCP.600 and CCP.700 adsorbents

Table 6 Thermodynamic parameters of the adsorption of amoxicillin onto CCP.600 and CCP.700 activated carbons (Lima et al. 2019)

Temperature (K)	283	293	298	303	313	318
CCP.600						
K_g (L mol^{-1})	$1.228 \cdot 10^5$	$8.977 \cdot 10^4$	$7.578 \cdot 10^4$	$6.320 \cdot 10^4$	$4.430 \cdot 10^4$	$4.004 \cdot 10^4$
K_e [a]	$1.228 \cdot 10^5$	$8.977 \cdot 10^4$	$7.578 \cdot 10^4$	$6.320 \cdot 10^4$	$4.430 \cdot 10^4$	$4.004 \cdot 10^4$
$\Delta G°$ (kJ mol^{-1})	− 27.57	− 27.78	− 27.84	− 27.85	− 27.84	− 28.02
$\Delta H°$ (kJ mol^{-1})	–	–	− 24.72	–	–	–
$\Delta S°$ (J K^{-1} mol^{-1})	–	–	10.26	–	–	–
R^2_{adj}	0.9958	–	–	–	–	–
SD	0.02747	–	–	–	–	–
CCP.700						
K_g (L mol^{-1})	$1.181 \cdot 10^5$	$8.950 \cdot 10^4$	$7.245 \cdot 10^4$	$6.208 \cdot 10^4$	$4.597 \cdot 10^4$	$3.931 \cdot 10^4$
K_e	$1.181 \cdot 10^5$	$8.950 \cdot 10^4$	$7.245 \cdot 10^4$	$6.208 \cdot 10^4$	$4.597 \cdot 10^4$	$3.931 \cdot 10^4$
$\Delta G°$ (kJ mol^{-1})	− 27.48	− 27.78	− 27.73	− 27.80	− 27.94	− 27.97
$\Delta H°$ (kJ mol^{-1})	–	–	− 23.83	–	–	–
$\Delta S°$ (J K^{-1} mol^{-1})	–	–	13.10	–	–	–
R^2_{adj}	0.9961	–		–	–	–
SD	0.02567	–		–	–	–

[a] K_e, the thermodynamic equilibrium constant was calculated as described previously (Lima et al. 2019). The γ of amoxicillin was considered 1.00

were recorded (190 to 400 nm, see Fig. 7). Therefore, the integration under the curves to obtain the total areas (190 to 400 nm) was employed to calculate the total percentage (sum of all organic compounds) of removal of each effluent by the activated carbons. For effluent 1, the percentage of removal of all organic compounds was 98.01 (CCP.600) and 98.60% (CCP.700). For effluent 2, the percentual of removal was 97.28 (CCP.600) and 97.76% (CCP.700).

The percentage of removal of these effluents is very close for both activated carbons in agreement with the chemical and physical properties discussed previously and also with the maximum sorption capacity based on the Liu isotherm obtained for both adsorbents.

Based on the results of total removal of synthetic effluent, it is possible to state that the *capsule of cashew of Para* (*B. excelsa* capsules) activated carbons present potentiality for being used in treatment real hospital effluents.

Conclusion

In this study, *B. excelsa* capsules were used as carbon precursor for the preparation of activated carbons. The textural characterization of the CCP.600 and CCP.700 activated carbons prepared presented high specific surface area and total pore volumes. These activated carbons were employed for the removal of the antibiotic amoxicillin from aqueous solutions and simulated hospital effluents.

The Avrami fractional kinetic model and the Liu isotherm models were the best models to describe the kinetics and equilibrium of the adsorption, respectively. The maximum adsorption capacities of 451.0 (CCP.600) and 454.7 mg g^{-1} (CCP.700) were obtained at 45 °C for both adsorbents.

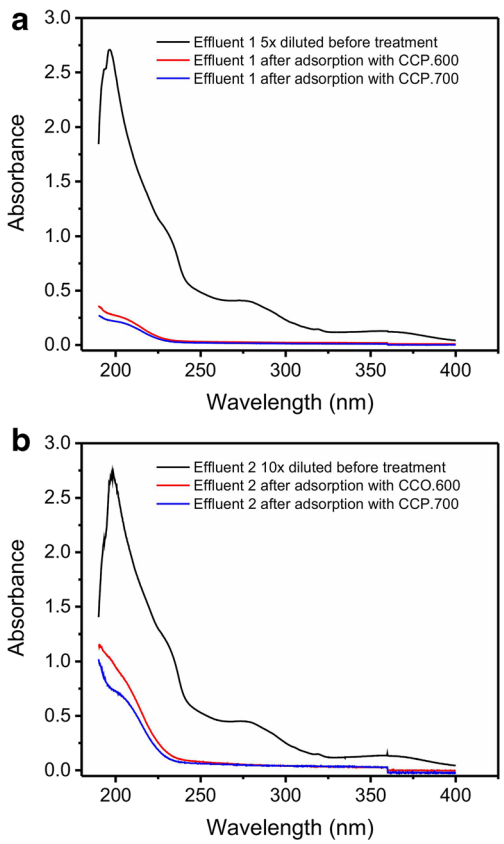

Fig. 7 Simulated effluents. **a** Effluent 1 and **b** effluent 2. For the chemical composition of effluents, see Table 1

The thermodynamic parameters of adsorption indicate that the uptake of amoxicillin is favorable and spontaneous.

CCP.600 and CCP.700 were efficiently used in the treatment of synthetic hospital effluents, containing elevated concentrations of organic and inorganics and showing their potentiality for being used in real hospital effluents.

Acknowledgments We are also grateful to Chemaxon for giving us an academic research license for the Marvin Sketch software, Version 19.2.0 (http://www.chemaxon.com), 2019 used for molecule physical-chemical properties.

Funding information The authors thank the National Council for Scientific and Technological Development (CNPq, Brazil) and Coordination of Improvement of Higher Education Personnel (CAPES, Brazil) for financial support and sponsorship.

References

Abazari R, Mahjoub AR, Shariati J (2019) Synthesis of a nanostructured pillar MOF with high adsorption capacity towards antibiotics pollutants from aqueous solution. J Hazard Mater 366:439–451

Babaei AA, Lima EC, Takdastan A, Alavi N, Goudarzi G, Vosoughi M, Hassani G, Shirmardi M (2016) Removal of tetracycline antibiotic from contaminated water media by multi-walled carbon nanotubes: operational variables, kinetics, and equilibrium studies. Water Sci Technol 74:1202–1216

Bondarczuk K, Piotrowska-Seget Z (2019) Microbial diversity and antibiotic resistance in a final effluent-receiving lake. Sci Total Environ 650:2951–2961

Cunha MR, Lima EC, Cimirro NFGM, Thue PS, Dias SLP, Gelesky MA, Dotto GL, dos Reis GS, Pavan FA (2018) Conversion of Eragrostis plana Nees leaves to activated carbon by microwave assisted pyrolysis for the removal of organic emerging contaminants from aqueous solutions. Environ Sci Pollut Res 25:23315–23327

dos Reis GS, Bin Mahbub MK, Wilhelm M, Lima EC, Sampaio CH, Saucier C, Dias SLP (2016a) Activated carbon from sewage sludge for removal of sodium diclofenac and nimesulide from aqueous solutions. Korean J Chem Eng 33:3149–3161

dos Reis GS, Sampaio CH, Lima EC, Wilhelm M (2016b) Preparation of novel adsorbents based on combinations of polysiloxanes and sewage sludge to remove pharmaceuticals from aqueous solutions. Colloids Surf A Physicochem Eng Asp 497:304–331

Goertzen SL, Theriault KD, Oickle AM, Tarasuk AC, Andreas HA (2010) Standardization of the Boehm titration. Part I. CO_2 expulsion and endpoint determination. Carbon 48:1252–1261

Hoppen MI, Carvalho KQ, Ferreira RC, Passing FH, Pereira IC, Rizzo-Domingues RCP, Lenzi MK, Bottini RCR (2019) Adsorption and desorption of acetylsalicylic acid onto activated carbon of babassu coconut mesocarp. J Environ Chem Eng 7:102862. https://doi.org/10.1016/j.jece.2018.102862

Jagiello J, Thommes M (2004) Comparison of DFT characterization methods based on N_2, Ar, CO_2, and H_2 adsorption applied to carbons with various pore size distributions. Carbon 42:1227–1232

Kasperiski FM, Lima EC, Umpierres CS, dos Reis GS, Thue PS, Lima DR, Dias SLP, Saucier C, da Costa JB (2018) Production of porous activated carbons from *Caesalpinia ferrea* seed pod wastes: highly efficient removal of captopril from aqueous solutions. J Clean Prod 197:919–929

Khadhri N, Saad MEK, Mosbah M, Moussaoui Y (2019) Batch and continuous column adsorption of indigo carmine onto activated carbon derived from date palm petiole. J Environ Chem Eng 7:102775. https://doi.org/10.1016/j.jece.2018.11.020

Kosikova, D. (2018) Brazil nut market—globalization on the Brazil nut market. https://www.indexbox.io/blog/Globalization-on-the-Brazil-Nut-Market/ website visited on December 18th, 2018

Krzeminski P, Tomei MC, Karaolia P, Langenhoff A, Almeida CMR, Felis E, Gritten F, Andersen HR, Fernandes T, Manaia CM, Rizzo L, Fatta-Kassinos D (2019) Performance of secondary wastewater treatment methods for the removal of contaminants of emerging concern implicated in crop uptake and antibiotic resistance spread: a review. Sci Total Environ 648:1052–1081

Le TH, Ng C, Tran NH, Chen H, Gin KYH (2018) Removal of antibiotic residues, antibiotic-resistant bacteria and antibiotic resistance genes in municipal wastewater by membrane bioreactor systems. Water Res 145:498–508

Leite AB, Saucier C, Lima EC, dos Reis GS, Umpierres CS, Mello BL, Shirmardi M, Dias SLP, Sampaio CH (2018) Activated carbons from avocado seed: optimization and application for removal several emerging organic compounds. Environ Sci Pollut Res 25:7647–7661

Leite AJB, Sophia AC, Thue PS, dos Reis GS, Dias SLP, Lima EC, Vaghetti JCP, Pavan FA, de Alencar WS (2017) Activated carbon from avocado seeds for the removal of phenolic compounds from aqueous solutions. Desalin Water Treat 71:168–181

Li D, Shi W (2016) Recent developments in visible-light photocatalytic degradation of antibiotics. Chin J Catal 37:792–799

Li H, Hu J, Cao Y, Li X, Wang X (2017) Development and assessment of a functional activated fore-modified bio-hydrochar for amoxicillin removal. Bioresour Technol 246:168–175

Li Y, Ding X, Guo Y, Wang L, Rong C, Qu Y, Ma X, Wang Z (2011) A simple and highly effective process for the preparation of activated carbons with high surface area. Mater Chem Phys 127:495–500

Lima EC, Barbosa RV, Brasil JL, Santos AHDP (2002) Evaluation of different permanent modifiers for the determination of arsenic, cadmium and Lead in environmental samples by electrothermal atomic absorption spectrometry. J Anal At Spectrom 17:1523–1529

Lima EC, Adebayo MA, Machado FM (2015) Chapter 3: kinetic and equilibrium models of adsorption. In: Bergmann CP, Machado FM (eds) Carbon nanomaterials as adsorbents for environmental and biological applications. Springer International Publishing, pp 33–69

Lima EC, Barbosa F Jr, Krug FJ, Guaita U (1999) Tungsten-rhodium permanent chemical modifier for lead determination in digests of biological materials and sediments by electrothermal atomic absorption spectrometry. J Anal At Spectrom 14:1601–1605

Lima EC, Fenga PG, Romero JR, de Giovani WF (1998a) Electrochemical behaviour of $[Ru(4,4'\text{-}Me_2bpy)_2(PPh_3)(H_2O)](ClO_4)_2$ in homogeneous solution and incorporated into carbon paste electrodes. Application to oxidation of benzylic compounds. Polyhedron 17:313–318

Lima EC, Hosseini-Bandegharaei A, Moreno-Piraján JC, Anastopoulos I (2019) A critical review of the estimation of the thermodynamic parameters on adsorption equilibria. Wrong use of equilibrium constant in the Van't Hoof equation for calculation of thermodynamic parameters of adsorption. J Mol Liq 273:425–434

Lima EC, Krug FJ, Nóbrega JA, Nogueira ARA (1998b) Determination of ytterbium in animal faeces by tungsten coil electrothermal atomic absorption spectrometry. Talanta 47:613–623

Lima EC, Barbosa F Jr, Krug FJ (2000) The use of tungsten–rhodium permanent chemical modifier for cadmium determination in decomposed samples of biological materials and sediments by electrothermal atomic absorption spectrometry. Anal Chim Acta 409:267–274

Lu J, Sun J, Chen X, Tian S, Chen D, He C, Xiong Y (2019) Efficient mineralization of aqueous antibiotics by simultaneous catalytic ozonation and photocatalysis using $MgMnO_3$ as a bifunctional catalyst. Chem Eng J 358:48–57

McConnell MM, Hansen LT, Jamieson RC, Neudorf KD, Yost CK, Tong A (2018) Removal of antibiotic resistance genes in two tertiary level municipal wastewater treatment plants. Sci Total Environ 643:292–300

Moreira NFF, Orge CA, Ribeiro AR, Faria JL, Nunes OC, Pereira MFR, Silva AMT (2015) Fast mineralization and detoxification of amoxicillin and diclofenac by photocatalytic ozonation and application to an urban wastewater. Water Res 87:87–96

Oickle AM, Goertzen SL, Hopper KR, Abdalla YO, Andreas HA (2010) Standardization of the Boehm titration: part II. Method of agitation, effect of filtering and dilute titrant. Carbon 48:3313–3322

Prola LDT, Machado FM, Bergmann CP, de Souza FE, Gally CR, Lima EC, Adebayo MA, Dias SLP, Calvete T (2013) Adsorption of Direct Blue 53 dye from aqueous solutions by multi-walled carbon nanotubes and activated carbon. J Environ Manag 130:166–175

Puchana-Rosero MJ, Adebayo MA, Lima EC, Machado FM, Thue PS, Vaghetti JCP, Umpierres CS, Gutterres M (2016) Microwave-assisted activated carbon obtained from the sludge of tannery-treatment effluent plant for removal of leather dyes. Colloids Surf A Physicochem Eng Asp 504:105–115

Qiu W, Sun J, Fang M, Luo S, Tian Y, Dong P, Xu B, Zheng C (2019) Occurrence of antibiotics in the main rivers of Shenzhen, China: association with antibiotic resistance genes and microbial community. Sci Total Environ 653:334–341

Ramanathan R, Weibel DE (2012) Novel liquid-solid adhesion superhydrophobic surface fabricated using titanium dioxide and trimethoxypropyl silane. Appl Surf Sci 258:7950–7955

Roy J (2012) An introduction to pharmaceutical sciences production, chemistry, techniques and technology. Woodhead Pub, Cambridge, p 239

Saucier C, Karthickeyan P, Ranjithkumar V, Lima EC, dos Reis GS, de Brum IAS (2017) Efficient removal of amoxicillin and paracetamol from aqueous solutions using magnetic activated carbon. Environ Sci Pollut Res 24:5918–5932

Schwarz GE (1978) Estimating the dimension of a model. Ann Stat 6: 461–464

Silva CP, Jaria G, Otero M, Esteves VI, Calisto V (2018) Waste-based alternative adsorbents for the remediation of pharmaceutical contaminated waters: has a step forward already been taken? Bioresour Technol 250:888–901

Skoog DA, Holler FJ, Crouch SR (2007) Principles of instrumental analysis, 6th edn. Thomson Brooks, Canada

Sophia CA, Lima EC (2018) Removal of emerging contaminants from the environment by adsorption. Ecotoxicol Environ Saf 150:1–17

Sophia CA, Lima EC, Allaudeen N, Rajan S (2016) Application of graphene-based materials for adsorption of pharmaceutical traces from water and wastewater—a review. Desalin Water Treat 57: 27573–27586

Souza PR, Dotto GL, Salau NPG (2018) Artificial neural network (ANN) and adaptive neuro-fuzzy interference system (ANFIS) modelling for nickel adsorption onto agro-wastes and commercial activated carbon. J Environ Chem Eng 6:7152–7160

Suo F, Liu X, Li C, Yuan M, Zhang B, Wang J, Ma Y, Lai Z, Ji M (2019) Mesoporous activated carbon from starch for superior rapid pesticides removal. Int J Biol Macromol 121:806–813

Takdastan A, Mahvi AH, Lima EC, Shirmardi M, Babaei AA, Goudarzi G, Neisi A, Farsani MH, Vosoughi M (2016) Preparation, characterization, and application of activated carbon from low-cost material for the adsorption of tetracycline antibiotic from aqueous solutions. Water Sci Technol 74:2349–2363

Tang S, Yuan D, Rao Y, Zhang J, Qu Y, Gu J (2018) Evaluation of antibiotic oxytetracycline removal in water using a gas phase dielectric barrier discharge plasma. J Environ Manag 226:22–29

Thommes M, Kaneko K, Neimark AV, Olivier JP, Rodriguez-Reinoso F, Rouquerol J, Sing KSW (2015) Physisorption of gases, with special reference to the evaluation of surface area and pore size distribution (IUPAC Technical Report). Pure Appl Chem 87:1051–1069

Thue PS, Adebayo MA, Lima EC, Sieliechi JM, Machado FM, Dotto GL, Vaghetti JCP, Dias SLP (2016) Preparation, characterization and application of microwave-assisted activated carbons from wood chips for removal of phenol from aqueous solution. J Mol Liq 223:1067–1080

Thue PS, dos Reis GS, Lima EC, Sieliechi JM, Dotto GL, Wamba AGN, Dias SLP, Pavan FA (2017a) Activated carbon obtained from Sapelli wood sawdust by microwave heating for *O-cresol* adsorption. Res Chem Intermed 43:1063–1087

Thue PS, Lima EC, Sieliechi JM, Saucier C, Dias SLP, Vaghetti JCP, Rodembusch FS, Pavan FA (2017b) Effects of first-row transition metals and impregnation ratios on the physicochemical chemical properties of microwave-assisted activated carbons from wood biomass. J Colloid Interface Sci 486:163–175

Umpierres CS, Thue PS, dos Reis GS, de Brum IAS, Lima EC, de Alencar WA, Dias SLP, Dotto GL (2018) Microwave activated carbons from Tucumã (*Astrocaryum aculeatum*) waste for efficient removal of 2-nitrophenol from aqueous solutions. Environ Technol 39:1173–1187

Wang L, Ben W, Li Y, Liu C, Qiang Z (2018) Behavior of tetracycline and macrolide antibiotics in activated sludge process and their subsequent removal during sludge reduction by ozone. Chemosphere 206:184–191

WHO (2015) Model list of essential medicines. The 19th edition, April 2015. Available in: https://www.google.com/search?q=Model+list+of+essential+medicines.+The+19th+edition%2C+April+2015&rlz=1C1CHBD_pt-PTBR841BR841&oq=Model+list+of+essential+medicines.+The+19th+edition%2C+April+2015&aqs=chrome..69i57.743j0j8&sourceid=chrome&ie=UTF-8

Zhu J, Li Y, Xu L, Liu Z (2018) Removal of toluene from waste gas by adsorption-desorption process using corncob-based activated carbons as adsorbents. Ecotoxicol Environ Saf 165:115–125

Colloids and Surfaces A 583 (2019) 123966

Contents lists available at ScienceDirect

Colloids and Surfaces A

journal homepage: www.elsevier.com/locate/colsurfa

Efficient acetaminophen removal from water and hospital effluents treatment by activated carbons derived from Brazil nutshells

Diana R. Lima[a], Ahmad Hosseini-Bandegharaei[b,c], Pascal S. Thue[d,**], Eder C. Lima[a,d,e,*], Ytallo R.T. de Albuquerque[a], Glaydson S. dos Reis[a,f], Cibele S. Umpierres[d], Silvio L.P. Dias[a,d], Hai Nguyen Tran[g]

[a] Postgraduate Program in Mine, Metallurgical, and Materials Engineering (PPGE3M), School of Engineering, Federal University of Rio Grande do Sul (UFRGS), Av. Bento Gonçalves 9500, Porto Alegre, RS, Brazil
[b] Department of Environmental Health Engineering, Faculty of Health, Sabzevar University of Medical Sciences, Sabzevar, Iran
[c] Department of Engineering, Kashmar Branch, Islamic Azad University, P.O. Box 161, Kashmar, Iran
[d] Graduate Program in Science of Materials (PGCIMAT). Institute of Chemistry, Federal University of Rio Grande do Sul (UFRGS), Av. Bento Gonçalves 9500, Porto Alegre, RS, Brazil
[e] Institute of Chemistry, Federal University of Rio Grande do Sul (UFRGS), Av. Bento Gonçalves 9500, P.O. Box 15003, 91501-970, Porto Alegre, RS, Brazil
[f] The French Institute of Science and Technology for Transport, Spatial Planning, Development, and Networks (IFSTTAR), MAST, GPEM, F-44344, Bouguenais, France
[g] Institute of Fundamental and Applied Sciences, Duy Tan University, Ho Chi Minh City 700000, Vietnam

GRAPHICAL ABSTRACT

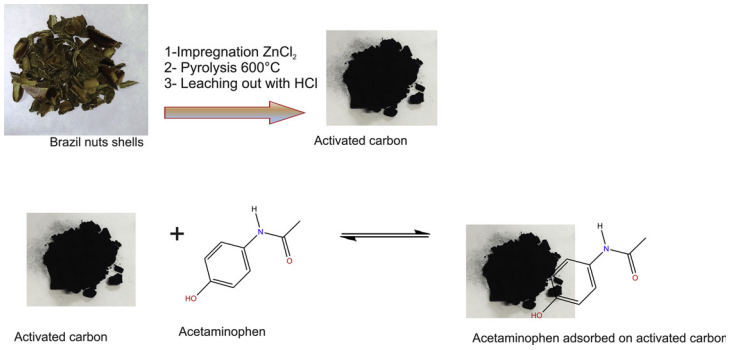

ARTICLE INFO

Keywords:
Brazil nutshells
Acetaminophen
Carbon adsorbents
Adsorption
Synthetic hospital effluents

ABSTRACT

Activated carbons from Brazil nutshells were produced by $ZnCl_2$-activation at different biomass: $ZnCl_2$ ratios of 1.0:1.0 and 1.0:1.5 at 600 °C and the samples were denominated as BNS1.0 and BNS1.5, respectively. The obtained activated carbons were used in the adsorption of acetaminophen (paracetamol) and for the treatment of synthetic hospital effluents. Several analytical techniques were used to characterize the activated carbons. The N_2 isotherms presented the S_{BET} values of the BNS1.0 and BNS1.5 are very high, 1457 and 1640 $m^2 g^{-1}$, respectively. The FTIR and Boehm titration analysis demonstrated the presence of several surface functional groups on both ACs surfaces, which can influence the acetaminophen adsorption. The adsorption studies revealed that the maximum adsorption capacities (Q_{max}) are very high for both ACs; however, the BNS1.5 capacity

* Corresponding author at: Institute of Chemistry, Federal University of Rio Grande do Sul (UFRGS), Av. Bento Gonçalves 9500, P.O. Box 15003, 91501-970, Porto Alegre, RS, Brazil.
** Corresponding author.
E-mail addresses: ahoseinib@yahoo.com (A. Hosseini-Bandegharaei), pascalsilasthue@gmail.com (P.S. Thue), profederlima@gmail.com, eder.lima@ufrgs.br (E.C. Lima).

https://doi.org/10.1016/j.colsurfa.2019.123966
Received 5 July 2019; Received in revised form 8 September 2019; Accepted 10 September 2019
Available online 11 September 2019

is higher (411.0 mg g^{-1}) than that of BNS1.0 (309.7 mg g^{-1}). The thermodynamic assessments revealed that the process of acetaminophen adsorption is spontaneous, energetically favorable, and exothermic, and the magnitude of enthalpy is compatible with physisorption. Besides, it suggests that the acetaminophen adsorption on both ACs is dominated by van der Walls forces and microporous filling mechanism. The use of activated carbons for treatment of synthetic hospital effluents, containing different pharmaceuticals as well as organics and inorganic salts, presented a high percentage of removal (up to 98.83%). The adsorbent was magnificently regenerated up to 74% with a mixture of 0.1 mol L^{-1} NaOH + 20% EtOH solution and can be reused up to four cycles ensuring sustainable use of proposed adsorbent for acetaminophen removal from aqueous media. In the light of these results, it is possible to say that Brazil nutshell is an excellent raw material to prepare efficient ACs which can be successfully used in the treatment of real hospital effluents.

1. Introduction

Contamination of the environment is a non-negligible problem that affects people's health and quality of life [1]. Large amounts of pollutants are laid-off into natural waters without any treatment [1]. There are many types of water contaminants, and they can be categorized into big classes such as organic contaminants, nutrients, pathogens, agricultural runoff, inorganic pollutants (salts and metals), and others.

However, over the last few years, a new class of pollutants, so-called emerging concern pollutants (ECPs) has gained attention from environmental researchers [1–4]. ECPs can be comprehended in any naturally-occurring or synthetic chemical, and any microorganism that is not regularly measured in the environment with possible human health or ecological effects [2–4]. The emerging concern pollutants consist mainly of pharmaceuticals, hormones, personal care products, flame retardants, fuel additives, pesticides, plasticizers, several chemicals used in the industry, solvents, and surfactants [1–4].

Therefore, the vast majority of emerging pollutants comes from municipal and industrial wastewater treatment plants which fail to eliminate this kind of pollutions, since they exploit conventional treatment technologies which are not explicitly designed to remove residual concentrations of such organic compounds [3,4].

One of the emerging pollutants is acetaminophen, most know as paracetamol, which is frequently consumed as a painkiller, analgesic, and antipyretic compound worldwide [5]. It was reported that 58–68% of acetaminophen is excreted by human urine [5]. This pharmaceutical is also prone to bioaccumulation in aquatic organisms. Its presence was reported in all kind of waters in several European countries [5,6]. The degradation of acetaminophen produces carcinogenic and highly toxic compounds, such as, 4-aminophenol, that cause mutagenic effects in human cells [5,6]. In light of these facts, acetaminophen is considered as an emerging contaminant and should be removed from wastewaters before releasing in the environment.

The literature shows several methods for treatment of waters and wastewaters polluted with the acetaminophen such as Advanced Oxidative Process [7,8], biological treatments [5,9], filtration in membranes [10,11], and adsorption [12–14]. However, some of these treatment methods have some drawbacks, such as high costs and high solid (e.g., sludges) generation [7,9]. In contrast to these disadvantageous methods, adsorption as a treatment method of effluents presents some advantages such as the low initial price for implementation and smooth operation, and it can be useful for removal of acetaminophen even in low traces [4,14].

Amongst the adsorbents used in the adsorption processes, one of the most widespread adsorbents used for the removal of contaminants from water is activated carbon (AC) [15–18] which, because of its pore structures and surface area confers an outstanding adsorption capacity. Different AC adsorbents can be manufactured by exploiting a wide different variety of carbonaceous precursors (e.g., biomass wastes), resulting in the production of a variety of adsorbents with different characteristics and quality.

The use of biomass wastes for preparing activated porous carbon materials has enhanced considerably in the last years. Some residual biomasses used for fabrication of activated carbons are coffee wastes [15], grass [16], ironwood seed pod wastes [17], avocado seed [12], tucumã seed [18], cotton stalk [19], coals [20], tannery sludge [21], and pulp mill sludge [22], and others.

In this work, usage of residual biomass of Brazil nuts shell is proposed as a raw material for developing ACs, in order to give valorization to these wastes which are currently generated and underutilized in Brazil [23,24]. The Brazil nut tree (*Bertholletia excelsa*) is native to South America and grows in well-drained and upland areas of the Amazon rainforest (Brazil, Colombia, and Venezuela), as well as in neighboring areas of Bolivia, Guyana, and Peru [23,24]. The groves occupy over 320 million ha distributed among these countries where Brazil has the largest occupied area [23,24].

In this research, the feasibility of the production of suitable ACs for efficient acetaminophen removal will be demonstrated. This research will be subdivided into three parts:

(i) Production of the ACs from Brazil nutshell using chemical activation with $ZnCl_2$ and subsequent pyrolysis in a conventional furnace, obtaining carbon adsorbent with most excellent properties in terms of high specific surface areas and porosities as well as chemical composition.
(ii) Applying these ACs as adsorbents for removing acetaminophen from aqueous solution as well as to treat synthetic effluents containing many ECPs and evaluating their efficiencies.
(iii) Demonstration of the reusability of the adsorbent applying adsorption experiments

2. Materials and methods

2.1. Materials

All the reagents were of analytical grade and utilized as received without any additional purification. Acetaminophen was purchased from Sigma Aldrich (DE). Deionized water (Permution) was used throughout the experiments for preparing solutions.

2.2. Activated carbon

The ACs were produced by the following described procedure: First, 80.0 g of Brazil nuts shells (CS) was processed and grounded (ϕ < 260 μm) and blended with two weight ratios of $ZnCl_2$, i.e., $ZnCl_2$: biomass ratios of 1.0:1.0 and 1.5:1.0. During the mixing, small amounts of water were added to optimize the mixing by forming a homogeneous paste [16]. Each paste was disposed in a quartz reactor in a vertical furnace, and it was heated from the ambient temperature up to 600 °C using a heating rate of 10 °C min^{-1} under a flow rate 150 ml min^{-1} of nitrogen as a purge gas. The temperature of the furnace was kept fixed at the maximum temperature for 30 min. Afterward, the furnace was shut down. However, the nitrogen stream was kept until the temperature reached < 200 °C. In order to rid the zinc metal from the pyrolyzed material, an HCl solution (1 HCl + 1 H_2O) was mixed with a known amount of pyrolyzed material under reflux for 60 min [16,17]. The

samples were denominated as BNS1.0 and BNS1.5 according to the ratio of 1.0:1.0 and 1.5:1.0 of $ZnCl_2$: biomass, respectively. The two ratios were made in order to study the effect of $ZnCl_2$ amount.

2.3. Characterization

Isotherms of N_2 adsorption-desorption (at −196 °C) were obtained by a Tristar II Kr 3020 Micromeritics equipment for analyzing the surface, after 12 h degassing of the samples under vacuum at 120 °C. The specific surface area (S_{BET}) was measured by the BET multipoint method [25], and the pore size distribution was estimated by exploiting the DFT (Density Functional Theory) method [26].

CHN/O elemental analysis was carried out by an elemental analyzer (Thermo Fisher Scientific) for measuring the amounts of C, H, N, and O (%) in the BNS1.0 and BNS1.5 samples [17].

Fourier-transform infrared spectroscopy (FTIR) was exploited to determine the functional groups of the carbon materials. The FTIR spectra were recorded over the wavenumber range of 4000–400 cm^{-1}, utilizing a Thermo Scientific Nicolet IZ10 spectrometer with an acquisition of 64 scans min^{-1} and resolution of 4 cm^{-1} [16].

The thermal stabilities of both ACs were checked by thermogravimetric analysis (TGA) exploiting a thermogravimetric analyzer (TA model SDT Q600). The activated carbons were heated up from 20° to 800 °C under inert N_2 (10 °C min^{-1}), and from 800° to 1000 °C, under oxidant atmosphere [16].

The hydrophobicity/hydrophilicity balance (HI) was performed as recommended [18,27].

Scanning electron images of the activated carbons were obtained using a scanning electron microscope furnished by Jeol model JSM-6610LV [28].

The determination of the point of zero charge pH_{pzc} of the adsorbents was obtained according to the procedure previously described [18,29]. Boehm method was used for measuring the total quantity (mmol g^{-1}) of acidic and basic groups of the two ACs [30].

2.4. Adsorption and desorption studies

The experiments of adsorption were carried out using the BNS1.0 and BNS1.5 activated carbon and acetaminophen as sorbing specie [15–17]. More details are shown in the Supplementary material.

The analytical determination of acetaminophen was carried as described elsewhere [31–35]. More details are shown in the Supplementary material.

Desorption experiments were carried out using as detailed in Supplementary material.

The statistical evaluation of the nonlinear models was performed using standard deviation (SD), $R^2_{adjusted}$, and the Bayesian Information Criterion (*BIC*) [36,37]. Details are shown in Supplementary material.

2.5. Kinetic and isotherms of adsorption models

The pseudo-first-order [38], pseudo-second-order [39], and Avrami fractional-order [40] models were utilized to fit the experimental kinetic data.

The Langmuir [41], Freundlich [42], and Liu [43] isotherm equations were utilized for the equilibrium data. Details are shown in Supplementary material [38–42].

2.6. Thermodynamics of adsorption

The thermodynamic data were evaluated using previous conditions [36,44]. Details are shown in Supplementary material.

2.7. Simulated effluents

In order to simulate real hospital effluents, two effluents containing several organic and inorganic compounds, which are commonly found in hospital effluents, were prepared. Table 1 shows the composition of simulated hospital effluents [45]. The idea of performing adsorption tests with simulated hospital effluents is to verify the possibility of the prepared ACs to be used as adsorbents for treating real hospital effluents.

Table 1
The chemical contents of the synthetic effluents.

Effluent contents	Concentration (mg L^{-1})	
	Effluent 1	Effluent 2
Pharmaceuticals		
Acetaminophen	40	80
Enalapril	15	30
Nicotinamide	15	30
Diclofenac	15	30
Metformin	15	30
Sugars		
Saccharose	30	50
Glucose	30	50
Organic components		
Sodium dodecyl sulfate	5	10
Humic acid	10	20
Citric acid	10	20
Urea	10	20
Inorganic components		
Sodium chloride	50	70
Ammonium chloride	20	30
Sodium sulfate	10	20
Ammonium phosphate	20	30
Sodium carbonate	10	20
Calcium nitrate	10	20
Magnesium chloride	10	20
Potassium nitrate	10	20
pH*	7	7

3. Results and discussion

3.1. Isotherms of adsorption of N_2

The nitrogen adsorption-desorption isotherms of both ACs are exhibited in Fig. 1A. The samples exhibit type Ib of pore models [25], revealing that the activated carbons have pore size distributions include a broad range consisting of wider micropores and possibly narrow mesopores (< 5.0 nm). Such porosity is suitable for adsorption since micropores have a significant influence on the adsorption of small molecules [46].

Fig. 1B exhibits the pore size distribution curve obtained using the DFT method [26]. BNS1.0 presents micropores ≤ 1.1 nm (higher amount), and a lower percentage of micropores between 1.1 and 2.0 nm. Also, BNS1.0 presents some mesopores in the region of 2–4 nm. On the other hand, BNS1.5 does not present micropores < 1 nm. This carbon material presents a fraction of micropores in the region of 1.0–2.0 and, also, a reasonable amount of mesopores in the region of 2–4 nm. Based on these results, both BNS1.0 and BNS1.5 are predominantly microporous material. However, it may also contain a lower amount of mesopores. The difference in the pore size distribution of BNS1.0 and BNS1.5 activated carbons is supposed to influence the acetaminophen adsorption because the adsorption of a sorbing species is affected by the pore sizes [12].

From the S_{BET} assessments, ACs presented values of 1457 and 1640 $m^2 g^{-1}$ for BNS1.0 and BNS1.5 surface, respectably, showing an increase of 12.6% in the surface area of the AC prepared with a ratio of 1:1.5 (biomass: $ZnCl_2$). The total pore volumes, according to Horvath-Kawazoe method, are 0.6661 and 0.9290 $cm^3 g^{-1}$ for the BNS1.0 and BNS1.5 (39.5% higher for BNS1.5), respectively. Using the DFT

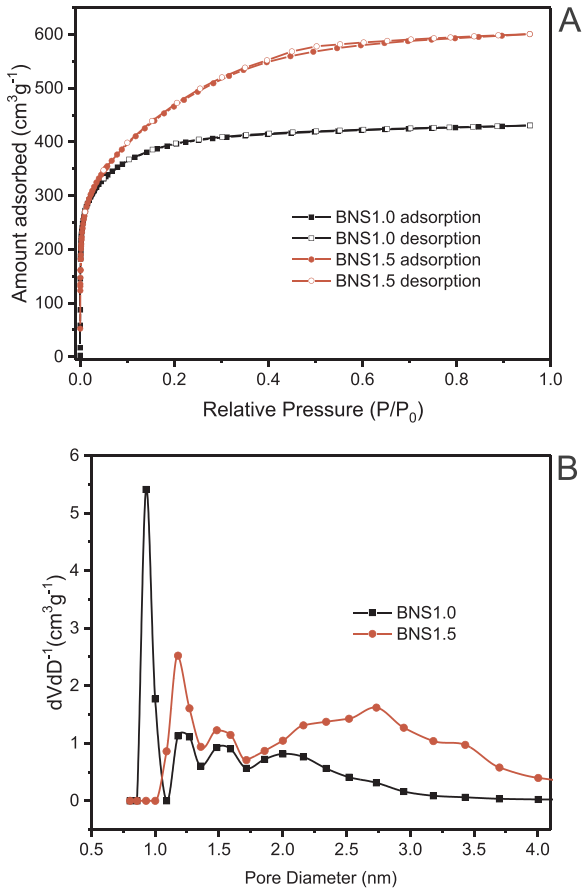

Fig. 1. Textural characteristics of BNS1.0 and BNS1.5 activated carbon. A- isotherms of adsorption and desorption of N2; B- Pore size distribution curve.

analysis, the total pore volumes are 0.5486 and 0.7947 $cm^3\,g^{-1}$ for BNS1.0 and BNS1.5 (44.9% higher than BNS1.0) respectively. Although using different methods for calculating the total volume of pores leads to different results, the volume of pores of BNS1.5 is remarkably higher than BNS1.0, the fact that would affect the adsorption capacity of these activated carbons. These results indicate that the $ZnCl_2$ provokes an increase in the surface area of ACs, by increasing the number of pores that is responsible for adsorption of a higher amount of N_2. The improved S_{BET} and pore volumes might enhance the active sites on the carbon surface, which can enhance the acetaminophen adsorption. The good porosity is also favorable for the rapid inter-diffusion of the acetaminophen through the pores of the activated carbons [25].

3.2. Surface analysis

FTIR analysis is an analytical technique that provides qualitative information concerning the functional groups existing on the surface of activated carbons. These groups play a crucial role in the adsorption of adsorbate from aqueous solutions. Fig. 2 shows the FTIR spectra of BNS1.0 and BNS1.5. As can be seen, both spectra are very similar to each other, denoting that the $ZnCl_2$ amount did not influence the chemical surface group, which is in contrast with its influence on the physical changes highlighted in the S_{BET} analysis.

The FTIR identified chemical groups on the surface of both ACs such as the broad peaks in 3424 cm^{-1} (BNS1.0) and 3432 cm^{-1} (BNS1.5) which are related to OH group stretching [15–17]. The two bands at 2920 cm^{-1} and 2855 cm^{-1} are assignable to the stretching vibrations of C–H groups, respectively to asymmetric and symmetric ones [18,21]. The band at 1632 cm^{-1} is attributable to O=C stretching in esters or carboxylic acids [16,17,27]. The small peaks at 1429 cm^{-1} are assigned to ring modes of aromatics [27,47,48]. The small peaks at 1376 and 1335 cm^{-1} is attributable to C–N stretching of amines or amides or bending of C–H bonds [47,48]. The bands at 1157, 1115, are attributed to C–O-C stretching of ether or C-C–O of esther [47,48.], and the band 1064 cm^{-1} is attributed to C–O stretching of phenolic or carboxylate groups [47,48].

Although the FTIR is critical to designate the presence of functional groups on the carbon surfaces, it cannot be used to quantify them. In this regards the use of Boehm- titration is required to quantitatively determine the amounts of total acidic and basic sites available on the activated carbon surface [18,30,48].

Considering the results shown in Table 2, it is possible to see that the quantity of acidic groups is higher than the basic groups on the surface of BNS1.0 and BNS1.5 activated carbons, indicating that the use of $ZnCl_2$ as activating agent for production of activated carbons generate carbons with higher amount of acidic functional groups on their surface.

The ratios of the sum of acidic groups divided by sum of basic groups are 1.59 (for BNS1.0) and 1.84 (for BNS1.5), reflecting that BNS1.5 would be more acidic than BNS1.0, although the total acidity of BNS1.0 (0.3520 mmol g^{-1}) is higher than that of BNS1.5 (0.3130 mmol g^{-1}). These results are following the pH_{pzc} values (reported in Table 2) which imply that, in ACs, having a higher ratio of the total acid groups divided by total basic groups leads to lower values of pH_{pzc}. The ACs presented pH_{pzc} values of 6.46 (BNS1.0) and 5.86 (BNS1.5). Taking into consideration the Boehm titration and pH_{pzc} results, it is possible to state that these results are in total accordance with hydrophobic/hydrophilic ratio (HI) characteristics of the surface of BNS1.0 and BNS1.5 adsorbents (see Table 2). Considering that acidic and basic groups increase the hydrophilic behavior of carbon surface [18,27], the higher the total amount of polar functional groups, the lower will be the value of HI [18,27]. The total sum of functional groups of the studied carbons are 0.5734 mmol g^{-1} (BNS1.0) and 0.4833 mmol g^{-1} (BNS1.5), and the values of HI obtained are 0.8151 (BNS1.0) and 0.9821 (BNS1.5). Although both ACs exhibited to have hydrophilic surfaces, because their HI values were < 1.00, BNS1.0 is more hydrophilic than BNS1.5. Therefore, the results of HI are in complete consistency with the total acidity and basicity of the activated carbons.

The elemental analyses (C, H, N, O) of BNS1.0 and BNS1.5 are exhibited in Table 2. The prepared ACs present percentages of carbon that are similar to commercial activated carbons (75–85%), which itself is a fact that justifies the use of Brazil nuts shells as a source of carbon. The percentage of nitrogen and oxygen are in agreement with the quantity of functional groups present on BNS1.0 and BNS1.5 activated carbons. BNS1.5 displays the highest %C (84.40%) and the lowest %O (11.89%)

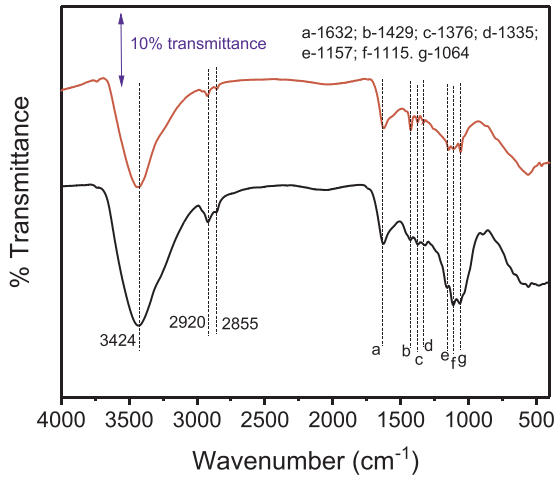

Fig. 2. FTIR of BNS1.0 and BNS1.5 activated carbon. Values inside the graphs are wavenumber of vibrational bands.

Table 2
CHN/O analysis, total acidity and basicity, and hydrophobiC–Hydrophilicity behavior of BNS1.0 and BNS 1.5.

adsorbent	%C	%H	%N	%O	%Ashes	Total acidity (mmol g^{-1})	Total basicity (mmol g^{-1})	pH_{pzc}	HI
BNS1.0	77.10	2.99	1.38	18.25	0.28	0.3520	0.2369	6.46	0.8151
BNS1.5	84.40	2.29	1.45	11.70	0.16	0.3130	0.1703	5.86	0.9821

compared to BNS1.0 (77.10% C; 18.25% O) (see Table 2). It is possible to infer that an increase of $ZnCl_2$ as activated agent results in increases of the %C and the HI values. As a consequence, there is a diminishing in the total amount of functional groups present on ACs, producing a carbon adsorbent with lower hydrophilic behavior [12].

3.3. Scanning electron microscopic images (SEM)

The textural surface properties of BNS1.0 and BNS1.5 was investigated by SEM (as shown in Fig. 3). From the images, it is possible to observe on the surface of both activated carbons several holes that allow the passage of solvent during the adsorption acetaminophen from aqueous media. However, BNS1.5 seems to show plenty and spherical holes compared to BNS1.0. BNS1.0 exhibited an irregular, heterogeneous and lowered holed surface structure, indicating relatively lower surface areas, while BNS1.5 exhibited plenty of holes and pits on its surface. This result match with the results of the textural analysis presented in Section 3.1, was the pore volumes and S_{BET} values of BNS1.5 is remarkably higher than BNS1.0. However, both activated carbons can be adequately used as adsorbents for the removal of pharmaceuticals contaminated water as it will be shown later in future sections.

3.4. Thermal analysis

TGA is performed to investigate the thermal stability of the material in a determined atmosphere. Both carbons materials were subjected to this analysis using an inert atmosphere (N_2) from ambient temperature up to 800 °C, where practically the weight loss of the functional groups occurs (Fig. 4) [16,48]. From 800 °C up to 1000 °C, an oxidizing ambiance was applied using ultrapure synthetic air. As previously reported [16], usage of a stream of ultra-pure air for temperatures ≥800 °C intent to convert the contents of the activated carbons into ash in a single run of TGA analysis [16].

Fig. 4A and B present the weight loss curves for BNS1.0 and BNS1.5, in which as can be seen the TG curves for both ACs are very similar. The thermogravimetric curves of the carbon materials show four sections of weighing loss for BNS1.0 and five sections for BNS1.5. For BNS 1.0, the first section corresponds to losses of moisture and adsorbed water on the carbon surface. For BNS 1.5, this moisture loss is not observed. However, the second section of BNS1.0 and the first section of weight loss in BNS1.5 correspond to the weight of hydration water that is present in the structure of the carbon matrix [16,47]. This stage takes place at 516.4 and 555.4 °C for BNS1.0 and BNS1.5, respectively. The following section of weight loss ranging from 516.4 to 784.3 °C and 555.4–795.5 °C for BNS1.0 and BNS1.5, respectively, corresponds to a remarkable weight loss which is ascribed to the losses of functional groups existing on the activated carbon surface, taking place by releasing the most volatile organic compounds [16,18]. At 800 °C, the atmosphere is changed from inert N_2 to oxidizing atmosphere (synthetic air). Therefore, the fourth region of weight loss of BNS1.0 and the third region of BNS1.5 correspond to complete degradation of the matrix of activated carbon [16,18,47], which are finished at 819.2 °C (for BNS1.0) and 816.5°V (for BNS1.5). Then, the temperature is raised to 1000 °C; however, the weight loss is a minute loss of only about 0.41–0.44%, where all the carbon is eliminated, and only inorganic ashes are remained [16,46,48]. Therefore, the remaining residual mass at 1000 °C (respectively 0.28% and 0.16% for BNS1.0 and BNS1.5) are the inorganic ashes of the ACs, because the atmosphere utilized at this temperature was synthetic air [16].

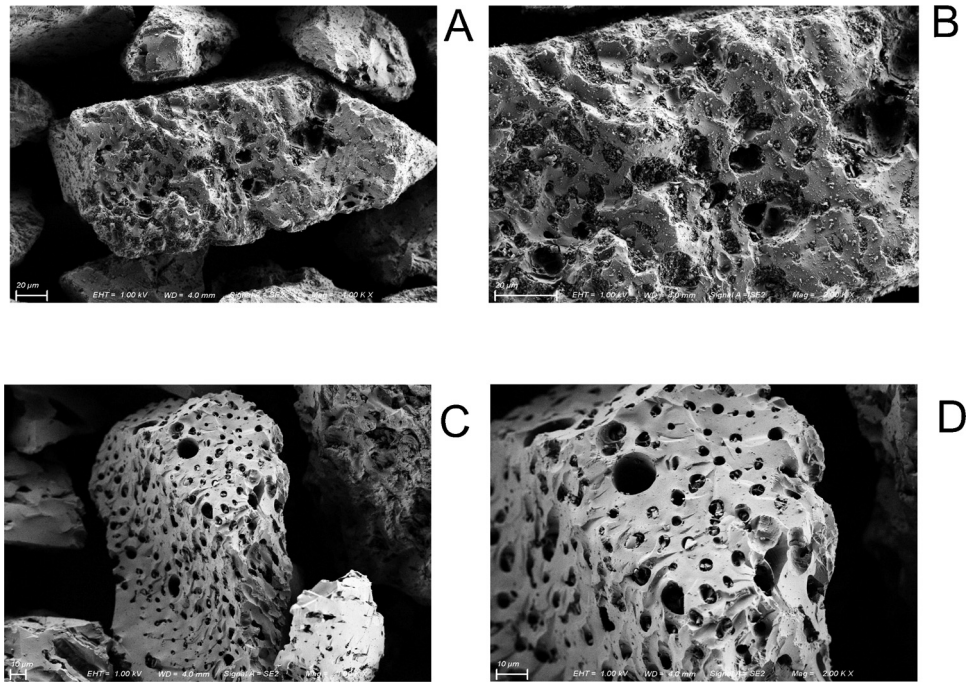

Fig. 3. SEM images of BNS 1.0 and magnification of ×1000 (A); BNS 1.0 and magnification of ×2000 (B); BNS 1.5 and magnification of ×1000 (C); and BNS 1.5 and magnification of ×2000 (D).

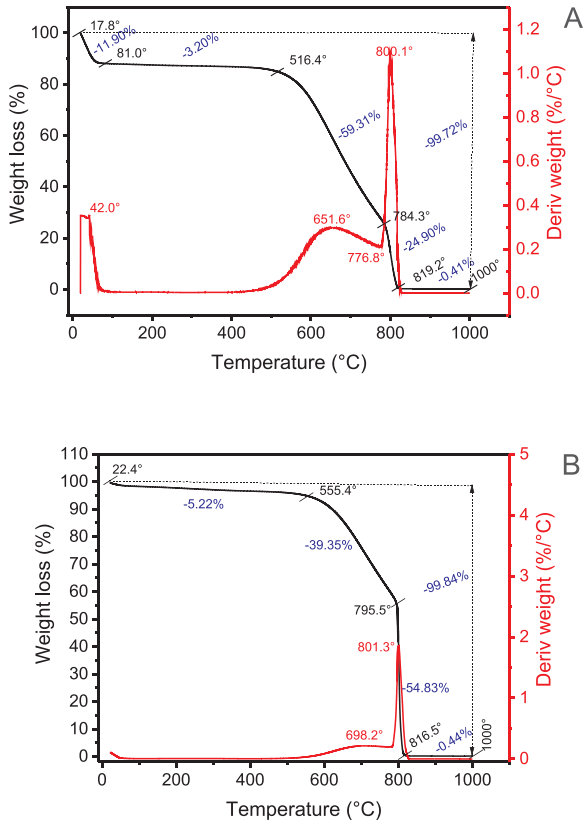

Fig. 4. Thermogravimetric (TG) and differential thermogravimetric curves (DTA) of A- BNS1.0; B- BNS-1.5.

3.5. Kinetic study of the adsorption

The kinetic study of adsorption was performed to establish the optimal time for adsorption of acetaminophen onto ACs made from Brazil nuts. Besides, kinetic studies also furnish information about the adsorption mechanism. The results show that the adsorption process is speedy, reaching the equilibrium around 10 min after contacting the BNS1.0 and BNS1.5 with acetaminophen solutions having the concentrations of 400 and 800 mg L^{-1} (Fig. 5). These results show that for both acetaminophen concentrations, there is a large number of active sites unoccupied to be fulfilled, leading to a high driving force for the mass transfer from the bulk solution to the surface of ACs, which results in fast adsorption to takes place [49,50]. The fastness of adsorption rate of acetaminophen onto ACs and the largeness of adsorption sites probably results from sizeable total pore volume and S_{BET} of the ACs. The hydrophilicity of the ACs also improves the accessibility of the acetaminophen molecules to the active sites and pores and interconnect porous structure, and the kinetics on the activated carbons are fast due to short diffusion path of ultrathin pores wall [49,50].

The acetaminophen molecule (see Supplementary Fig. 1) presents a maximum diagonal length of 0.88 nm, a dipole moment of 3.63 Debye (hydrophilic molecule), HLB (Hydrophilic-lipophilic balance) of 6.53–9.53, and Log P 0.49 (hydrophilic substance). Based on these physicochemical properties of acetaminophen, it is a compound of intermediate affinity to water and has some affinity to carbon surfaces; however, it also presents an affinity for carbon surfaces, facts that explain its adsorption onto activated carbon.

Concerning the kinetic models, three models were selected for fitting with the data, i.e., pseudo-first-order, pseudo-second-order, and Avrami models. The fitting results are summed up in Table 3. It illustrates that the kinetic data is more suitable to be characterized by the Avrami fractional-order model.

The extent of abiding the empirical data from the studied models was evaluated using the adjusted determination coefficient (R^2_{adj}), and standard deviation of residues (*SD*). Lower *SD* values and R^2_{adj} values nearer to 1.00 denote that the model is better abided by the data, and the difference between theoretical and experimental sorption capacities are negligible.

According to the kinetic data displayed in Table 3, the Avrami kinetic adsorption model is the best-fitted model and best describe the data obtained in the experiments, because Avrami model presented

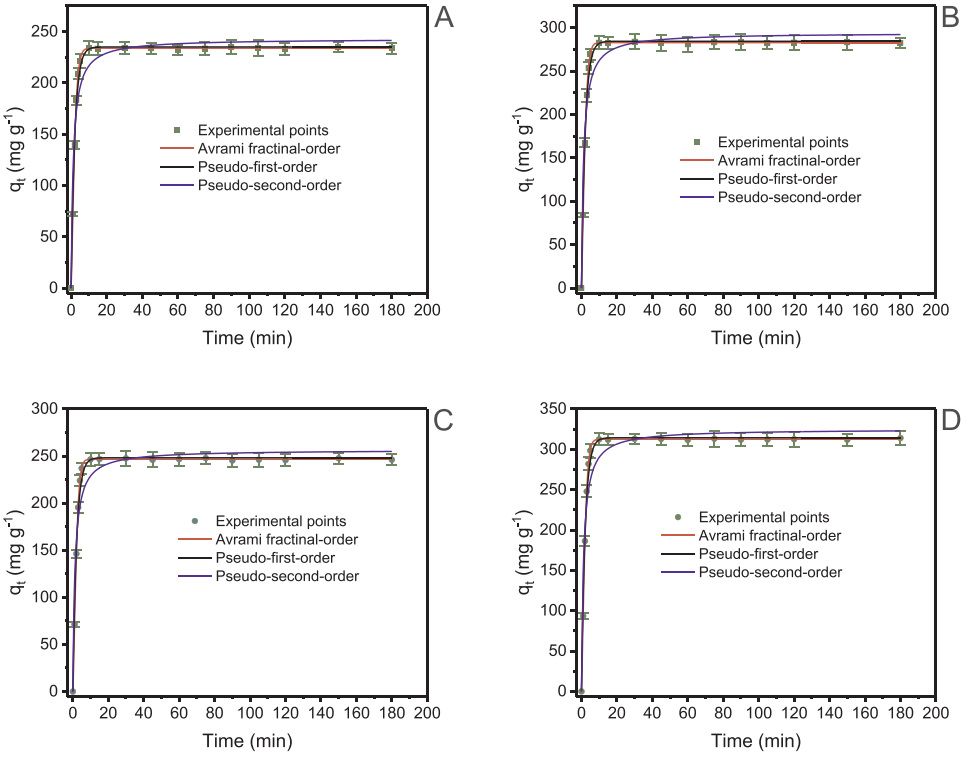

Fig. 5. Kinetic curves of adsorption of acetaminophen onto BNS1.0 and BNS1.5 activated carbons. A- 400 mg L^{-1} acetaminophen and BNS1.0; B- 800 mg L^{-1} acetaminophen and BNS1.0; C- 400 mg L^{-1} acetaminophen and BNS1.5; D- 800 mg L^{-1} acetaminophen and BNS1.5. Conditions: initial pH 7.0; adsorbent dosage 1.5 g L^{-1}, 25 °C.

Table 3
Avrami-fractional order, pseudo-first-order and pseudo-second-order parameters for adsorption of acetaminophen onto BNS1.0 and BNS1.5 adsorbents. Conditions adsorbent mass of 30 mg; initial pH of acetaminophen 7.0; the temperature of 25 °C. Values are expressed with four significant digits (average), and the standard error is given between parenthesis.

C_0 (mg L^{-1})	BNS1.0		BNS1.5	
	400	800	400	800
Avrami fractional-order				
q_e (mg g^{-1})	233.9 (0.2)	282.7 (0.2)	246.6 (0.2)	312.4 (0.2)
k_{AV} (min^{-1})	0.4630 (0.0018)	0.4604 (0.0016)	0.4631 (0.0018)	0.4656 (0.0012)
n_{AV}	1.295 (0.009)	1.341 (0.009)	1.398 (0.011)	1.354 (0.007)
$t_{1/2}$ (min)	1.627	1.652	1.662	1.638
$t_{0.95}$ (min)	5.04	4.924	4.732	4.831
R^2 adjusted	0.9999	0.9999	0.9999	0.9999
SD (mg g^{-1})	0.6734	0.7364	0.7298	0.6199
BIC	−5.412	−2.372	−2.676	−8.229
Pseudo-first-order				
q_e (mg g^{-1})	235.0 (1.7)	284.3 (2.4)	248.1 (2.4)	314.3 (2.7)
k_1 (min^{-1})	0.4721 (0.019)	0.4702 (0.021)	0.4744 (0.024)	0.4760 (0.021)
$t_{1/2}$ (min)	1.468	1.474	1.461	1.456
$t_{0.95}$ (min)	6.346	6.371	6.315	6.293
R^2_{adj}	0.9928	0.9908	0.9881	0.9903
SD (mg g^{-1})	5.732	7.883	7.883	8.946
BIC	65.74	76.57	76.57	80.87
Pseudo-second-order				
q_e(mg g^{-1})	243.0 (5.2)	294.0 (6.6)	256.6 (6.0)	324.9 (7.3)
k_2 (g mg^{-1} min^{-1})	0.003376 (0.0002)	0.002768 (0.0001)	0.0032 (0.0002)	0.002543 (0.0001)
$t_{1/2}$(min)	1.219	1.229	1.218	1.21
$t_{0.95}$ (min)	23.16	23.35	23.14	23
R^2_{adj}	0.9493	0.9449	0.9389	0.9438
SD (mg g^{-1})	15.26	19.33	17.83	21.56
BIC	99.02	107.1	104.3	110.8

lower *SD* values (0.6199 to 0.7364) and R^2_{adj} values nearer to unity (0.9999), for both BNS1.0 and BNS1.5 at two different initial concentrations of acetaminophen (Table 3). These results point out that the theoretical values of q_t calculated from the Avrami-fractional equation are the nearest to the experimental ones. Besides the evaluation of the nonlinear models using R^2_{adj} and SD values, the Bayesian Information Criterion (*BIC*) was also employed [36,37].

This statistical parameter gives a conclusive decision about what is the better physical model to be used. When the difference of BIC between two models is ≤2.0, the model with a lower number of parameters (simpler physical model) is the most suitable since this difference of BIC values (Δ BIC ≤2) is not relevant [37]. On the other hand, when Δ BIC is ≥ 10 for two different models, the one with the lower BIC value is undoubtedly the best-fitted model [37]. The Δ BIC values between the Avrami model and pseudo-first-order were 71.2–89.1, and the BIC differences between Avrami model and pseudo-second-order were 104.4-119.0. All these values are much higher than 10, therefore form the statistical point of view, the Avrami fractional model is the most suitable kinetic model for describing the kinetic data.

In Table 3 also is presented the $t_{1/2}$ and $t_{0.95}$ which were defined previously in several adsorption studies [16–18,47,50]. Knowing that the best-fitted model is the Avrami fractional-order model, the time to attain the half of saturation was computed which was around 1.6 min, and the time to attain 95% of saturation was around 5.0 min. Considering that it is essential to use a higher amount time of contact to guarantee the enoughness of time for equilibrium to be attained at higher concentrations of sorbing species, the contact time for further experiments was fixed at 30 min.

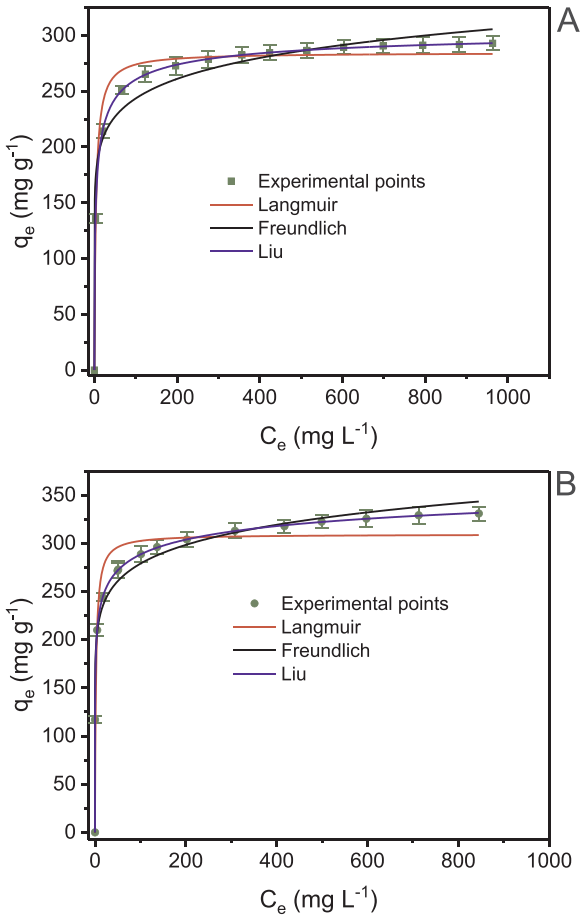

Fig. 6. Isotherms of adsorption of acetaminophen onto BNS1.0 and BNS1.5 activated carbons at 25 °C. A-BNS1.0; B-BNS-1.5. Conditions: initial pH 7.0; adsorbent dosage 1.5 g L^{-1}, time of contact fixed at 30 min.

3.6. Equilibrium models and recycling

There are several isotherm models described in the literature by which researchers analyze the equilibrium data. Liu, Langmuir, and Freundlich isotherms were used to model the adsorption equilibrium data of acetaminophen onto BNS1.0 and BNS1.5 activated carbons.

The adsorption equilibrium isotherms of acetaminophen onto both ACs at 25 °C are displayed in Fig. 6. Also, Table 4 contains the computed parameters for the studied isotherm models. From the results, the increase in the adsorption capacity (Q_{max} values) when increasing the temperature from 10° to 25 °C is apparent; however, the capacity suffers from a remarkable decrease when the temperature is raised from 25° to 45 °C. Otherwise, it is observed that the equilibrium constant (K) experienced a regular decrease as the temperature was raised. Such results denote that the adsorption process is of an exothermic kind [36,44], which will be more discussed in the next sections.

The goodness of fit of experimental equilibrium data with Langmuir, Freundlich, and Liu isotherms was evaluated using the R^2_{Adj}, *SD,* and *BIC* values.

In the light of R^2_{Adj}, *SD* and *BIC* values, the isothermal adsorption process is more suitable to be described with Liu model, because it is the highest R^2_{Adj} and the lowest *SD* and *BIC* values, in comparison with Langmuir and Freundlich models (see Table 4). This finding means that Langmuir and Freundlich's isotherms models do not offer a reasonable description of the process. Likewise, the *q* values provided by Liu model were closer to those obtained experimentally.

For the data of adsorption of acetaminophen onto BNS1.0, the Δ*BIC* values between the Langmuir and Liu model varied from 39.03 to 119.2

Table 4
Parameters of the isotherm of Langmuir, Freundlich and Liu models for the adsorption of acetaminophen onto BNS1.0 and BNS1.5 adsorbents. Conditions contact time of BNS1.0 and BNS1.5 and acetaminophen was adjusted at 30 min. Values are expressed with four significant digits (average), and the standard error is given between parenthesis.

BNS1.0						
Langmuir	10 °C	20 °C	25 °C	30 °C	40 °C	45 °C
Q_{max} (mg g^{-1})	229.9 (3.9)	243.5 (1.6)	284.6 (3.5)	232.8 (4.9)	236.0 (4.8)	232.6 (3.3)
K_L (L mg^{-1})	0.4480 (0.013)	0.2487 (0.009)	0.2569 (0.012)	0.8115 (0.041)	0.5126 (0.026)	0.1887 (0.006)
R^2_{adj}	0.9660	0.9943	0.9792	0.9334	0.9433	0.973
SD (mg g^{-1})	12.87	5.224	11.59	17.14	16.5	10.63
BIC	82.62	55.58	79.48	91.22	90.08	76.88
Freundlich						
K_F (mg g^{-1} (mg $L^{-1})^{-1/nF}$)	119.4 (3.7)	133.9 (5.4)	153.4 (5.4)	137.3 (4.2)	124.1 (4.3)	122.0 (6.1)
n_F	9.121 (0.37)	10.40 (0.49)	9.973 (0.51)	10.90 (0.47)	9.307 (0.52)	9.621 (0.48)
R^2_{adj}	0.9682	0.9481	0.9711	0.9913	0.9827	0.9833
SD (mg g^{-1})	12.45	15.72	13.67	6.199	9.127	8.354
BIC	81.62	88.63	84.43	60.71	72.31	69.66
Liu						
Q_{max} (mg g^{-1})	258.0 (4.6)	250.8 (0.4)	309.7 (0.5)	308.2 (1.4)	289.8 (0.8)	265.6 (0.9)
K_g (L mg^{-1})	0.2929 (0.009)	0.2483 (0.002)	0.2291 (0.002)	0.2072 (0.007)	0.1729 (0.003)	0.1581 (0.003)
n_L	0.4659 (0.002)	0.7264 (0.006)	0.5311 (0.004)	0.2803 (0.003)	0.3649 (0.003)	0.4552 (0.006)
R^2_{adj}	0.9977	0.9999	0.9999	0.9999	0.9999	0.9999
SD (mg g^{-1})	3.332	0.4885	0.4289	0.3064	0.3225	0.4777
BIC	43.59	−14.01	−17.91	−28.00	−26.46	−14.68
BNS1.5						
Langmuir	10 °C	20 °C	25 °C	30 °C	40 °C	45 °C
Q_{max} (mg g^{-1})	270.2 (4.6)	268.8 (2.8)	309.3 (8.7)	248.5 (3.6)	267.2 (3.9)	270.5 (6.2)
K_L (L mg^{-1})	0.3752 (0.011)	0.2896 (0.014)	0.4423 (0.022)	0.2661 (0.013)	0.2355 (0.012)	0.2465 (0.013)
R^2_{adj}	0.9632	0.9876	0.875	0.9713	0.9767	0.9589
SD (mg g^{-1})	14.90	8.853	32.61	11.79	12.44	18.53
BIC	87.03	71.4	110.5	80	81.62	93.56
Freundlich						
K_F (mg g^{-1} (mg $L^{-1})^{-1/nF}$)	150.2 (5.3)	137.6 (6.7)	177.9 (6.3)	135.4 (5.9)	126.3 (5.1)	119.5 (5.7)
n_F	10.11 (0.49)	8.971 (0.42)	10.25 (0.51)	10.08 (0.51)	8.153 (0.41)	7.291 (0.36)
R^2_{adj}	0.9785	0.9539	0.9848	0.9811	0.9579	0.9594
SD (mg g^{-1})	11.38	17.09	11.38	9.564	16.74	18.41
BIC	78.94	91.13	78.93	73.72	90.52	93.37
Liu						
Q_{max} (mg g^{-1})	306.6 (1.3)	284.5 (0.5)	411.0 (2.0)	281.3 (0.6)	292.3 (0.5)	313.4 (0.8)
K_g (L mg^{-1})	0.3172 (0.007)	0.2599 (0.002)	0.2405 (0.008)	0.2182 (0.002)	0.1784 (0.002)	0.1650 (0.003)
n_L	0.4341 (0.006)	0.6234 (0.005)	0.2689 (0.002)	0.4515 (0.003)	0.5573 (0.003)	0.4557 (0.003)
R^2_{adj}	0.9999	0.9999	0.9999	0.9999	0.9999	0.9999
SD (mg g^{-1})	0.7308	0.5156	0.5399	0.3305	0.4182	0.5362
BIC	−1.922	−12.39	−11.01	−25.73	−18.67	−11.21

and, its values between Freundlich and Liu model were from 38.03 to 102.6. For the data of adsorption of acetaminophen onto BNS1.5, the Δ BIC values between Langmuir and Liu models were from 83.79 to 121.5, and its values between Freundlich and Liu were 80.86 to 109.2.

It appears that all these *BIC* differences are much higher than 10. This result denotes that the Liu model was the most desirable equilibrium model which should be used to represent the experimental data.

Indeed, the Liu model is a mathematical combination of Langmuir and Freundlich isotherm models. The Liu model has three parameters, considering the adsorption sites as energetically different sites and occurrence of surface saturation.

Furthermore, the maximum adsorption capacities of acetaminophen onto BNS1.0 and BNS1.5 reached 309.7 and 411.0 mg/g, respectively, at 25 °C, as reported in Table 4. The S_{BET} surface area can explain the differences in the Q_{max} values obtained by BNS1.0 and BNS1.5 and, also, the total pore volume can be used for such explanation, as these values are higher in the BNS1.5. Besides, BNS1.5 presents a higher portion of pore size distribution at mesopore region (pores with a diameter ≥ 2 nm). Acetaminophen molecule presents a dimension of 0.887 nm (see Supplementary Fig. 1). In Fig. 1B, it is observed that BNS1.5 presents a portion of pore size distribution shifted to the mesopore region, and it does not present pores with size < 1 nm, unlike BNS1.0. Therefore, a higher sorption capacity is expected to be obtained for BNS1.5. Besides the textural characteristics of BNS1.5 are superior to BNS1.0, the former presents a higher HI (lower hydrophilicity behavior), and a lower total amount of functional groups on the surface (Table 2). Recently [12], it has been reported that higher HI values, the lower sum of acidic and basic groups in activated carbons leads to their higher affinity for adsorbing different emerging contaminants, such as acetaminophen.

Considering that BNS1.5 presented higher surface area and higher sorption capacity for acetaminophen, desorption of this specie from BNS1.5 activated carbon was investigated through applying continuous agitation of the system after it reached equilibrium with different eluent solutions. It appears from Table 5 that the mixture 0.5 M NaOH + 20% ETOH showed higher desorption efficiency among the thirteen solutions used as eluent. It is essential to notice that approximately 26% of acetaminophen remained adsorbed on the BNS1.5 pores. This result can be explained by the fact that some adsorbate molecules are seized in the pores of the material and are not removed by eluent. The desorption experiment also allows to state whether the interaction adsorbate – adsorbent was strengthened or not. Considering this result, it is possible also to state that the interaction adsorbent–acetaminophen molecule was weak. The mixture 0.5 M NaOH + 20% EtOH was further used for the recycling process.

As can be seen in Fig. 7, the produced activated carbon still has high adsorption properties even after four cycles of adsorption-desorption process. This proves a very good application of the activated carbon. However, it appeared also that the desorption efficiencies from the 2nd and 4th cycle were higher than the 1st. This uncommon observation is

Table 5
Desorption experiments of BNS1.5 for acetaminophen. Values are expressed with four significant digits (average), and the standard error is given between parenthesis.

Desorption solutions	Desorption percentage (%)
Water	20.76 (0.52)
0.1 M NaOH	66.79 (1.87)
0.2 M NaOH	64.80 (2.01)
0.3 M NaOH	62.29 (2.12)
0.4 M NaOH	59.80 (1.97)
1 M NaOH	54.88 (1.54)
1.5 M NaOH	51.26 (1.33)
2 M NaOH	42.00 (1.26)
2.5 M NaOH	35.68 (1.25)
0.1 M NaOH + 5% EtOH	69.55 (1.53)
0.1 M NaOH + 10% EtOH	70.48 (1.48)
0.1 M NaOH + 20% EtOH	73.99 (1.70)
0.1 M NaOH + 50% EtOH	70.87 (1.70)

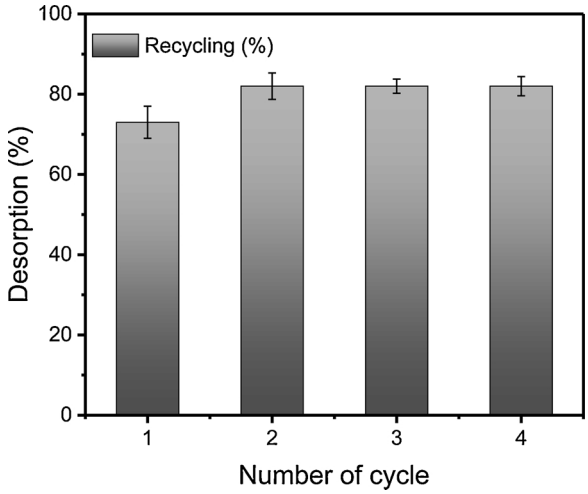

Fig. 7. Cycles of desorption of acetaminophen onto BNS1.5 activated carbon. Eluent: 0.5 mol L^{-1} NaOH + 20% ETOH.

consistent and can be explained in this way: At the second cycle of the adsorption-desorption process, the adsorption of acetaminophen molecules occurs more at the surface of BNS1.5 since the pores still contain the remaining adsorbate molecules seized within it in the 1st cycle. The same justification can be made for the 3rd and the 4th cycles. Therefore, the desorption efficiency was higher after the 1st cycle. However, it is crucial to notice that the desorption efficiency remain constant and do not increase any more after the 2nd cycle and reached 82%. This is due by the fact that almost all the molecules adsorbed during the adsorption process, are also desorbed. Thus, the recycling process ensures the potential application on a large scale of the produced material.

3.7. Comparison of adsorption capacities with those of different adsorbents

Table 6 shows the comparison of maximum sorption capacities (Q_{max}) of several adsorbents used in the removal of acetaminophen from aqueous media [22,51–60]. It appears from this data that the ACs prepared from Brazil nut shells presented Q_{max} values of 309.7 and 411.0 mg g^{-1}, which are the highest adsorption capacities amongst 16 different adsorbents. This result is significant because it indicates that the adsorbents prepared in this work could be very useful for the treatment of aqueous effluents containing pharmaceuticals.

3.8. Adsorption thermodynamics and mechanism of adsorption

For the adsorption processes, in order to infer whether the process is spontaneous or not, both energy and entropy changes should be considered. Practical application of a process for large-scale treatment plants also can be inferred from the calculated values of thermodynamic parameters. The change in Gibbs free energy (ΔG°, kJ mol^{-1}), enthalpy (ΔH°, kJ mol^{-1}) and entropy (ΔS°, J mol^{-1} K^{-1}) are important thermodynamic parameters which can act as crucial indicators for such assessments. The values obtained from these parameters also determine and explain if the adsorption process has an exothermic or endothermic nature [36,44].

In order to deduce these thermodynamic parameters for adsorption of acetaminophen on both ACs, experiments were conducted at temperatures varying from 283 to 318 K (10–45 °C), and the values of these thermodynamic parameters were depicted in Table 7 [36,44]. Details about how these parameters were obtained have been included in Supplementary material.

The results in Table 7 shows that, for both ACs, the values of ΔS° and ΔG° are positive and negative, respectively, denoting that the adsorption of acetaminophen occurs spontaneously and is favorable at 283–318 K for both ACs [34]. Also, positive ΔS° denotes that, at the solid/liquid interface, an increase in randomness happens during the occurrence of adsorption.

The negative value of ΔH° implies that the adsorption is exothermic. ΔH° values ≤ 40 kJ mol^{-1} means that the process is of a physical type [61].

Based on the adsorption studies discussed previously, a proposal of the mechanism of adsorption of acetaminophen onto the ACs could be given. This mechanism should occur by hydrogen bonds, electron donor-acceptor, $\pi-\pi$ interactions, and dispersion interactions [16–18]. In the surfaces of activated carbons are present polar groups such as −O, −COO, −OH, and −NH, (see Table 2 and Fig. 3) and these groups could interact with the O−H, and N−H group of acetaminophen molecules forming hydrogen bonds [16]. Acetaminophen adsorption on BNS1.0 and BNS1.5 carbon could also take place by $\pi-\pi$ interactions (between the π electrons of the aromatic ring in acetaminophen (see Supplementary Fig. 1) with the π electrons of the aromatic rings of the activated carbons, and “donor-acceptor complex” formation between the carbonyl groups (electron donors) on the ACs surfaces and the aromatic ring of acetaminophen acting as the electron acceptor. Also, dispersion interactions of C–H of acetaminophen with C−C of activated carbon can take place [62].

3.9. Treatment of a simulated effluent

The effectiveness of the activated carbons obtained from Brazil nutshells as carbon sources in the treatment of simulated hospital effluents was also evaluated in this work. Such effluents are composed of several emerging pollutants plus many other chemicals that are

Table 6
Comparison of adsorption capacities of different adsorbents for acetaminophen.

Adsorbent	Q_{max}	References
Pyrolyzed pulp mill sludge	19.74	[22]
MCM-41	121.9	[51]
Oak fruits	45.45	[51]
sludge-based activated carbon	58.73	[52]
biomass-derived activated carbon	100.0	[53]
AC from industrial pre-treated cork	118.6	[54]
Activated carbons from sisal waste	190.0	[55]
Magnetic activated carbon	147.1	[56]
Grape stalk	2.18	[57]
Activated carbons from plastics wastes	137.0	[57]
Activated carbons from urban residues	159.0	[58]
AC Prepared from Rice Husk	20.96	[59]
Polymeric resin	6.90	[60]
Commercial Activated carbon	235.0	[60]
BNS1.0	309.7	This work
BNS1.5	411.0	This work

Table 7
Thermodynamic parameters of the adsorption of emerging pollutant acetaminophen onto BNS1.0 and BNS1.5 adsorbents. Values are expressed with four significant digits (average), and the standard error is given between parenthesis.

Temperature (K)	283	293	298	303	313	318
BNS1.0						
K_g (L mol^{-1})	4.427.10^4 (0.1360.10^4)	3.753.10^4 (0.0302.10^4)	3.463.10^4 (0.0302.10^4)	3.131.10^4 (0.1058.10^4)	2.613.10^4 (0.0453.10^4)	2.390.10^4 (0.0453.10^4)
$\Delta G°$ (kJ mol^{-1})	−25.17 (0.77)	−25.66 (0.21)	−25.90 (0.23)	−26.08 (0.88)	−26.47 (0.46)	−26.65 (0.51)
$\Delta H°$ (kJ mol^{-1})	–	–	−13.66 (0.40)	–	–	–
$\Delta S°$ (J K^{-1} mol^{-1})	–	–	40.97 (1.32)	–	–	–
R^2_{adj}	–	–	0.9957	–	–	–
BNS1.5						
K_g (L mol^{-1})	4.795.10^4 (0.1072.10^4)	3.929.10^4 (0.0302.10^4)	3.635.10^4 (0.1209.10^4)	3.298.10^4 (0.0302.10^4)	2.697.10^4 (0.0302.10^4)	2.494.10^4 (0.0453.10^4)
$\Delta G°$ (kJ mol^{-1})	−25.36 (0.57)	−25.77 (0.20)	−26.02 (0.87)	−26.21 (0.24)	−26.55 (0.30)	−26.77 (0.49)
$\Delta H°$ (kJ mol^{-1})	–	–	−14.10 (0.35)	–	–	–
$\Delta S°$ (J K^{-1} mol^{-1})	–	–	39.87 (1.16)	–	–	–
R^2_{adj}	–	–	0.9975	–	–	–

commonly found in hospital effluents. The chemical contents of the studied effluents are shown in Table 1. The results of the treatment of the simulated effluents might be essential to verify the adequacy of BNS1.0 and BNS1.5 in real treatment plants of hospital wastewaters.

The UV–vis spectra of the effluents before adsorption and after adsorption (190–400 nm) were used to determine the removed amounts of the compounds from simulated effluents (Fig. 8). The UV–vis bands were used to calculate the total percentage of removal of all organic compounds for each effluent, through an integration method of the areas [17,45]. Performing the integration of the area under the UV–vis band of the treated effluent and dividing it by the area under the curve of the initial effluent, it is possible to calculate the total removal of organic compounds present in the effluents [17,45]. For effluent 1, the total removals obtained were 98.29% and 98.83% for BNS1.0 and BNS1.5, respectively. For effluent 2, the removal amounts were 96.38 and 97.04% for BNS1.0 and BNS1.5, respectively. Using the chemometric approach previously reported in the literature [45], the concentration of acetaminophen found in the effluents after the adsorption was 0.32 and 0.36 for effluents 1 and 2 using BNS1.0 adsorbent, and below the detection limit (see Supplementary material) for both effluents using BNS1.5 adsorbent.

The performance of BNS1.5 is slightly better than BNS1.0 for the treatment of effluents 1 and 2 (see Table 1). Such a result is consistent with the porosity and physical properties of the ACs, already discussed earlier. Besides, the results provided by Fig. 7 also match with the results of the total functional groups, and HI, which discussed previously. In comparison to BNS1.0, BNS1.5 presents higher S_{BET} and well-developed porosity, which lead to higher efficiencies in treating simulated effluents, showing its higher potential for being applied in real wastewater treatments. In light of these results, it is possible to state that Brazil nutshell is an excellent raw material for producing efficient ACs which can be successfully used in the treatment of real hospital effluent.

4. Conclusion

The high surface area activated carbons obtained from Brazil nutshells as carbon source was successfully prepared under chemical activation with $ZnCl_2$. These carbon materials were applied for acetaminophen removal from aqueous effluents as well for treating simulated hospital effluents.

The N_2 physisorption showed that the SBET values of the BNS1.0 and BNS1.5 are very high, 1457 and 1639 $m^2 g^{-1}$ respectively. The FTIR and Boehm titration analysis has demonstrated the presence of several surface groups on both AC surfaces, which can influence the acetaminophen adsorption.

The adsorption studies revealed that the maximum adsorption capacities (Q_{max}) are very high for both ACs. However, the BNS1.5 capacity is higher (411.0 mg g^{-1}) than that of BNS1.0 (309.7 mg g^{-1}), which can be stemmed back from a difference in the porosity and S_{BET} values. These values reveal that the maximum sorption capacities (Q_{max}) of BNS1.0 and BNS1.5 are higher when compared with other adsorbents reported in the literature for adsorption of acetaminophen. The preparation method of chemical activation forming a paste of biomass with zinc salts with no excess of water, carbonizing it under an inert atmosphere, and carrying out a leaching procedure with HCl, leads to activated carbon with better textural characteristics that leads improvement in the sorption capacities obtained.

The thermodynamic assessments revealed that the adsorption of acetaminophen was spontaneous and favorable and the interactions between adsorbate and adsorbent could occur by physical forces such as

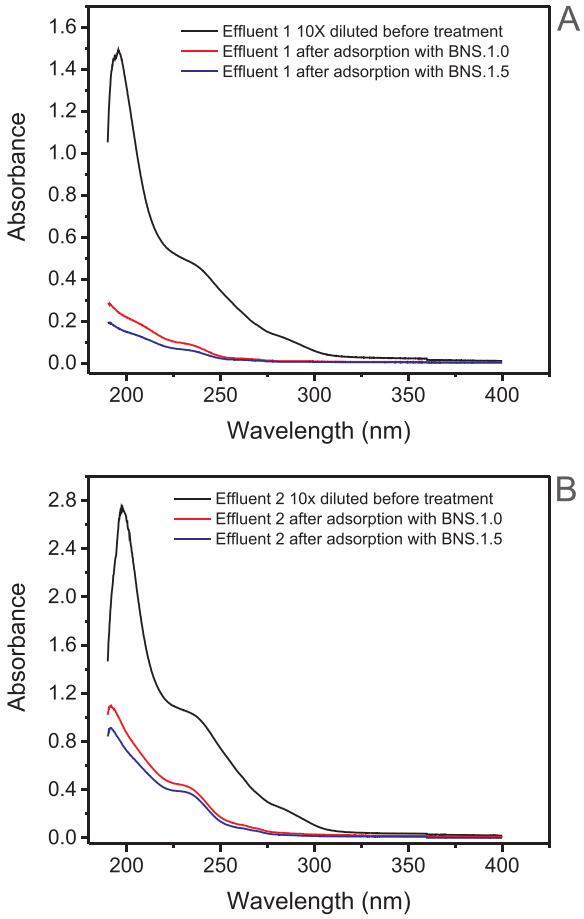

Fig. 8. Use of BNS1.0 and BNS1.5 as adsorbents for treatment of simulated. hospital effluents. A-Effluent 1; B- Effluent 2. For composition of effluents, see Table 1.

hydrogen bond, electron donor-acceptor, π-π interactions, and dispersion interactions.

The use of BNS1.0 and BNS1.5 for treating simulated hospital wastewaters, containing several pharmaceuticals, organics, and inorganic salts, presented up to 98.83% of total removal. The adsorbent was magnificently regenerated up to 74% with a mixture of NaOH 0.1 M + 20% EtOH solution and can be reused up to four cycles ensuring sustainable use of proposed adsorbent for acetaminophen removal from aqueous media. In light of these results, it is possible to say that Brazil nutshell is an excellent raw material for the production of efficient ACs with promissory application in the treatment of hospital wastewaters.

Acknowledgments

The authors thank the Foundation for Research Support of the State of Rio Grande do Sul (FAPERGS), National Council for Scientific and Technological Development (CNPq, Brazil) and Coordination of Improvement of Higher Education Personnel (CAPES, Brazil) for financial support and sponsorship. Dr. Glaydson Simões Dos Reis and Pascal Silas Thue are grateful to the CAPES for the postdoctoral scholarship granted through the National Postdoctoral Program (PNPD). Authors are grateful to Nanoscience and Nanotechnology Center (CNANO-UFRGS), and Microscopy and Microanalysis Center (CME-UFRGS) of Federal University of Rio Grande do Sul (UFRGS). We are also grateful to Chemaxon for giving us an academic research license for the Marvin Sketch software, Version 19.16.0, (http://www.chemaxon.com), 2019 used for molecule physical-chemical properties.

Appendix A. Supplementary data

Supplementary material related to this article can be found, in the online version, at doi:https://doi.org/10.1016/j.colsurfa.2019.123966.

References

[1] M. Taheran, M. Naghdi, S.K. Brar, M. Verma, R.Y. Surampalli, Emerging contaminants: here today, there tomorrow!, Environ. Nanotechnol. Monit. Manag. 10 (2018) 122–126.
[2] S. Sauve, M. Desrosiers, A review of what is an emerging contaminant, Chem. Cent. J. 8 (2014) 1–7.
[3] S. Kim, K.H. Chu, Y.A.J. Al-Hamadani, C.M. Park, Min Jang, D.H. Kim, M. Yu, J. Heo, Y. Yoon, Removal of contaminants of emerging concern by membranes in water and wastewater: a review, Chem. Eng. J. 335 (2018) 896–914.
[4] C.A. Sophia, E.C. Lima, Removal of emerging contaminants from the environment by adsorption, Ecotoxicol. Environ. Saf. 150 (2018) 1–17.
[5] J. Żur, D. Wojcieszyńska, K. Hupert-Kocurek, A. Marchlewicz, U. Guzik, Paracetamol – toxicity, and microbial utilization. *Pseudomonas moorei* KB4 as a case study for exploring the degradation pathway, Chemosphere 206 (2018) 192–202.
[6] N. Pi, J.Z. Ng, B.C. Kelly, Bioaccumulation of pharmaceutically active compounds and endocrine-disrupting chemicals in aquatic macrophytes: results of hydroponic experiments with *Echinodorus horemanii* and *Eichhornia crassipes*, Sci. Total Environ. 601–602 (2017) 812–820.
[7] W.C. Yun, K.Y.A. Lin, W.C. Tong, Y.F. Lin, Y. Du, Enhanced degradation of paracetamol in water using sulfate radical-based advanced oxidation processes catalyzed by 3-dimensional Co_3O_4 nanoflower, Chem. Eng. J. 373 (2019) 1329–1337.
[8] S.O. Ganiyu, N. Oturan, S. Raffy, M. Cretin, C. Causserand, M.A. Oturan, Efficiency of plasma elaborated sub-stoichiometric titanium oxide (Ti4O7) ceramic electrode for advanced electrochemical degradation of paracetamol in different electrolyte media, Sep. Purif. Technol. 208 (2019) 142–152.
[9] D. Dionisi, C.C. Etteh, Effect of process conditions on the aerobic biodegradation of phenol and paracetamol by open mixed microbial cultures, J. Environ. Chem. Eng. 7 (2019) 103282, , https://doi.org/10.1016/j.jece.2019.10328.
[10] M. Nadour, F. Boukraa, A. Benaboura, Removal of Diclofenac, Paracetamol and Metronidazole using a carbon-polymeric membrane, J. Environ. Chem. Eng. 7 (2019) 103080, , https://doi.org/10.1016/j.jece.2019.103080.
[11] J. Li, Q. Zhou, L.C. Campos, The application of GAC sandwich slow sand filtration to remove pharmaceuticals and personal care products, Sci. Total Environ. 635 (2018) 1182–1190.
[12] A.B. Leite, C. Saucier, E.C. Lima, G.S. dos Reis, C.S. Umpierres, B.L. Mello, M. Shirmardi, S.L.P. Dias, C.H. Sampaio, Activated carbons from avocado seed: optimization and application for removal several emerging organic compounds, Environ. Sci. Pollut. Res. 25 (2018) 7647–7661.
[13] L. Spessato, K.C. Bedin, A.L. Cazetta, I.P.A.F. Souza, V.A. Duarte, L.H.S. Crespo, M.C. Silva, R.M. Pontes, V.C. Almeida, KOH-super activated carbon from biomass waste: insights into the paracetamol adsorption mechanism and thermal regeneration cycles, J. Hazard. Mater. 371 (2019) 499–505.
[14] S. Wong, Y. Lim, N. Ngadi, R. Mat, O. Hassan, I.M. Inuwa, N.B. Mohamed, J.H. Low, Removal of acetaminophen by activated carbon synthesized from spent tea leaves: equilibrium, kinetics and thermodynamics studies, Powder Technol. 338 (2018) 878–886.
[15] S. Rovani, M.T. Censi, S.L. Pedrotti-Jr, E.C. Lima, R. Cataluña, A.N. Fernandes, Development of a new adsorbent from agro-1 industrial waste and its potential use in endocrine disruptor compound removal, J. Hazard. Mater. 271 (2014) 311–320.
[16] M.R. Cunha, E.C. Lima, N.F.G.M. Cimirro, P.S. Thue, S.L.P. Dias, M.A. Gelesky, G.L. Dotto, G.S. dos Reis, F.A. Pavan, Conversion of *Eragrostis plana Nees* leaves to activated carbon by microwave-assisted pyrolysis for the removal of organic emerging contaminants from aqueous solutions, Environ. Sci. Pollut. Res. 25 (2018) 23315–23327.
[17] F.M. Kasperiski, E.C. Lima, C.S. Umpierres, G.S. dos Reis, P.S. Thue, D.R. Lima, S.L.P. Dias, C. Saucier, J.B. da Costa, Production of porous activated carbons from *Caesalpinia ferrea* seed pod wastes: highly efficient removal of captopril from aqueous solutions, J. Clean. Prod. 197 (2018) 919–929.
[18] C.S. Umpierres, P.S. Thue, G.S. dos Reis, I.A.S. de Brum, E.C. Lima, W.A. de Alencar, S.L.P. Dias, G.L. Dotto, Microwave activated carbons from Tucumã (Astrocaryum aculeatum) waste for efficient removal of 2- nitrophenol from aqueous solutions, Environ. Technol. 39 (2018) 1173–1187.
[19] K. Li, Z. Rong, Y. Li, C. Li, Z. Zheng, Preparation of nitrogen-doped cotton stalk microporous activated carbon fiber electrodes with a different surface area from hexamethylenetetramine-modified cotton stalk for electrochemical degradation of methylene blue, Results Phys. 7 (2017) 656–664.
[20] J. Lladó, Montserrat Solé-Sardans, Conxita Lao-Luque, E. Fuente, B. Ruiz, Removal of pharmaceutical industry pollutants by coal-based activated carbons, Process Saf. Environ. Prot. 104 (2016) 294–303.
[21] M.J. Puchana-Rosero, M.A. Adebayo, E.C. Lima, F.M. Machado, P.S. Thue, J.C.P. Vaghetti, C.S. Umpierres, M. Gutterres, Microwave-assisted activated carbon obtained from the sludge of tannery-treatment effluent plant for removal of leather dyes, Colloids Surf. A Physicochem. Eng. Asp. 504 (2016) 105–115.
[22] R.N. Coimbra, V. Calisto, C.I.A. Ferreira, V.I. Esteves, M. Otero, Removal of pharmaceuticals from municipal wastewater by adsorption onto pyrolyzed pulp mill sludge, Arab. J. Chem. (2015), https://doi.org/10.1016/j.arabjc.2015.12.001.
[23] A.C. Baquião, P. Zorzete, T.A. Reis, E. Assunção, S. Vergueiro, B. Correa, Mycoflora and mycotoxins in field samples of Brazil nuts, Food Control 28 (2012) 224–229.
[24] J. Yang, Brazil nuts and associated health benefits: a review, Food Sci. Technol. 42 (2009) 1573–1580.
[25] M. Thommes, K. Kaneko, A.V. Neimark, J.P. Olivier, F. Rodriguez-Reinoso, J. Rouquerol, K.S.W. Sing, Physisorption of gases, with special reference to the evaluation of surface area and pore size distribution (IUPAC Technical Report), Pure Appl. Chem. 87 (2015) 1051–1069.
[26] J. Jagiello, M. Thommes, Comparison of DFT characterization methods based on N_2, Ar, CO_2, and H_2 adsorption applied to carbons with various pore size distributions, Carbon 42 (2004) 1227–1232.
[27] G.S. dos Reis, C.H. Sampaio, E.C. Lima, M. Wilhelm, Preparation of novel adsorbents based on combinations of polysiloxanes and sewage sludge to remove pharmaceuticals from aqueous solutions, Colloids Surf. A: Physicochem. Eng. Asp. 497 (2016) 304–315.
[28] P.R. Souza, G.L. Dotto, N.P.G. Salau, Artificial neural network (ANN) and adaptive neuro-fuzzy interference system (ANFIS) modelling for nickel adsorption onto agro-wastes and commercial activated carbon, J. Environ. Chem. Eng. 6 (2018) 7152–7160.
[29] P.S. Thue, A.C.A. Sophia, E.C. Lima, A.G.N. Wamba, W.S. de Alencar, G.S. dos Reis, F.S. Rodembusch, S.L.P. Dias, Synthesis and characterization of a novel organic-inorganic hybrid clay adsorbent for the removal of Acid Red 1 and Acid Green 25 from aqueous solutions, J. Clean. Prod. 171 (2018) 30–44.
[30] Y.S. Kim, S.J. Yang, H.J. Lim, T. Kim, K. Lee, C.R. Park, Effects of carbon dioxide and acidic carbon compounds on the analysis of Boehm titration curves, Carbon 50 (2012) 1510–1516.
[31] E.C. Lima, F. Barbosa-Jr, F.J. Krug, U. Guaita, Tungsten-rhodium permanent chemical modifier for lead determination in digests of biological materials and sediments by electrothermal atomic absorption spectrometry, J. Anal. At. Spectrom. 14 (1999) 1601–1605.
[32] E.C. Lima, R.V. Barbosa, J.L. Brasil, A.H.D.P. Santos, Evaluation of different permanent modifiers for the determination of arsenic, cadmium, and lead in environmental samples by electrothermal atomic absorption spectrometry, J. Anal. At. Spectrom. 17 (2002) 1523–1529.
[33] E.C. Lima, F. Barbosa Jr., F.J. Krug, The use of tungsten–rhodium permanent chemical modifier for cadmium determination in decomposed samples of biological materials and sediments by electrothermal atomic absorption spectrometry, Anal. Chim. Acta 409 (2000) 267–274.
[34] E.C. Lima, F.J. Krug, J.A. Nóbrega, A.R.A. Nogueira, Determination of ytterbium in animal faeces by tungsten coil electrothermal atomic absorption spectrometry, Talanta 47 (1998) 613–623.
[35] E.C. Lima, P.G. Fenga, J.R. Romero, Wagner F. de Giovani, Electrochemical behaviour of $[Ru(4,4'\text{-}Me_2bpy)_2(PPh_3)(H_2O)](ClO_4)_2$ in homogeneous solution and incorporated into carbon paste electrodes. Application to oxidation of benzylic compounds, Polyhedron 17 (1998) 313–318.
[36] E.C. Lima, M.A. Adebayo, F.M. Machado, Kinetic and equilibrium models of adsorption, Chapter 3, in: C.P. Bergmann, F.M. Machado (Eds.), Carbon Nanomaterials as Adsorbents for Environmental and Biological Applications, Springer International Publishing, 2015, pp. 33–69.
[37] G.E. Schwarz, Estimating the dimension of a model, Ann. Stat. 6 (1978) 461–464.

[38] S. Lagergren, About the theory of so-called adsorption of soluble substances, Kungliga Suensk Vetenskapsakademiens Handlingar 241 (1898) 1–39.
[39] G. Blanchard, M. Maunaye, G. Martin, Removal of heavy metals from waters by means of natural zeolites, Water Res. 18 (1984) 1501–1507.
[40] E.C.N. Lopes, F.S.C. dos Anjos, E.F.S. Vieira, A.R. Cestari, An alternative Avrami equation to evaluate kinetic parameters of the interaction of Hg(II) with thin chitosan membranes, J. Colloid Interface Sci. 263 (2003) 542–547.
[41] I. Langmuir, The adsorption of gases on plane surfaces of glass, mica, and platinum, J. Am. Chem. Soc. 40 (1918) 1361–1403.
[42] H.M.F. Freundlich, Adsorption in solution, Phys. Chem. Soc. 40 (1906) 1361–1368.
[43] Y. Liu, H. Xu, S.F. Yang, J.H. Tay, A general model for biosorption of Cd^{2+}, Cu^{2+}, and Zn^{2+} by aerobic granules, J. Biotechnol. 102 (2003) 233–239.
[44] E.C. Lima, A. Hosseini-Bandegharaei, J.C. Moreno-Piraján, I. Anastopoulos, A critical review of the estimation of the thermodynamic parameters on adsorption equilibria. Wrong use of equilibrium constant in the Van't Hoof equation for calculation of thermodynamic parameters of adsorption, J. Mol. Liq. 273 (2019) 425–434.
[45] D.R. Lima, A.A. Gomes, E.C. Lima, C.S. Umpierres, P.S. Thue, J.C.P. Panzenhagen, G.L. Dotto, G.A. El-Chaghaby, W.S. de Alencar, Evaluation of efficiency and selectivity in the sorption process assisted by chemometric approaches: removal of emerging contaminants from water, Spectrochim. Acta Part A 218 (2019) 366–373.
[46] W.J. Liu, K. Tian, H. Jiang, H.Q. Yu, Facile synthesis of highly efficient and recyclable magnetic solid acid from biomass waste, Sci. Rep.-Uk 3 (2013) 2419, https://doi.org/10.1038/srep02419.
[47] P.S. Thue, M.A. Adebayo, E.C. Lima, J.M. Sieliechi, F.M. Machado, G.L. Dotto, J.C.P. Vaghetti, S.L.P. Dias, Preparation, characterization, and application of microwave-assisted activated carbons from wood chips for removal of phenol from aqueous solution, J. Mol. Liq. 223 (2016) 1067–1080.
[48] P.S. Thue, E.C. Lima, J.M. Sieliechi, C. Saucier, S.L.P. Dias, J.C.P. Vaghetti, F.S. Rodembusch, F.A. Pavan, Effects of first–row transition metals and impregnation ratios on the physicochemical properties of microwave-assisted activated carbons from wood biomass, J. Colloid Interface Sci. 486 (2017) 163–175.
[49] S. Zhang, M. Zeng, J. Li, J. Li, J. Xu, X. Wang, Porous magnetic carbon sheets from biomass as an adsorbent for the fast removal of organic pollutants from aqueous solution, J. Mater. Chem. A 2 (2014) 4391–4397.
[50] A.G.N. Wamba, E.C. Lima, S.K. Ndi, P.S. Thue, J.G. Kayem, F.S. Rodembusch, G.S. dos Reis, W.S. de Alencar, Synthesis of grafted natural pozzolan with 3-aminopropyltriethoxysilane: preparation, characterization, and application for removal of Brilliant Green 1 and Reactive Black 5 from aqueous solutions, Environ. Sci. Pollut. Res. 24 (2017) 21807–21820.
[51] S.O. Akpotu, B. Moodley, Application of as-synthesised MCM-41 and MCM-41 wrapped with reduced graphene oxide/graphene oxide in the remediation of acetaminophen and aspirin from the aqueous system, J. Environ. Manage. 209 (2018) 205–215.
[52] H. Nourmoradi, K.F. Moghadam, A. Jafari, B. Kamarehie, Removal of acetaminophen and ibuprofen from aqueous solutions by activated carbon derived from Quercus brantii (Oak) acorn as a low-cost biosorbent, J. Environ. Chem. Eng. 6 (2018) 6807–6815.
[53] F.J. García-Mateos, R. Ruiz-Rosas, M.D. Marqués, L.M. Cotoruelo, J. Rodríguez-Mirasol, T. Cordero, Removal of paracetamol on biomass-derived activated carbon: modeling the fixed bed breakthrough curves using batch adsorption experiments, Chem. Eng. J. 279 (2015) 18–30.
[54] A.S. Mestre, R.A. Pires, I. Aroso, E.M. Fernandes, M.L. Pinto, R.L. Reis, M.A. Andrade, J. Pires, S.P. Silva, A.P. Carvalho, Activated carbons prepared from industrial pre-treated cork: sustainable adsorbents for pharmaceutical compounds removal, Chem. Eng. J. 253 (2014) 408–417.
[55] A.S. Mestre, A.S. Bexiga, M. Proença, M. Andrade, M.L. Pinto, I. Matos, I.M. Fonseca, A.P. Carvalho, Activated carbons from sisal waste by chemical activation with K_2CO_3: kinetics of paracetamol and ibuprofen removal from aqueous solution, Bioresour. Technol. 102 (2011) 8253–8260.
[56] L. Sellaoui, E.C. Lima, G.L. Dotto, A.B. Lamine, Adsorption of amoxicillin and paracetamol on modified activated carbons: equilibrium and positional entropy studies, J. Mol. Liq. 234 (2017) 375–381.
[57] I. Villaescusa, N. Fiol, J. Poch, A. Bianchi, C. Bazzicalupi, Mechanism of paracetamol removal by vegetable wastes: the contribution of π–π interactions, hydrogen bonding, and hydrophobic effect, Desalination 270 (2011) 135–142.
[58] I. Cabrita, B. Ruiz, A.S. Mestre, I.M. Fonseca, A.P. Carvalho, C.O. Ania, Removal of an analgesic using activated carbons prepared from urban and industrial residues, Chem. Eng. J. 163 (2010) 249–255.
[59] N.A.G. Nche, A. Bopda, D.R.T. Tchuifon, C.S. Ngakou, I.-H.T. Kuete, A.S. Gabche, Removal of paracetamol from aqueous solution by adsorption onto activated carbon prepared from rice husk, J. Chem. Pharm. Res. 9 (3) (2017) 56–68.
[60] R.N. Coimbra, C. Escapa, M. Otero, Adsorption separation of analgesic pharmaceuticals from ultrapure and waste water: batch studies using a polymeric resin and an activated carbon, Polymers 10 (2018) 958, https://doi.org/10.3390/polym10090958.
[61] R. Chang, J.W. Thoman Jr., Intermolecular forces, Chapter 17, Physical Chemistry for Chemical Sciences, University Science Books, 2014, pp. 779–808.
[62] P. Lipkowski, A. Koll, A. Karpfen, P. Wolschann, An approach to estimate the energy of the intramolecular hydrogen bond, Chem. Phys. Lett. 10 (2002) 256–263.

Journal of Environmental Chemical Engineering 9 (2021) 105865

Contents lists available at ScienceDirect

Journal of Environmental Chemical Engineering

journal homepage: www.elsevier.com/locate/jece

Comparison of acidic leaching using a conventional and ultrasound-assisted method for preparation of magnetic-activated biochar

Diana R. Lima [a], Eder C. Lima [a,b,c,*], Pascal S. Thue [a,c], Silvio L.P. Dias [b,c], Fernando M. Machado [d], Moaaz K. Seliem [e], Farooq Sher [f], Glaydson S. dos Reis [g], Mohammad Reza Saeb [h], Jörg Rinklebe [i,j]

[a] Postgraduate program in Mine, Metallurgical, and Materials Engineering (PPGE3M). School of Engineering, Federal University of Rio Grande do Sul (UFRGS), Av. Bento Gonçalves 9500, Porto Alegre, RS, Brazil
[b] Institute of Chemistry, Federal University of Rio Grande do Sul (UFRGS), Av. Bento Goncalves 9500, Postal Box, 15003, Porto Alegre, RS 91501-970, Brazil
[c] Postgraduate program in Science of Materials (PGCIMAT). Institute of Chemistry, Federal University of Rio Grande do Sul (UFRGS), Av. Bento Gonçalves 9500, Porto Alegre, RS 91501-970, Brazil
[d] Technology Development Center, Federal University of Pelotas, 1 Gomes Carneiro St., 96010-610 Pelotas, RS, Brazil
[e] Faculty of Earth Science, Beni-Suef University, 62511, Egypt
[f] Department of Engineering, School of Science and Technology, Nottingham Trent University, Nottingham NG11 8NS, UK
[g] Swedish University of Agricultural Sciences, Department of Forest Biomaterials and Technology, Biomass Technology Centre, SE-901 83 Umeå, Sweden
[h] Center of Excellence in Electrochemistry, School of Chemistry, College of Science, University of Tehran, Tehran, Iran
[i] University of Wuppertal, School of Architecture and Civil Engineering, Institute of Foundation Engineering, Water, and Waste-Management, Laboratory of Soil, and Groundwater-Management, Pauluskirchstraße 7, 42285 Wuppertal, Germany
[j] University of Sejong, Department of Environment, Energy and Geoinformatics, Guangjin-Gu, Seoul 05006, Republic of Korea

ARTICLE INFO

Editor: Dr. GL Dotto

Keywords:
Biochar
Ultrasound-assisted-leaching
Materials characterization
Magnetic adsorbents
Pyrolysis
Pore-forming

ABSTRACT

Four magnetic biochars (MBs) were prepared from two mixtures of Sappeli sawdust with $NiCl_2$ solution or Sappeli sawdust with $NiCl_2$ plus $ZnCl_2$ solutions. These mixtures formed two pastes that were dried and further pyrolyzed at 700 °C under nitrogen flow. The pyrolyzed material was leached out with 0.1 M HCl under conventional reflux (AL- 80 °C, 2 h) or assisted by ultrasound-leaching (US- 15 min, 600 W), obtaining four biochars: SNiAL, SNiUS, SNiZnAL, SNiZnUS. The biochars were characterized by VSM, XRD, FTIR, isotherms of adsorption and desorption of nitrogen, pH_{pzc}, hydrophobically characteristics (HI), TGA, elemental analysis (CHN/O). The data show that using the leaching process assisted by ultrasound can obtain biochars that present good magnetization saturation, with a lower leaching time than conventional leaching. The four biochar were tested as adsorbents to remove ten emerging contaminants and four dyes of aqueous effluents. It was observed that the impregnation of zinc chloride in the samples led to an increase in the surface areas of the magnetic biochars, which influenced the most of sorption capacities of the adsorbents for the different sorbing species. Making a ratio of sorption capacities of SNiAL/SNiZnAL and SNiUS/SNiZnUS, it was obtained the values, respectively, of 0.9761, and 0.9710 (Acid Red 1), 2.057, and 3.030 (Reactive Blue 4), 4.192, and 1.971 (Basic Violet 3), 3.359, and 1.129 (Basic Green 1), 1.673, and 1.835 (Paracetamol), 3.612, and 3.779 (Propranolol), 5.871, and 5.171 (Sodium Diclofenac), 1.457, and 1.607 (Nicotinamide), 1.094 and 1.093 (Caffeine), 1.167, and 2.398 (4-chloroaniline), 1.009 and 0.9965 (2-nitrophenol), 1.156 and 1.341 (Resorcinol), 1.299 and 1.331 (Hydroquinone), 0.9975 and 1.019 (4-bromophenol).

1. Introduction

Carbon materials (activated carbon, biochar, carbon nanotubes, graphene, and carbon composites) are efficient adsorbents for removing toxic species from aqueous effluents [1–5].

Due to the physical-chemical characteristics of the carbon-based adsorbent such as, chemical nature that allows the formation of hydrogen bonding, π-π stacking, van der Walls interactions with organic

* Corresponding author at: Postgraduate program in Mine, Metallurgical, and Materials Engineering (PPGE3M). School of Engineering, Federal University of Rio Grande do Sul (UFRGS), Av. Bento Gonçalves 9500, Porto Alegre, RS, Brazil.
E-mail addresses: profederlima@gmail.com, eder.lima@ufrgs.br (E.C. Lima).

https://doi.org/10.1016/j.jece.2021.105865
Received 28 April 2021; Received in revised form 10 June 2021; Accepted 12 June 2021
Available online 25 June 2021

compounds [6–8], also these carbon materials possesses several functional groups that could coordinate with metallic ions [9,10]; also, carbon-based materials present good textural properties (high surface area, high total pore volume, structured pores) that also allow the adsorption of several pollutants [6–10].

One of the main problems of using powder carbon-based adsorbents is separating the carbon adsorbent from the liquid solution. When organic compounds such as dyes, pesticides, hormones, pharmaceuticals, and other organic compounds are used as the sorbing specie, an efficient centrifuge is required to separate the liquid phase (aqueous solution) from the solid phase (adsorbent) [2,6]. However, this issue could be solved if a magnetic adsorbent is used [11,12].

To date, different MBs have been used for removal of emerging contaminants [13,14], dyes [15,16], and mettalic ions [17,18] from aqueous effluents.

The co-precipitation of the magnetic material over carbon-based adsorbent principally produces magnetic carbon-adsorbent [19–21]. Alternatively, the carbon material's impregnation with salts of iron, nickel, or cobalt and subsequent heating at higher temperatures forms the adsorbent matrix impregnated with magnetized material [11,22, 23]]. The third method of preparing magnetically carbon-based adsorbent is soaking biomass with iron or nickel salts and subsequent pyrolysis under an inert atmosphere. During this last step, the carbonization and magnetization co-occur in one single step [12,24–26].

This preparation method of magnetic adsorbents is not frequently reported in the literature [12,24–26]. Considering this less traditional method of preparing magnetic adsorbents, Thue et al. [12] prepared an excellent magnetic activated carbon using $NiCl_2$ plus $ZnCl_2$ as impregnating reagents for the tucumã biomass. After the pyrolysis, the authors performed a partially leach-out of the inorganics procedure using 0.1 M HCl. This procedure aims to remove the salts of zinc (that are used to create pores in the carbonized material) and the minimum nickel salts (that produce magnetism on the adsorbent) [12]. Nevertheless, this traditional leaching procedure [2,6,7,12] is time-consuming (1–2 h of reflux), followed by extensive washing with water and drying. On the other hand, the extraction of inorganic salts from diverse kinds of samples could get faster if ultrasound-assisted leaching is utilized [27–33].

In this paper, four magnetic biochars were prepared from African wood sawdust, Sapeli [12], mixing this biomass with $NiCl_2$ in proportion 1:1, and Sapeli: $ZnCl_2$: $NiCl_2$ (1:1:1). Please see Fig S1 for the denomination of the materials. These four magnetic biochars were characterized by X-ray diffraction (XRD); vibrational spectroscopy in the infrared region with Fourier transform (FTIR); Vibrating Sample Magnetometry (VSM); isotherms of adsorption and desorption of nitrogen to obtain total pore volume, pore size distribution, and surface area; pH_{pzc}; hydrophobic/hydrophilic balance (HI); thermal gravimetric analysis; and TGA, CHN/O elemental analysis.

After a full characterization of these four biochars, they were tested as adsorbents to remove ten emerging contaminants and four dyes from aqueous effluents.

2. Materials and methods

2.1. Reagents and biomass

The pharmaceuticals (paracetamol, sodium diclofenac, propranolol hydrochloride, nicotinamide, caffeine), emerging contaminants (4-chloro-aniline, 2-nitro-phenol, resorcinol, hydroquinone, 4-bromophenol), and the dyes (acid red 1, reactive blue 4, basic green 1, and basic violet 3) are shown in Fig S2. These reagents were acquired from Sigma-Aldrich and were used as received.

Deionized water was used throughout the adsorption tests to prepare all solutions.

Sapelli sawdust, with $\phi < 250$ μm, was obtained from Ngaoundere city sawmills (Cameroon), as previously reported [34]. Sapelli sawdust (*Entandrophragma cylindricum*) was used as a precursor for the biochars' preparation.

2.2. Sapelli magnetic biochars preparation

A single pyrolysis step prepared the magnetic biochars as following: First, 100.0 g of the Sapelli sawdust was mixed with weight ratios of $NiCl_2$, of 1:1, or Sapelli sawdust was mixed with $NiCl_2$ + $ZnCl_2$ in the proportion 1:1:1. During the mixing, about 75.0 mL of water was added to help the formation of pastes [34]. These two pastes were dried in an oven at 85 °C for 4 h, and then they were introduced in a quartz reactor in a conventional vertically-split oven, and it was heated up from 20 °C up to 700 °C in a ramp that lasts 68 min, under nitrogen (150 mL min^{-1}). The furnace's temperature was held at 700 °C for 30 min; then, the furnace was turned off, keeping nitrogen flow until the temperature was <200 °C, and turning it off until the furnace attain room temperature.

The pyrolyzed materials containing $NiCl_2$ or $NiCl_2$ + $ZnCl_2$ were partially leached out by conventional leaching (0.1 M HCl, at 80 °C, for 2 h) [12] or assisted by ultrasound (0.1 M HCl, 20 kHz, 600 W, 15 min).

Briefly, the ultrasound procedure took place by adding 5 g of biochar into a beaker containing 250 mL 0.1 M HCl, inserted in an Ultrasonic Disruptor chamber (Eco-sonics, Indaiatuba, SP, Brazil) with a macro probe (Potency ranging from 200 W to 750 W). The slurries were sonicated by a cycle of 15 min using a potency of 600 W (80% of total Potency) at 20 kHz. The sample was then filtered and washed abundantly with deionized water until the washing waters' pH attain pure water value.

After the conventional acidic leaching (AL), two biochars were obtained, denominated SNiAL and SNiZnAL. For the ultrasound-assisted extraction, the other two biochars were denominated as SNiUS and SNiZnUS. As previously reported [12], nickel salts' function is to produce magnetism to the biochar, and the $ZnCl_2$ function is the formation of pores [12].

Fig S1 summarizes the preparation of the magnetic biochars from Sappeli sawdust.

2.3. Characterization of magnetic biochars

The carbon adsorbents' magnetic features were evaluated by using an EZ9MicroSense VSM with a magnetic field (*H*) ranging from − 20 kOe until + 20 kOe [12].

X-ray diffraction technique was employed to obtain the patterns of powder adsorbents utilizing a Philips X′pert MPD diffractometer, operating at 40 kV, 17 mA with CuK_α (radiation wavelength of $\lambda = 1.5406$ Å). Diffractograms were taken from $5 \leq 2\theta \leq 90°$ using a scanning step of $0.016° \ s^{-1}$ [35]. Scherrer's equation was applied to find the Ni's average crystallite size (D) from SNiZiAL, SNiZiUS, SNiAL, and SNiUS samples [12].

X-ray fluorescence (Shimadzu XRF1800 X-ray Fluorescence Spectrometer, Japan) was used to determine the contents of Ni and Zn from SNiZiAL, SNiZiUS, SNiAL, and SNiUS samples.

N_2 isotherms, total pore volume, specific surface area, and pores size distribution were obtained by a Micrometrics instrument volumetric analyzer (TriStar II 3020) at −196 °C. Before collecting the data of isotherms, the magnetic biochar samples were degassed under a vacuum at 150 °C. The determination of surface area was calculated using the BET multipoint method [36], and the pore diameter was attained using the DFT method [37] and BJH Method [38].

The mass loss of the samples as a function of temperature (20–800 °C) under N at 10 °C/min and (800–1000 °C under O_2 [39].

Elemental composition (CHN/O) was obtained from a Thermo Fisher Scientific analyzer to quantify the proportions (%) of C, H, N, and O present in the adsorbents [40]. The functionalities present on biochars surfaces were identified by FTIR using a Shimadzu spectrophotometer [41]. The pH_{pzc} and hydrophobicity index (HI) of the carbon materials were obtained as described in references elsewhere [6,42,43].

2.4. Batch contact adsorption procedure

The performance as adsorbent of SNiAL, SNiUS, SNiZnAL, SNiZnUS was checked using 30.0 mg of each biochar with 20.00 mL of pharmaceuticals (paracetamol, propranolol, diclofenac, caffeine, nicotinamide), emerging contaminants (4-chloro-aniline, 2-nitro-phenol, resorcinol, hydroquinone, 4-bromophenol), and the dyes (acid red 1, reactive blue 4, basic green 1, and basic violet 3). The solutions' pH was fixed at pH 7 for pharmaceuticals [2,7,11,12,35,39–43] and emerging contaminants [6,7,44], pH 2 for anionic dyes [45], and pH 9 for cationic dyes [46]. These conditions have been extensively reported and exhaustively studied in the authors' laboratory. The slurry (30.0 mg biochar plus 20.00 mL sorbing solution) was shaken for six hours. Afterward, the solid phase was separated from the solution. The initial and final adsorbates' concentration was determined by UV-Vis [39–46] using a T90 + spectrophotometer (PG Instruments). Sorption capacities were determined as previously described [39–46].

3. Results and discussion

3.1. Biochar magnetic properties

Fig. 1 shows the magnetization curves of the SNiAL, SNiUS, SNiZnAL, and SNiUS biochars. The biochars that utilized $ZnCl_2$ in the biomass's impregnation presented a lower saturation magnetization (M_S) than the biochars prepared only with $NiCl_2$ independently on the leaching process used. These values were 6.86 (SNiZnAL), 10.81 (SNiZnUS), 15.00 (SNiAL), and 12.59 (SNiUS) emu g^{-1} (see Table 1). The remanence indexes (M_R) were 0.29 (SNiZnAL), 0.26 (SNiZnUS), 1.18 (SNiAL), and 1.12 emu g^{-1} (SNiUS). The coercivity indexes (H_C) were 46.65 (SNiZnAL), 25.81 (SNiZnUS), 35.29 (SNiAL), and 35.27 Oe (SNiUS). However, it is noting that SNiZnUS showed high M_S compared to SNiZnAL – showing that ultrasound-assisted extraction might be a preferable road to leach out zinc metal and keep Ni in the biochar structure to enhance the magnetic properties. On the other hand, when used Ni salt alone to prepare the magnetic biochar, conventional acidic leaching might be preferable to ultrasound-assisted extraction to keep a high M_S. It is worth adding here that M_S is not the only parameter that should be considered to evaluate the magnetic biochar materials efficiency. Other parameters such as functional groups and pore size distribution are also essential and are discussed in this work.

As displayed in Table 1, the adsorbents showed to be superparamagnetic biochars. The superparamagnetic feature means that the materials show zero or insignificant remanence (M_R) and coercivity (Hc)

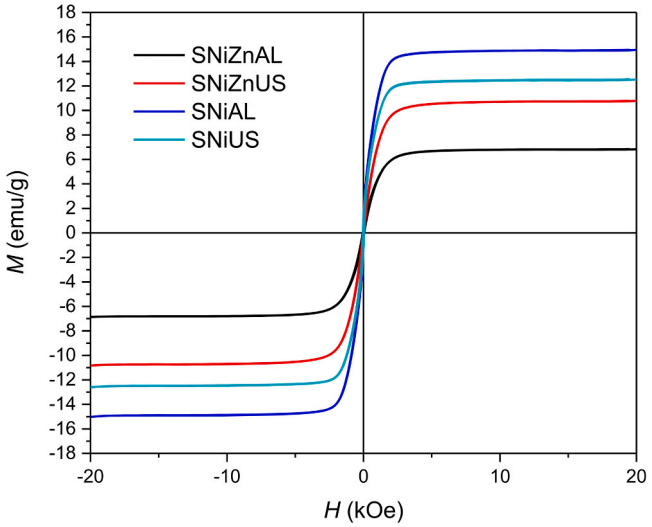

Fig. 1. Magnetization curves of Sappeli biochars.

Table 1
Magnetic properties of the magnetic biochar materials.

Biochar magnetic Samples	Saturation magnetization M_S (emu/g)	Coercivity, HC (Oe)	Remanence, M_R (emu/g)	M_R/M_S
SNiZnAL	6.86	46.65	0.29	0.042
SNiZnUS	10.81	25.81	0.26	0.024
SNiAL	15.00	35.29	1.18	0.078
SNiUS	12.59	35.27	1.12	0.088

values [47]. In fact, superparamagnetism appears when the crystal size becomes sufficiently small. This is discussed in the next section, which displays the XRD patterns. Usually, it is not observed a hysteresis loop on the magnetization curves, and the ratio of saturation remanence divided by saturation magnetization (M_R/M_S) is to be $< 25\%$ [22]. The data presented in Table 1 show that the ratio M_R/M_S was between 2.4% and 8.8%, which confirms the superparamagnetic characteristics of biochars synthesized in this research. Indeed, this property is vital for the easy separation of the materials after it is used in the wastewater treatment and for reusing and regenerating the biochars without reuniting the materials' magnetization or losing efficiency. When the external magnetic field (H) is turned off, the magnetic biochar materials will not join together and be demagnetized entirely. This feature allows the magnetic biochars to be regenerated and reused again (see Fig. 1).

Although adding $ZnCl_2$ in the biochar formulation provoked a decrease in the saturation magnetization (M_S), these saturation values obtained in this work are enough for the complete magnetic separation of the adsorbent from the liquid phase to the ending of the process. The M_S values showed to be comparable or higher than other magnetic biochars (MB) early reported in other works [48–50]. For example, Zhu et al. [48] reported a porous MB prepared via simultaneous activation and magnetization, and it presented a lower M_S value equal to 0.76 emu g^{-1} at 300 K. The materials were used to remove tetracycline from aqueous solution. Also, porous MB was prepared from almond shells [49], which exhibited an M_S equal to 4.47 emu g^{-1} at 300 K. The MB was used for trinitrophenol removal from water. Zhang et al. [50] reported a single-step synthesis of magnetic activated carbon from a peanut shell with M_S values of 5.61 emu g^{-1} and 8.64 emu g^{-1}. Thue et al. [12] reported MB's preparation to remove propranolol and nicotinamide from aqueous, with a saturation magnetization between 7.14 and 14.91 emu g^{-1}. Therefore, it can be concluded that the MB prepared in this research exhibited superparamagnetic properties, as their ratios of Mr/Ms were found even to be less than 10% and could be easily separated from the liquid solution.

The benefits of using $ZnCl_2$ for biochar activation are significant because this salt increases the adsorbent's total pore volume and surface area [6,7,12,39,40]. These benefits will be shown in the next subsections.

This decrease of magnetization in SNiZnAL and SNiZnUS is due to the partial leaching process with 0.1 M HCl at 80 °C for 2 h or with 0.1 M HCl in an ultrasound-assisted extraction (20 kHz, 600 W, 15 min), for partial leaching out of nickel and zinc compounds after the pyrolysis. This behavior is further discussed In the section below. However, the biochars' saturation magnetization values were still comparable with the literature [12,48–50] and were promptly separated using a magnet from the aqueous solution.

The acidic leaching of inorganics works as solubilizing the inorganics compounds forming soluble chlorides species. Conversely, the acoustic cavitation provoked by the ultrasound leads to the formation of microbubbles in the water [51,52]. These microbubbles grow and collapse at a higher frequency. The collapse of microbubbles generating temperatures up to 5000 K and pressures up to 1700 bar at the point of the collapse of the bubbles [51]. The shock of these bubbles in a solid sample will cause cavitation erosion, releasing the inorganic species from the carbonaceous biochar [52]. Sonication has been reported as an activated

procedure for increasing the surface area of biochar [53] and biomass-based adsorbents [54,55] because the sonication effect leads to the extraction of inorganics and organic species from the solid sample [52].

3.2. X-rays diffraction of biochars

Fig. 2 shows the X-ray diffraction patterns of SNiAL (Fig. 2A), SNiUS (Fig. 2B), SNiZnAL (Fig. 2C), and SNiZnUS (Fig. 2D) biochars. All diffractometers show the characteristic peaks of the quartz (SiO_2, JCPDS card 00–001–0649) at $2\theta \approx 26.58°$ from the organic precursor, and Ni° (JCPDS card 00–004–0850) at $2\theta \approx 44.5°$, 51.8°, and 76.4°, independently of the method of leaching used (conventional and ultrasound-assisted). This result is very relevant because metallic Ni, which confers the biochars' magnetic properties, was not wholly lost in the treatment with 0.1 M HCl under conventional leaching or ultrasound-assisted treatment. From the crystallite size obtained using Scherrer's equation [12], it is observed that both leaching methods were employed to obtain nanostructured Ni particles for all adsorbents samples, with an average crystallite size between 36.1 and 49.9 nm (see Table 2). These small crystallite particle's size also confirms the MB materials' superparamagnetic properties prepared in this work, as previously mentioned [47].

For samples from which $ZnCl_2$ was used (SNiZnAL and SNiZnUS), it is possible to confirm that simonkelleita ($Zn_5(OH)_8Cl_2{\cdot}H_2O$; JCPDS Card 00–007–0155) was formed during the pyrolysis, which indicates that zinc compounds were not completed leached under the studied leaching out methods. However, the simonkelleita peaks have lower intensity in SNiZnAL, and the material seems to be more amorphous compared to others – proving that the conventional HCl extraction was more effective in removing zinc compounds from the pyrolyzed material. Furthermore, the leaching process (conventional or ultrasonic-assisted) did not affect the crystallinity of the materials when the nickel salt alone was employed in the preparation of magnetic biochars. However, there was a difference found in the magnetic properties, as shown in Section 1.

Table 2
The crystallite size (*D*) of Ni particles for SNiZnAL, SNiZnUS, SNiAL, and SNiUS biochars.

Adsorbent	*D* (nm)
SNiZnAL	45.9
SNiZnUS	45.9
SNiAL	36.1
SNiUS	45.4

3.3. Textural characteristics

Fig. 3 shows the N_2 isotherm curves for the SNiAL (Fig. 3A), SNiUS (Fig. 3B), SNiZnAL (Fig. 3C), and SNiZnUS (Fig. 5D) magnetic biochars. The pore size distribution curves of these magnetic biochars are presented in Fig. 4.

The isotherms of SNiAL and SNiUS biochars could be considered Type IVa [36], with hysteresis type H3 [36]. On the other hand, the isotherm of type Ib [36] seems to be followed for SNiZnAL and SNiZnUS. The isotherm Type IVa are characteristics of mesoporous materials [36],

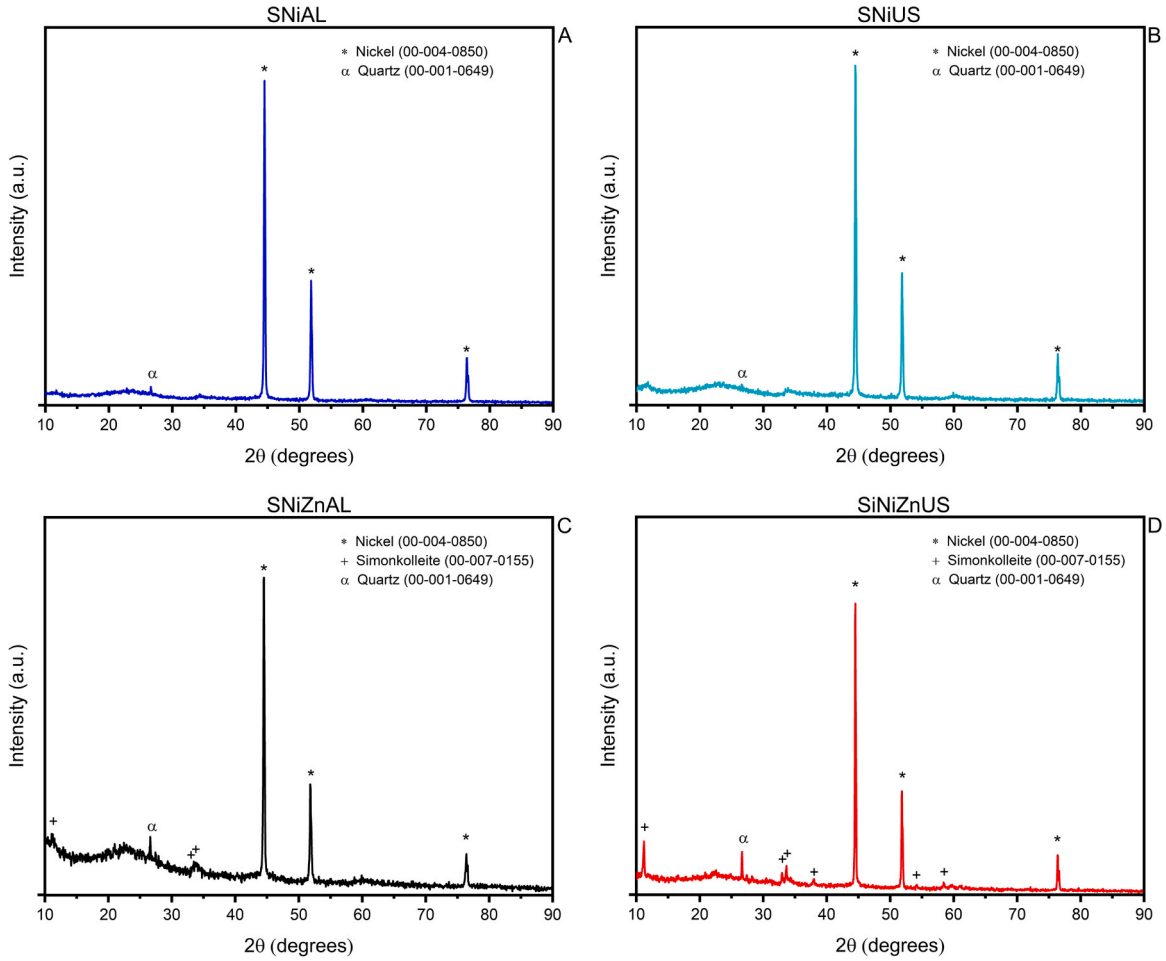

Fig. 2. XRD diffractograms of A-SNiAL, B-SNiUS, C-SNiZnAL, D-SNiZnUS.

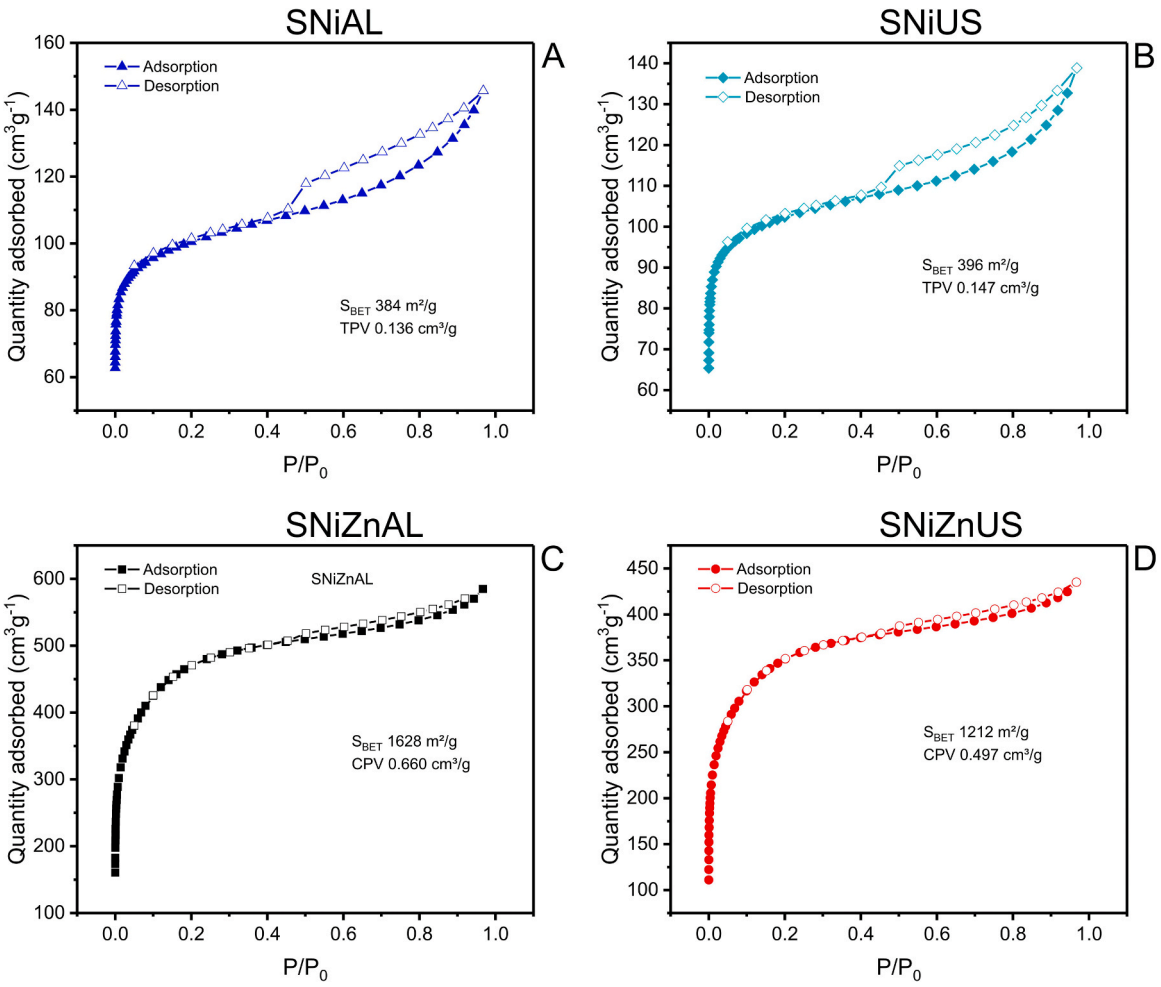

Fig. 3. *N_2 isotherms of magnetic carbon materials.*

while the isotherm of type Ib is the characteristics of micropores, with some pores attaining the low region of mesopores (pores < 2.8 nm) [36].

The SNiAL and SNiUS presented lower volumes of nitrogen adsorbed per gram of the biochars, which were 145.7 (SNiAL) and 139.9 $cm^3\ g^{-1}$ (SNiUS). The SNiZnAL and SNiZnUS presented much higher values for volume of nitrogen adsorbed per gram of the biochars, attaining 585.0 (SNiZnAL) and 435.1 $cm^3\ g^{-1}$ (SNiZnUS). These increases in the volume of nitrogen adsorbed per gram of biochar will reflect on the BET surface area obtained for the materials that are: 385 (SNiAL), 396 (SNiUS), 1628 (SNiZnAL), and 1212 $m^2\ g^{-1}$ (SNiZnUS).

Based on these results reported above and observing Figs. 3 and 4, the biochars that were not treated with $ZnCl_2$ presented lower surface area; however, they presented pores with a higher diameter range (from micro to mesopores). On the other hand, the addition of $ZnCl_2$ during the impregnation of the Sappeli biomass allowed the formation of biochars predominantly microporous, with a small fraction of mesopores with pore diameter <2.8 nm (Fig. 4).

Analyzing Figs. 3 and 4, it is possible to state that $ZnCl_2$ increased the surface area of the biochars by 4.23-times when the surface area of SNiZnAL was divided by the surface area SNiAL. Also, an increase of 3.06 times when the surface area of SNiZnUS is divided by the surface area of SNiUS. When this ratio is made using the total pore volume, the increase using $ZnCl_2$ was 4.85 and 3.38 times, for the total pore volume ratio SNiZnAL/SNiAL and SNiZnUS/SNiUS, respectively. It is well known that biomass impregnated with $ZnCl_2$ forms complexes [34] and acts as a catalyst in pyrolysis, inhibiting bio-oil formation [34].

After the pyrolysis, a leaching procedure is required to remove zinc salts from the carbonaceous matrix [6,7,12,34]. When it is leached, the zinc salts' volume forms void pores on the carbonaceous matrix. This increase in pores' formation is responsible for increasing the biochars' surface area impregnated with $ZnCl_2$. On the other hand, during the leaching of metallic salts, such as nickel [34], from pyrolyzed material, the leaching efficiency is much lower than $ZnCl_2$, as earlier reported by Thue et al. [34]. Therefore the use of $ZnCl_2$ during the impregnation of the biomass is recommended for the production of activated carbons [2, 6], magnetic carbon materials [12], and consequently for magnetic biochar used in this research.

Comparing AL and US methods of leaching inorganics after the pyrolysis of the biochar, for production of pores on the biochar, the conventional leaching using 0.1 M HCl, under reflux (80 °C) for a while of 2 h, produced a material with higher surface area (SNiZnAL) when compared with the ultrasound-assisted extraction using 0.1 M HCl, a macro probe operating at 20 kHz, using a power of 600 W for 15 min (SNiZnUS), because the elimination of inorganic compounds, was more efficient. However, the saturation of the magnetization of SNiZnUS (10.81 emu g^{-1}) was superior to SNiZnAL (6.81 emu g^{-1}), as seen above. Therefore, the use of ultrasonic partial-leaching of the inorganics could be a useful tool for producing magnetic biochars with adequate surface area and good magnetic properties such as SNiZnUS biochar.

3.4. Thermal stability of biochars

Fig. 5 brings the thermogravimetric curves of SNiAL (Fig. 5A), SNiUS (Fig. 5B), SNiZnAL (Fig. 5C), and SNiZnUS (Fig. 5D).

All the samples' thermal behavior suffered five weight variations, being at least four of weight losses and one of the winnings of mass for all

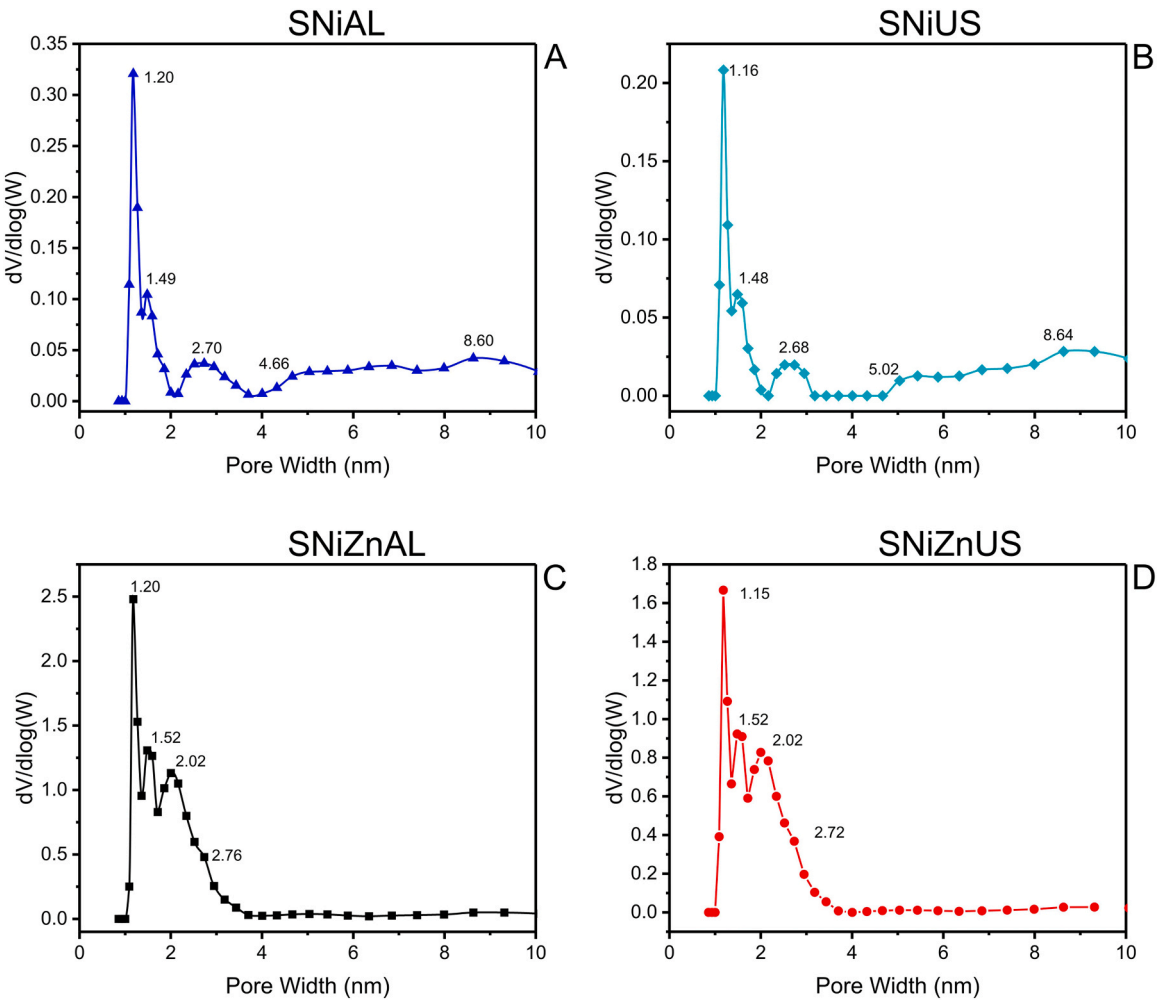

Fig. 4. Pore size distribution curves for magnetic biochars.

the samples, except SNiAL. The atmosphere was N_2 from room temperature up to 800 °C, and synthetic air for temperatures ranging from 800 ° to 1000 °C. This strategy of changing the atmosphere during the thermal analysis is useful because up to 800 °C, all the thermal behavior of the biochars are studied under an inert atmosphere, and in the same run, it is possible to obtain the contents of ashes using synthetic air, to decompose the carbon matrix entirely up to 1000 °C [6,12,39]. The first step (a) corresponds to the elimination of moisture; the second step (b) corresponds to the elimination of interstitial water [40,43], and it is associated with the elimination of water formed by the decomposition of organic functional groups present on the biochar [40,43]. The third step (c) corresponds to the carbonaceous matrix's degradation under N_2, where some volatiles acids, bases could be released [40,43]. The fourth step (d) corresponds to the complete oxidation of all organic matrices with oxygen present in the air [40,43], and the fifth step is the formation of the ashes, with the possibility of some recombination of the inorganics with oxygen, forming the ashes [40,43]. This recombination of some metals with oxygen leads to the formation of oxides responsible for the mass winning at the last step for SiNiUS, SiNiZnAL, and SiNiZnUS.

Therefore the residual mass at 1000 °C of a carbon-based material corresponds to the ash formed, which are 44.82% (SNiAL), 41.37% (SNiUS), 25.77% (SNiZnAL), and 35.50% (SNiZnUS). These values of the percentage of residual ashes agree with the previous results, where the samples with $ZnCl_2$ were more easily leached than samples that did not use this salt to impregnate the biomass. The conventional acidic partial leaching using 0.1 M HCl led to a material with a high surface area, more amorphous, and low contents of ashes, however, with the lowest magnetization. On the other hand, the material containing $ZnCl_2$ in the biomass's impregnation and the partial leaching assisted by ultrasound led to a material with good magnetization and surface area values $> 1000\ m^2/g$.

Concerning the thermal stability of the biochars, these materials are thermally stable under nitrogen atmosphere up to 674° (SNiAL), 608° (SNiUS), 581°(SNiZnAL), and 575 °C (SNiZnUS), which is also another critical characteristic of these carbon-based magnetic materials.

The DTA curves of these biochars are presented in Fig S3. The peaks correspond to the maximum temperature, where the thermal effect took place.

3.5. *Chemical characteristics of magnetic biochars*

Fig. 6 presents the FTIR spectra of the magnetic biochars. The band assignments of the vibrational spectra of SNiAL (Fig. 6 A), SNiUS (Fig. 6B), SNiZnAL (Fig. 6 C), and SNiZnUS (Fig. 6D) are presented in Table 3.

As seen in Table 3, all the biochars contain the chemical functions of aromatics, alcohol, phenol, carboxylic acid, silica (that is also seen in Fig. 4), and Metal-O, or Metal-N groups. However, it is possible to observe some differences in the spectra. SNiAL and SNiUS seem to present more aromatic ring molecules compared to SNiZnAL and SNiZnUS. This can be observed by the four different peaks, characteristic of the ring modes of aromatic stretching, which reveals both magnetic biochars' aromatization [34]. This characteristic may lead to biochars with high hydrophobic properties since the HI is usually affected by

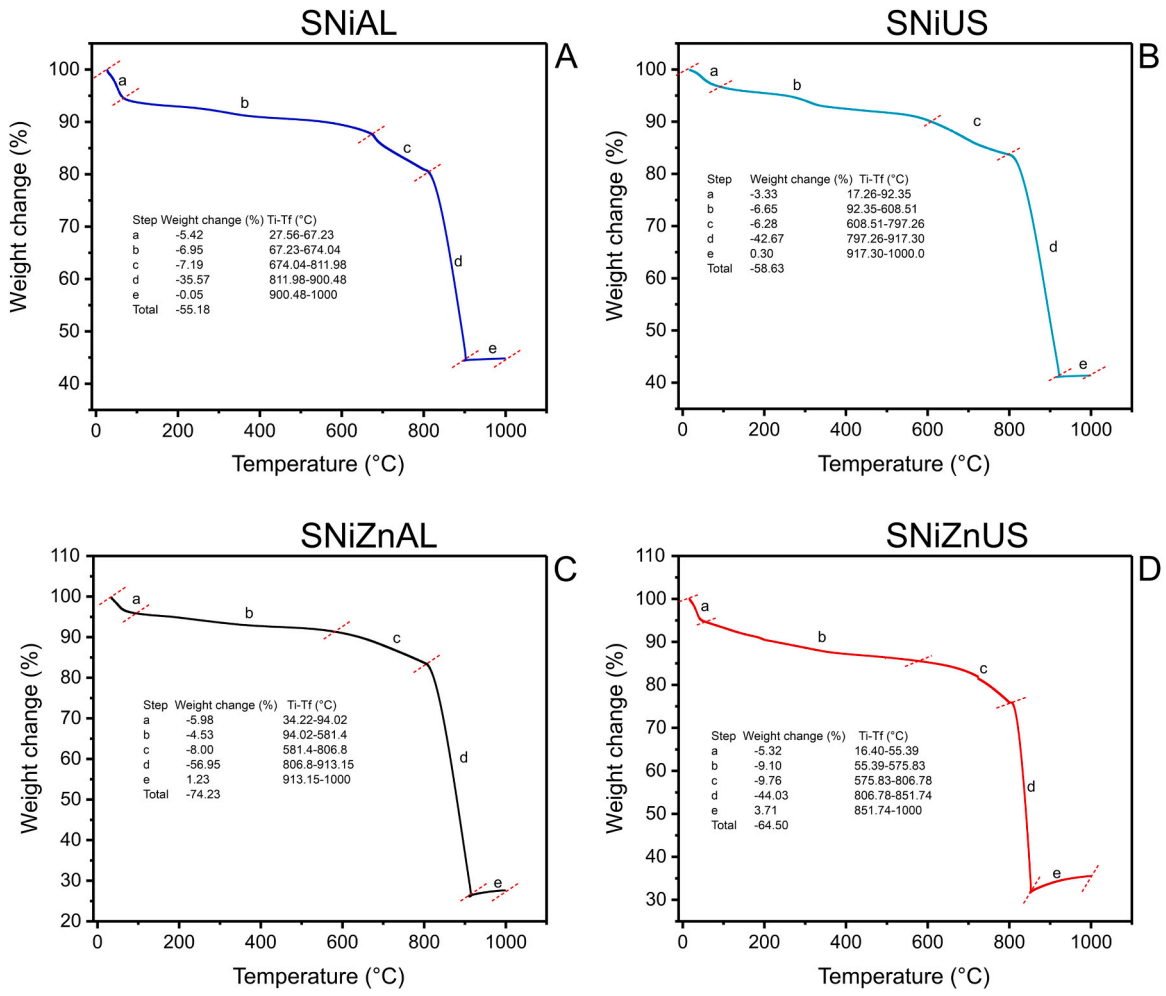

Fig. 5. Thermogravimetric curves of magnetic biochars.

aromatic groups' presence in the material's structure. Likewise, SNiZnAL and SNiZnUS presented some bands that were not found in SNiAL and SNiUS spectra. The bands in the 1400–1000 cm^{-1} region can be attributed to C-O of secondary alcohol (hydroxyl, ester, or ether), C-O of phenol, and O-H bending vibrations [34,48]. Considering that those groups are polar, SNiZnAL and SNiZnUS are expected to be more hydrophilic compared to SNiAL and SNiUS biochars. In fact, $ZnCl_2$ has been widely used as a catalytic agent in biomass conversion and an activating agent to prepare activated carbons [34]. According to the literature [34,43,44], biochars prepared with $ZnCl_2$ actually shows high polar surface functional groups. It was not possible to clearly observe through FTIR analysis the effect of the leaching procedure (conventional or ultrasound-assisted) on functional group development.

Table 4 present the results of CHN/O elemental analysis, hydrophobic/hydrophilic balance, pH_{pzc} of the magnetic biochars.

The CHN/O analysis of the four biochar showed that SNiZnAL presented the highest C contents above 60%. All other biochars presented the content of C around 50%. Nitrogen (> 4.4%) and hydrogen's (≈ 1%) contents are also higher in the samples that utilized $ZnCl_2$ for impregnating the biomass than the biochars that were impregnated only with $NiCl_2$ (values of N < 0.3% and H < 1.4%). Again, it is seen the effect of $ZnCl_2$ acting as a catalyst in the pyrolysis step.

Another essential characteristic of the biochar surfaces is the hydrophobic/hydrophilic balance (HI), which is defined by the quantity of vapor of n-heptane adsorbed per gram of adsorbed divided by the quantity of vapor of water adsorbed per gram of the adsorbent. When HI < 1, the surface presents good hydrophilicity, and when HI > 1, it predominates the hydrophobic character on the solid's surface. The SNiAL and SNiUS presented HI > 1, and contrasting this result, SNiZnAL and SNiZnUS presented HI < 1. This information is corroborated with FTIR analysis results and N and O contents present in the sample. Both nitrogen and oxygen present in the biochars are responsible for polar groups. When the %C is summed with %N, the following values are obtained: 3.90 (SNiAL), 6.07 (SNiUS), 8.90 (SNiZnAL), and 7.25 (SNiZnUS). The higher the sum of N + O, the higher is the polar character of the biochar, and the lower value of HI is obtained.

The pH_{pzc} of all these biochars are also listed in Table 4, and their values are within a narrow interval of 6.13–6.89. The unique, more acidic surface is SNiZnUS, whose pH_{pzc} is 6.13. All the others are in the interval of 6.86–6.89, which are practically the same value. Therefore, it is not expected a remarkable difference of these biochars for being used as adsorbents regarding the value of the adsorbate solution's initial pH.

3.6. *Biochars potentiality as adsorbents for removal of organic compounds*

After a careful characterization of the biochars obtained by conventional (0.1 M HCl; 80 °C under reflux, 2 h) or ultrasound-assisted extraction (0.1 M HCl; 20 kHz, 600 W, 15 min), the obtained materials were tested as potential adsorbents for removal of five pharmaceuticals, five emerging contaminants, and four dyes. Fig. 7 brings the sorption capacities obtained with the four magnetic biochars for these organic molecules.

The choice of suitable adsorbent dosage, initial pH for suitable

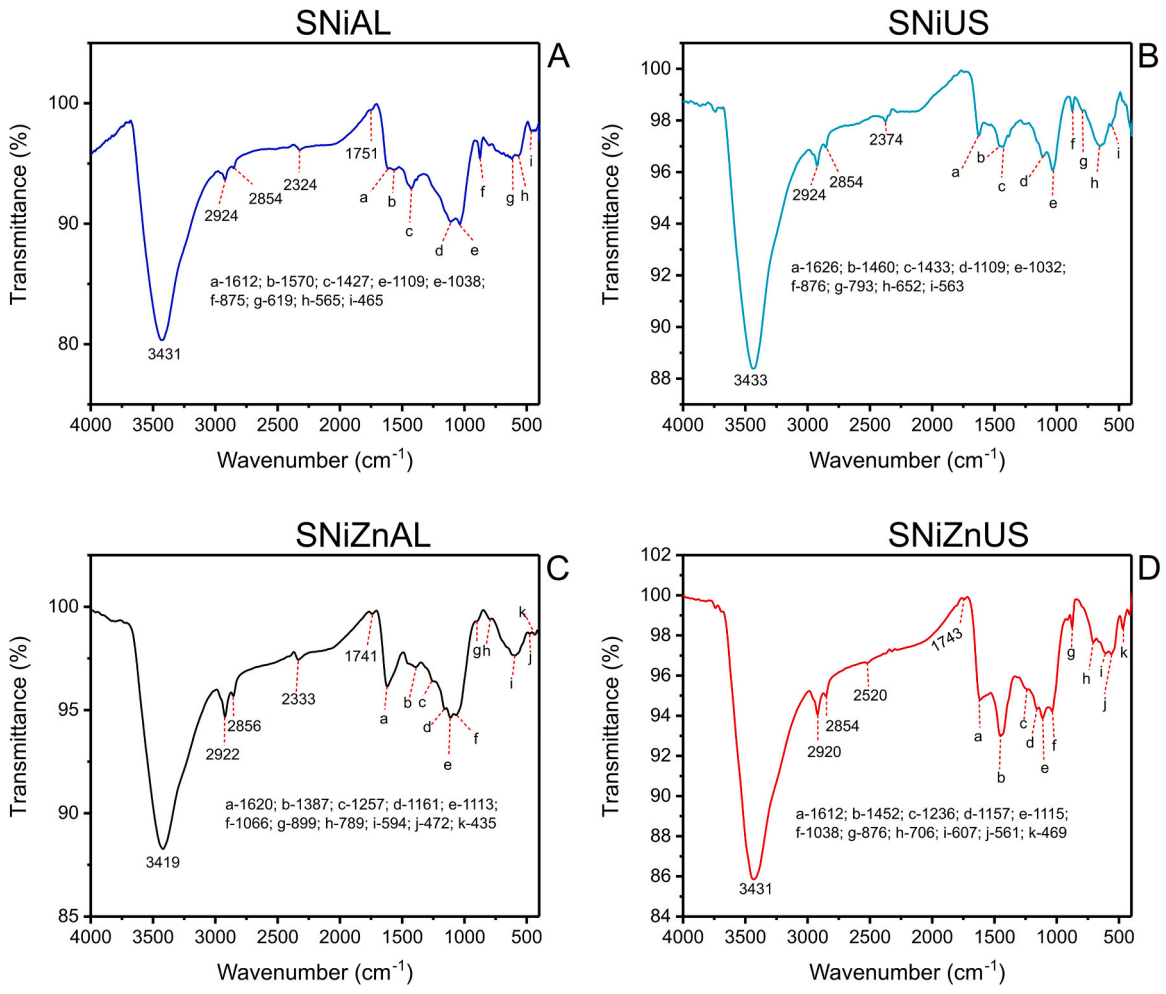

Fig. 6. FTIR spectra of magnetic biochars. A- SNiAL; B- SNiUS; C- SNiZnAL; D- SNiZnUS.

Table 3
FTIR band assignments [11,34,35,39,40].

	FTIR bands (cm^{-1})			
Band assignment	SNiAL	SNiUS	SNiZnAL	SNiZnUS
υO-H overlapping with υN-H of amines or amides	3431	3433	3419	3431
υC-H asymmetric	2924	2924	2922	2920
υC-H symmetric	2854	2854	2856	2854
υ CO_2	2324	2374	2333	2520
υ C═O aldehyde	1751	–	1741	1743
δ NH_2 of amides	1612	1626	1620	1612
δ Aromatic ring modes	1612	1626	1620	1612
	1570	1460		1452
	1427	1433		
δO-H;	–	–	1387	–
υ C-O of phenol	–	–	1257	1236
υ C-O of secondary alcohol	–	–	1161	1157
υ Si-O-Si	1109	1109	1113	1115
υ C-O primary alcohol	1038	1032	1066	1038
δ C-H out-of-plane of aromatics	875	876	899	876
		793	789	706
υ Ni-O; υ Ni-N	619	652	–	–
υ Ni-O; υ Ni-N	565	563	594	561
υ Ni-O; υ Zn-O; υ Ni-N; υ Zn-N	465	–	472	469
υ Zn-O; υ Zn-N	–	–	435	–

υ- stretching; δ-bending.

adsorption of the pharmaceuticals (Fig. 7A), emerging contaminants (Fig. 7B), and dyes (Fig. 7C) are based on our previous work dealing with different adsorbents and adsorbates in the last 15 years [2,6,7,11,12,35,39–46], and they are shown in the caption of Fig. 7.

We used a time of contact of 24 h, which has been much higher than the usual minimum time of contact necessary to attain the equilibrium to guarantee that contact was not a limit for attaining the equilibrium [2,6,7,11,12,35,39–46]. From Fig. 7, it is possible to infer that there are no remarkable differences in the performance as adsorbents between SNiZnAL and SNiZnUS, although the surface area and total pore volume of the first biochar is 34.23% and 32.80% superior to SNiZnUS. Notwithstanding, the surface area of SNiZnUS is superior to 1000 m^2g^{-1} and Leite et al. [7] have reported that different carbon-based adsorbents with surface area > 1000 $m^2\ g^{-1}$ did not present remarkable differences in several pharmaceuticals and other emerging contaminants' sorption capacities. On the other hand, SNiAL and SNiUS had lower sorption capacities than SNiZnAL and SNiZnUS. This considerable difference could be attributed to the low surface area and low total pore volume of these magnetic biochars prepared without the biomass's impregnation with $ZnCl_2$.

Making a ratio of sorption capacities of SNiAL/SNiZnAL and SNiUS/SNiZnUS, it was obtained the values, respectively, of 0.9761, and 0.9710 (Acid Red 1), 2.057, and 3.030 (Reactive Blue 4), 4.192, and 1.971 (Basic Violet 3), 3.359, and 1.129 (Basic Green 1), 1.673, and 1.835 (Paracetamol), 3.612, and 3.779 (Propranolol), 5.871, and 5.171 (Sodium Diclofenac), 1.457, and 1.607 (Nicotinamide), 1.094 and 1.093 (Caffeine), 1.167, and 2.398 (4-chloroaniline), 1.009 and 0.9965 (2-

Table 4
Chemical composition of the biochars.

	C (%)	H (%)	N (%)	O[1] (%)	ashes (%)[2]	Zn (%)[3]	Ni (%)[3]	HI[4]	pH_{pzc}
SNiAL	49.93	1.35	0.28	3.62	44.82	–	19.37	1.142	6.89
SNiUS	51.17	1.39	0.32	5.75	41.37	–	17.12	1.047	6.86
SNiZnAL	60.83	4.50	1.15	7.75	25.77	0.17	8.55	0.964	6.86
SNiZnUS	52.79	4.46	0.99	6.26	35.50	0.55	12.45	0.979	6.13

[1] Obtained by %O = 100% −(%C + %H + %N + %ashes).
[2] Obtained byTGA using synthetic air from 800 to 1000 °C (see Fig. 7.
[3] obtained by XRF
[4] HI: the amount of adsorbed of vapor of n-heptane (mg g^{-1}) divided by the amount adsorbed of vapor water (mg g^{-1})

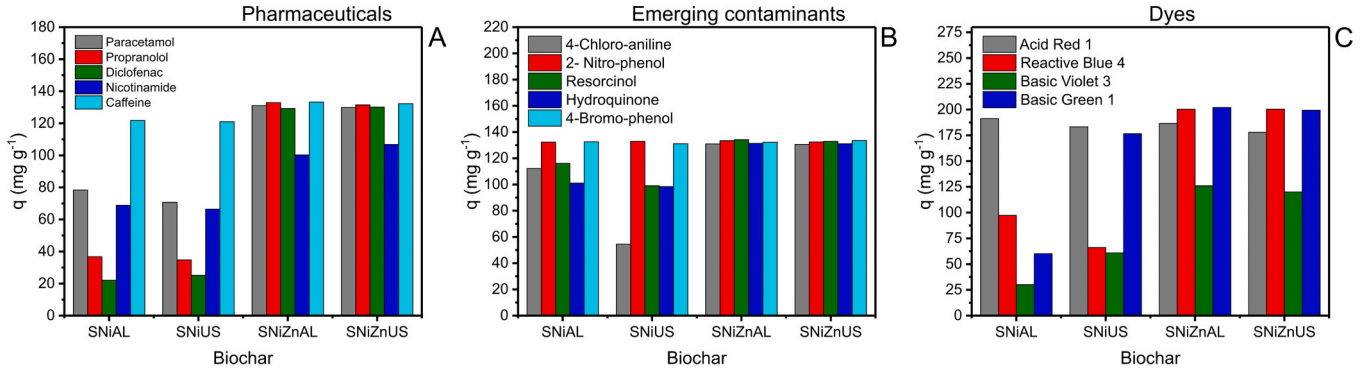

Fig. 7. Sorption capacities were obtained with SNiAL, SNiUS, SNiZnAL, and SNiZnUS biochars. A- initial adsorbate concentration 200 mg L^{-1}, pH 7; B- initial adsorbate concentration 200 mg L^{-1}, pH 7; C- initial adsorbate concentration 300 mg L^{-1}, pH 2 for Acid Red 1 and Reactive Red 4 (anionic dyes), and pH 9.0 for Basic Violet 3 and Basic Green 1 (cationic dyes). In all conditions, the adsorbent dosage used was 1.5 g L^{-1}, time of contact of 24 h, at 25 °C.

nitrophenol), 1.156 and 1.341 (Resorcinol), 1.299 and 1.331 (Hydroquinone), 0.9975 and 1.019 (4-bromophenol). Therefore, except for Acid Red 1 (SNiZnUS and SNiZnAL), 2-nitrophenol (SNiZnUS), 4-bromophenol (SNiZnAL), the sorption capacities of SNiZnAL and SNiZnUS presented higher sorption capacities when compared to the respective biochar without the impregnation of $ZnCl_2$.

Although SNiZnAL and SNiZnUS did not have a remarkable difference in sorption capacities for the different pollutants, the magnetism of SNiZnUS was superior to SNiZnAL (see Table 1).

4. Conclusion

Four magnetic biochars were prepared from Sapelli sawdust biomass: SNiAL, SNiUS, SNiZnAL, and SNiZnUS.

These magnetic biochars were characterized by FTIR (which shows some differences in the functional groups of the biochars containing zinc from the others that do not have it). The biochars were also characterized by XRD that detected metallic nickel in all the samples and salts of zinc in the biochar samples impregnated with it before the pyrolysis. By VSM technique showed that SNiZnUS (10.81 emu g^{-1}) presented higher magnetization of saturation than SNiZnAL (6.86 emu g^{-1}). The samples prepared with nickel alone presented higher magnetism than those containing zinc element; conversely, the biochars' surface area containing zinc was higher than those without it. As a compromise of magnetism and surface area, the best magnetic biochar was SNiZnUS that presented a surface area of 1212 m^2 g^{-1} and good magnetism.

Regarding employing the four magnetic biochars as adsorbents, SNiZnAL and SNiZnUS presented similar behavior, but they presented higher efficiency as adsorbents than SNiAL and SNiUS.

CRediT authorship contribution statement

Diana R. Lima: Conceptualization, Methodology, Investigation, data curation. **Eder C. Lima:** Supervision of the work, Funding acquisition, Writing - original draft, Visualization. **Pascal S. Thue:** Data curation, Formal analysis, Writing - review & editing. **Silvio L.P. Dias**: Resources. **Fernando M. Machado**: Formal analysis. **Moaaz K. Seliem**: Writing - review & editing. **Farooq Sher**: Writing - review & editing. **Glaydson S. dos Reis:** Writing - review & editing. **Mohammad Reza Saeb**: Visualization. **Jörg Rinklebe:** Writing - review & editing.

Declaration of Competing Interest

The authors declare that they have no known competing financial interests or personal relationships that could have appeared to influence the work reported in this paper.

Acknowledgments

The authors thank the Foundation for Research Support of the State of Rio Grande do Sul (FAPERGS, RS Brazil), National Council for Scientific and Technological Development (CNPq, Brazil), and Coordination of Improvement of Higher Education Personnel (CAPES, Brazil) for financial support and sponsorship. The authors are grateful to the Nanoscience and Nanotechnology Center (CNANO-UFRGS) of the Federal University of Rio Grande do Sul (UFRGS). We are also grateful to ChemAxon for giving us an academic research license for the Marvin Sketch software, Version 21.9 (http://www.chemaxon.com) 2021, used for molecule physical-chemical properties.

Appendix A. Supporting information

Supplementary data associated with this article can be found in the online version at doi:10.1016/j.jece.2021.105865.

References

[1] F. Sher, K. Hanif, A. Rafey, U. Khalid, A. Zafar, M. Ameen, E.C. Lima, Removal of micropollutants from municipal wastewater using different types of activated carbons, J. Environ. Manag. 278 (2021), 111302, https://doi.org/10.1016/j.jenvman.2020.111302.

[2] F.M. Kasperiski, E.C. Lima, C.S. Umpierres, G.S. dos Reis, P.S. Thue, D.R. Lima, S.L. P. Dias, C. Saucier, J.B. da Costa, Production of porous activated carbons from *Caesalpinia ferrea* seed pod wastes: highly efficient removal of captopril from aqueous solutions, J. Clean. Prod. 197 (2018) 919–929.

[3] H.N. Tran, F. Tomul, H.T.H. Nguyen, D.T. Nguyen, E.C. Lima, G.T. Le, C.T. Chang, V. Masindi, S.H. Woo, Innovative spherical biochar for pharmaceutical removal from water: Insight into adsorption mechanism, J. Hazard. Mater. 394 (2020), 122255, https://doi.org/10.1016/j.jhazmat.2020.122255.

[4] A.M.E. Khalil, F.A. Memon, T.A. Tabish, B. Fenton, D. Salmon, S. Zhang, D. Butler, Performance evaluation of porous graphene as filter media for the removal of pharmaceutical/emerging contaminants from water and wastewater, Nanomaterials 11 (2021) 79, https://doi.org/10.3390/nano11010079.

[5] M. Minale, Z. Gu, A. Guadie, D.M. Kabtamu, Y. Li, X. Wang, Application of graphene-based materials for removal of tetracyclines using adsorption and photocatalytic-degradation: a review, J. Environ. Manag. 276 (2020), 111310, https://doi.org/10.1016/j.jenvman.2020.111310.

[6] C.S. Umpierres, P.S. Thue, G.S. dos Reis, I.A.S. de Brum, E.C. Lima, W.A. de Alencar, S.L.P. Dias, G.L. Dotto, Microwave activated carbons from Tucumã (*Astrocaryum aculeatum*) waste for efficient removal of 2-nitrophenol from aqueous solutions, Environ. Technol. 39 (2018) 1173–1187.

[7] A.B. Leite, C. Saucier, E.C. Lima, G.S. dos Reis, C.S. Umpierres, B.L. Mello, M. Shirmardi, S.L.P. Dias, C.H. Sampaio, Activated carbons from avocado seed: optimization and application for removal several emerging organic compounds, Environ. Sci. Pollut. Res. 25 (2018) 7647–7661.

[8] M. Nasrollahzadeh, M. Sajjadi, S. Iravani, R.S. Varma, Carbon-based sustainable nanomaterials for water treatment: State-of-art and future perspectives, Chemosphere 263 (2021), 128005, https://doi.org/10.1016/j.chemosphere.2020.128005.

[9] S.A. Sajjadi, A. Meknati, E.C. Lima, G.L. Dotto, D.I. Mendoza-Castillo, I. Anastopoulos, F. Alakhras, E.I. Unuabonah, P. Singh, A. Hosseini-Bandegharaei, A novel route for the preparation of chemically activated carbon from Pistachio wood for highly efficient Pb(II) sorption, J. Environ. Manag. 236 (2019) 34–44.

[10] T.C. Egbosiuba, A.S. Abdulkareem, J.O. Tijani, J.I. Ani, V. Krikstolaityte, M. Srinivasan, A. Veksha, G. Lisak, Taguchi optimization design of diameter-controlled synthesis of multi-walled carbon nanotubes for the adsorption of Pb(II) and Ni(II) from chemical industry wastewater, Chemosphere 266 (2021), 128937, https://doi.org/10.1016/j.chemosphere.2020.128937.

[11] C. Saucier, P. Karthickeyan, V. Ranjithkumar, E.C. Lima, G.S. dos Reis, I.A.S. de Brum, Efficient removal of amoxicillin and paracetamol from aqueous solutions using magnetic-activated carbon, Environ. Sci. Pollut. Res. 24 (2017) 5918–5932.

[12] P.S. Thue, C.S. Umpierres, E.C. Lima, D.R. Lima, F.M. Machado, G.S. dos Reis, R. S. da Silva, F.A. Pavan, H.N. Tran, Single-step pyrolysis for producing magnetic activated carbon from tucumã (*Astrocaryum aculeatum*) seed and nickel(II) chloride and zinc(II) chloride. Application for removal of Nicotinamide and Propanolol, J. Hazard. Mater. 398 (2020), 122903, https://doi.org/10.1016/j.jhazmat.2020.122903.

[13] C. Wurzer, O. Mašek, Feedstock doping using iron-rich waste increases the pyrolysis gas yield and adsorption performance of magnetic biochar for emerging contaminants, Bioresour. Technol. 321 (2021), 124473, https://doi.org/10.1016/j.biortech.2020.124473.

[14] S. Zhuang, X. Zhu, J. Wan, Adsorptive removal of plasticizer (dimethyl phthalate) and antibiotic (sulfamethazine) from municipal wastewater by magnetic carbon nanotubes, J. Mol. Liq. 319 (2020), 114267, https://doi.org/10.1016/j.molliq.2020.114267.

[15] R. Tabatabaeian, M. Dinari, H.M. Aliabadi, Cross-linked bio-nano composites of hydrolyzed guar gum/magnetic layered double hydroxide as an effective sorbent for methylene blue removal, Carbohydr. Polym. 257 (2021), 117628, https://doi.org/10.1016/j.carbpol.2021.117628.

[16] M. Adel, M.A. Ahmed, A.A. Mohamed, Synthesis, and characterization of magnetically separable and recyclable crumbled $MgFe_2O_4$/reduced graphene oxide nanoparticles for removal of methylene blue dye from aqueous solutions, J. Phys. Chem. Solids 149 (2021), 109760, https://doi.org/10.1016/j.jpcs.2020.109760.

[17] T. Tatarchuk, M. Myslin, I. Lapchuk, A. Shyichuk, A.P. Murthy, R. Gargula, P. Kurzydło, B.F. Bogacz, A.T. Pędziwiatr, Magnesium-zinc ferrites as magnetic adsorbents for Cr(VI) and Ni(II) ions removal: cation distribution and anti-structure modeling, Chemosphere 270 (2021), 129414, https://doi.org/10.1016/j.chemosphere.2020.129414.

[18] L. Duan, C.G. Yuan, Q. Guo, S.L. Niu, K.Q. He, G.W. Xia, Preparation of halloysite nanotubes-encapsulated magnetic microspheres for elemental mercury removal from coal-fired flue gas, J. Hazard. Mater. 406 (2021), 124683, https://doi.org/10.1016/j.jhazmat.2020.124683.

[19] Z. Feng, H. Chen, H. Li, R. Yuan, F. Wang, Z. Chen, B. Zhou, Preparation, characterization, and application of magnetic activated carbon for treatment of biologically treated papermaking wastewater, Sci. Total Environ. 713 (2020), 136423, https://doi.org/10.1016/j.scitotenv.2019.136423.

[20] G.A. Saygili, H. Saygili, Pharmaceutical analysis by a novel spinel ferrite nanocomposite derived from a biomaterial-based activated carbon, J. Pharm. Biomed. Anal. 179 (2020), 112957, https://doi.org/10.1016/j.jpba.2019.112957.

[21] R. Saravanakumar, K. Muthukumaran, N. Selvaraju, Enhanced Pb (II) ions removal by using magnetic NiO/Biochar composite, Mater. Res. Express 6 (2019), 105504, https://doi.org/10.1088/2053-1591/ab2141.

[22] A.L. Cazetta, O. Pezoti, K.C. Bedin, T.L. Silva, A. Paesano-Jr, T. Asefa, V. C. Almeida, Magnetic activated carbon derived from biomass waste by concurrent synthesis: efficient adsorbent for toxic dyes, ACS Sustain. Chem. Eng. 4 (2016) 1058–1068.

[23] T. Han, X. Lu, Y. Sun, J. Jiang, W. Yang, P.G. Jönsson, Magnetic bio-activated carbon production from lignin via a streamlined process and its use in phosphate removal from aqueous solutions, Sci. Total Environ. 708 (2020), 135069, https://doi.org/10.1016/j.scitotenv.2019.135069.

[24] X. Bai, L. Yu, Z. Hua, Z. Tang, J. Zhang, Synthesis and characterization of superparamagnetic activated carbon adsorbents based on cyanobacteria, Mater. Chem. Phys. 163 (2015) 407–415.

[25] Q. Du, S. Zhang, J. Song, Y. Zhao, F. Yang, Activation of porous magnetized biochar by artificial humic acid for effective removal of lead ions, J. Hazard. Mater. 389 (2020), 122115, https://doi.org/10.1016/j.jhazmat.2020.122115.

[26] N.M. Mubarak, J.N. Sahu, E.C. Abdullah, N.S. Jayakumar, Plam oil empty fruit bunch based magnetic biochar composite comparison for synthesis by microwave-assisted and conventional heating, J. Anal. Appl. Pyrolysis 120 (2016) 521–528.

[27] J.L. Luque-Garcıa, M.D. Luque de Castro, Ultrasound: a powerful tool for leaching, Trends Anal. Chem. 22 (2003) 41–47.

[28] M. Esmaeili, S.O. Rastegar, R. Beigzadeh, T. Gu, Ultrasound-assisted leaching of spent lithium-ion batteries by natural organic acids and H_2O_2, Chemosphere 254 (2020), 126670, https://doi.org/10.1016/j.chemosphere.2020.126670.

[29] L. Zhang, H. Li, J. Peng, C. Srinivasakannan, S. Li, S. Yin, Microwave and ultrasound augmented leaching of complicated zinc oxide ores in ammonia and ammonium citrate solutions, Metals 7 (7) (2017) 216, https://doi.org/10.3390/met7060216.

[30] J. Chang, E.D. Zhang, L.B. Zhang, J.H. Peng, J.W. Zhou, C. Srinivasakannan, C. J. Yang, A comparison of ultrasound-augmented and conventional leaching of silver from sintering dust using acidic thiourea, Ultrason. Sonochem. 34 (2017) 222–231.

[31] H. Li, S. Li, J. Peng, C. Srinivasakannan, L. Zhang, S. Yin, Ultrasound augmented leaching of nickel sulfate in sulfuric acid and hydrogen peroxide media, Ultrason. Sonochem. 40 (2018) 1021–1030.

[32] J.J. John, V. De-Houwer, D. Van-Mechelen, T. Van-Gerven, Effect of ultrasound on leaching of lead from landfilled metallurgical residues, Ultrason. Sonochem. 69 (2020), 105239, https://doi.org/10.1016/j.ultsonch.2020.105239.

[33] X. Wang, C. Srinivasakannan, X.H. Duan, J.H. Peng, D.J. Yang, S.H. Ju, Leaching kinetics of zinc residues augmented with ultrasound, Sep. Purif. Technol. 115 (2013) 66–72.

[34] P.S. Thue, E.C. Lima, J.M. Sieliechi, C. Saucier, S.L.P. Dias, J.C.P. Vaghetti, F. S. Rodembusch, F.A. Pavan, Effects of first–row transition metals and impregnation ratios on the physicochemical properties of microwave-assisted activated carbons from wood biomass, J. Colloid Interface Sci. 486 (2017) 163–175.

[35] A.G.N. Wamba, S.K. Ndi, E.C. Lima, J.G. Kayem, P.S. Thue, T.M.H. Costa, A. B. Quevedo, E.V. Benvenutti, F.M. Machado, Preparation, characterization of titanate nanosheet–pozzolan nanocomposite and its use as an adsorbent for removal of diclofenac from simulated hospital effluent, J. Taiwan Inst. Chem. Eng. 102 (2019) 321–329.

[36] M. Thommes, K. Kaneko, A.V. Neimark, J.P. Olivier, F.J. Rodriguez-Reinoso, K. S. Rouquerol, W. Sing, Physisorption of gases, with special reference to the evaluation of surface area and pore size distribution (IUPAC technical report), Pure Appl. Chem. 87 (2015) 1051–1069.

[37] J. Jagiello, M. Thommes, Comparison of DFT characterization methods based on N_2, Ar, CO_2, and H_2 adsorption applied to carbons with various pore size distributions, Carbon 42 (2004) 1227–1232.

[38] F. Haghighatju, H.H. Rafsanjani, F. Esmaeilzadeh, Estimation of the dimension of micropores and mesopores in single-walled carbon nanotubes using the method Horvath–Kawazoe, Saito and Foley and BJH equations, Micro Nano Lett. 12 (2017) 1–5.

[39] M.R. Cunha, E.C. Lima, D.R. Lima, R.S. da Silva, P.S. Thue, M.K. Seliem, F. Sher, G. S. dos Reis, S.H. Larsson, Removal of captopril pharmaceutical from synthetic pharmaceutical-industry wastewaters: use of activated carbon derived from *Butia catarinensis*, J. Environ. Chem. Eng. 8 (2020), 104506, https://doi.org/10.1016/j.jece.2020.104506.

[40] D.R. Lima, A. Hosseini-Bandegharaei, P.S. Thue, E.C. Lima, Y.R.T. de Albuquerque, G.S. dos Reis, C.S. Umpierres, S.L.P. Dias, H.N. Tran, Efficient acetaminophen removal from water and hospital effluents treatment by activated carbons derived from Brazil nutshells, Colloids Surf. A Physicochem. Eng. Asp. 583 (2019), 123966, https://doi.org/10.1016/j.colsurfa.2019.123966.

[41] D.F. Caicedo, G.S. dos Reis, E.C. Lima, I.A.S. de Brum, P.S. Thue, B.G. Cazacliu, D. R. Lima, A.H. dos Santos, G.L. Dotto, Efficient adsorbent based on construction and demolition wastes functionalized with 3-aminopropyltriethoxysilane (APTES) for the removal ciprofloxacin from hospital synthetic effluents, J. Environ. Chem. Eng. 8 (2020), 103875, https://doi.org/10.1016/j.jece.2020.103875.

[42] G.S. dos Reis, C.H. Sampaio, E.C. Lima, M. Wilhelm, Preparation of novel adsorbents based on combinations of polysiloxanes and sewage sludge to remove pharmaceuticals from aqueous solutions, Colloids Surf. A Physicochem. Eng. Asp. 497 (2016) 304–315.

[43] D.R. Lima, E.C. Lima, C.S. Umpierres, P.S. Thue, G.A. El-Chaghaby, R.S. da Silva, F. A. Pavan, S.P. Dias, C. Biron, Removal of amoxicillin from simulated hospital effluents by adsorption using activated carbons prepared from capsules of cashew of Para, Environ. Sci. Pollut. Res. 26 (2019) 16396–16408.

[44] A.J.B. Leite, A.C. Sophia, P.S. Thue, G.S. dos Reis, S.L.P. Dias, E.C. Lima, J.C. P. Vaghetti, F.A. Pavan, W.S. de Alencar, Activated carbon from avocado seeds for the removal of phenolic compounds from aqueous solutions, Desalin. Water Treat. 71 (2017) 168–181.

[45] A.J.B. Leite, E.C. Lima, G.S. dos Reis, P.S. Thue, C. Saucier, F.S. Rodembusch, S.L. P. Dias, C.S. Umpierres, G.L. Dotto, Hybrid adsorbents of tannin and APTES (3-aminopropyltriethoxysilane) and their application for the highly efficient removal

of acid red 1 dye from aqueous solutions, J. Environ. Chem. Eng. 5 (2017) 4307–4318.
[46] A.G.N. Wamba, E.C. Lima, S.K. Ndi, P.S. Thue, J.G. Kayem, F.S. Rodembusch, G. S. dos Reis, W.S. de Alencar, Synthesis of grafted natural pozzolan with 3-amino-propyltriethoxysilane: Preparation, characterization, and application for removal of Brilliant Green 1 and Reactive Black 5 from aqueous solutions, Environ. Sci. Pollut. Res. 24 (2017) 21807–21820.
[47] S. Laurent, C. Henoumont, D. Stanicki, S. Boutry, E. Lipani, S. Belaid, R.N. Muller, L. Vander Elst, Magnetic properties. MRI Contrast Agents, From Molecules to Particles, first ed., Springer, 2017 https://doi.org/10.1007/978-981-10-2529-7. Chapter Two.
[48] X. Zhu, Y. Liu, F. Qian, C. Zhou, S. Zhang, J. Chen, Preparation of magnetic porous carbon from waste hydrochar by simultaneous activation and magnetization for tetracycline removal, Bioresour. Technol. 154 (2014) 209–214.
[49] D. Mohan, A. Sarswat, V.K. Singh, M. Alexandre-Franco, C. Pittman Jr, Development of magnetic activated carbon from almond shells for trinitrophenol removal from water, Chem. Eng. J. 172 (2011) 1111–1125.
[50] S. Zhang, L. Tao, M. Jiang, G. Gou, Z. Zhou, Single-step synthesis of magnetic activated carbon from peanut shell, Mater. Lett. 157 (2015) 281–284.
[51] M.P. Rayaroth, U.K. Aravind, C.T. Aravindakumar, Degradation of pharmaceuticals by the ultrasound-based advanced oxidation process, Environ. Chem. Lett. 14 (2016) 259–290.
[52] A.K. Krella, Cavitation erosion of monolayer PVD coatings – an influence of deposition technique on the degradation process, Wear 478–479 (2021), 203762, https://doi.org/10.1016/j.wear.2021.203762.
[53] T. Wang, G. Li, K. Yang, X. Zhang, K. Wang, J. Cai, J. Zheng, Enhanced ammonium removal on biochar from a new forestry waste by ultrasonic activation: characteristics, mechanisms, and evaluation, Sci. Total Environ. 778 (2021), 146295, https://doi.org/10.1016/j.scitotenv.2021.146295.
[54] G.L. Dotto, J.M.N. Santos, I.L. Rodrigues, R. Rosa, F.A. Pavan, E.C. Lima, Adsorption of Methylene Blue by ultrasonic surface-modified chitin, J. Colloid Interf. Sci. 446 (2015) 133–140.
[55] D.S.P. Franco, E.H. Tanabe, D.A. Bertuol, G.S. dos Reis, E.C. Lima, G.L. Dotto, Alternative treatments to improve the potential of rice husk as adsorbent for methylene blue, Water Sci. Technol. 75 (2017) 296–305, https://doi.org/10.2166/wst.2016.504.

5 CONCLUSÕES

O trabalho de tese proposto pela autora objetivava investigação de metodologias potencialmente inovadoras para o preparo de carvões ativados e compósitos magnéticos, tendo como precursores os resíduos agroindustriais da Castanha do Pará (*Bertholletia excelsa)* e da serragem do Sapelli *(Entandrophragma cylindricum)* e suas respectivas aplicações como adsorvente em contaminantes de preocupação emergente.

A investigação considerou os parâmetros influentes: temperatura de pirólise, a proporção do agente ativante cloreto de zinco, a potencialidade como carvão com propriedades magnéticas e o tipo de lixiviação, gerando então 7 carvões objetos do presente estudo: CCP600, CCP700, BNS 1:1.0, BNS 1:15; SNiAL, SNiUS, SNiZnAL, SNiZnUS.

Os estudos realizados indicaram que a ativação química com cloreto de zinco ($ZnCl_2$) e carbonização em atmosfera inerte propiciaram carvões ativados com alta área superficial. Os 6 carvões com uso desse ativante químico apresentaram área superficial superior a 1200 $m^2\ g^{-1}$. Em contramão, os 2 carvões que não foram sintetizados usando o ativante cloreto de zinco (SNiAL, SNiUS) apresentaram área superficial inferior a 400 $m^2\ g^{-1}$, indicando que a quantidade de cloreto de zinco na preparação dos carvões ativados teve a capacidade de aumentar no mínimo 3 vezes a área superficial dos materiais, chegando atingir 4 vezes no caso do BNS 1:1.5 e SNiZnAL. Ademais, na investigação do preparo dos carvões ativados magnéticos a presença do cloreto de zinco influenciou na lixiviação do sal cloreto de níquel, diminuindo o magnetismo dos materiais, levando a proposição que a relação entre sais esses dois sais deve ser investigada com maior atenção para assim garantir a alta área superficial e manutenção das propriedades magnéticas.

O estudo da influência da temperatura na carbonização dos carvões apontou que o gradiente de 100°C entre CCP600 e CCP700 não propiciou significativa modificação textural no carvão obtido.

As caracterizações indicaram a presença de grupos polares o que qualifica os carvões preparados como materiais hidrofílicos e com potencialidade para serem utilizados na adsorção de contaminantes emergentes. Os carvões CCP600 e CCP700 foram aplicados na adsorção do antibiótico Amoxicilina, os carvões BNS 1:0 e BNS 1: 1,5 foram ensaiados na adsorção do analgésico Paracetamol e os carvões SNiAL,

SNiUS, SNiZnAL, SNiZnUS foram colocados em contato com 6 fármacos (Paracetamos, Propranolol, Diclofenaco, Nicotidamina, Cafeina), 5 contaminantes emergentes (4-Cloro-anilina, 2-Nitrofenol, Resorcionol, Hidroquinona, 4-Bromofenol) e 4 corantes (Vermelho ácido 1, Azul reativo 4, Violeta básico 3, Verde básico 3).

Para as duas primeiras investigações foi possível obter os parâmetros cinéticos, de equilíbrio e termodinâmicos que regem o processo. Para ambas as investigações, influência da temperatura e influência da quantidade de cloreto de zinco, os dados experimentais foram ajustados para os modelos cinéticos de pseudo-primeira ordem, pseudo-segunda ordem e Avrami. Para os dados experimentais de equilíbrio os modelos aplicados foram às equações isotérmicas de Langmuir, Freundlich e Liu. Considerando ambos os estudos, o modelo cinético fracionário de Avrami e a isoterma de Liu foram os que melhor descreveram os dados experimentais de cinética e equilíbrio da adsorção, respectivamente. A capacidade máxima de adsorção de 451.0 $mg.g^{-1}$ (CCP.600) , 454.7 $mg.g^{-1}$ (CCP.700) foram obtidos a 45°C, enquanto 411.0 $mg.g^{-1}$ (BNS1.5) e 309.7 $mg.g^{-1}$ (BNS1,0) foram obtidos a 25 °C. Os parâmetros termodinâmicos da adsorção indicam que a adsorção de amoxicilina e do paracetamol é favorável e espontânea por ambos os carvões.

Para os carvões com propriedades magnéticas o emprego do ultrassom propiciou a proposição de técnica eficaz de lixiviação dos sais inorgânico, no que tange a eliminação dos agentes ativantes, além de reduzir o tempo dessa etapa de 2 horas para 15 min quando comparada com a lixiviação tradicional com ácido clorídrico. A técnica VSM mostrou que o carvão lixiviado com ultrassom (SNiZnUS) foi o que apresentou melhor relação entre área superficial e magnetismo (1212 $m^2.g^{-1}$; 10.81 emu g^{-1}).

Em relação ao emprego dos quatro *biochars* magnéticos como adsorventes, o SNiZnAL e o SNiZnUS apresentaram comportamento semelhante, mas apresentaram maior eficiência como adsorventes do que o SNiAL e o SNiUS, fato associado às melhores propriedades texturais obtidas via ativante cloreto de zinco.

Em complemento a agregação de valor do resíduo agroindustrial cápsulas de *Bertholletia excelsa* o estudo de dessorção e reutilização dos carvões BNS1.0 e BNS1.5 na adsorção do paracetamol foi realizada. Sendo identificada a regeneração de até 74% do adsorvente possibilitando ser reutilizado até quatro ciclos para a remoção do contaminante alvo do estudo.

REFERÊNCIAS BIBLIOGRÁFICAS

AHMED, S. F.; MOFIJUR, M.; NUZHAT, S.; CHOWDHURY, A. T.;RAFA, N.; UDDIN, M. A.; INAYAT,A.;MAHLIA, T.M.I.;ONG,H.C.;CHIA, W.Y.; SHOW, P. L. Recent developments in physical, biological, chemical, and hybrid treatment techniques for removing emerging contaminants from wastewater. **Journal of hazardous materials**, 416, 125912, 2021.

ALLEONI, L. R. F.; CAMARGO, O. A.; CASAGRANDE, J. C. Isotermas de Langmuir e de Freundlich na descrição da adsorção de boro em solos altamente intemperizados. **Scientia Agricola**, v. 55, n. 3, p. 379–387, 1998.

ÁLVAREZ-TORRELLAS, S.; RODRÍGUEZ, A.; OVEJERO, G.; GARCÍA, J. Comparative adsorption performance of ibuprofen and tetracycline from aqueous solution by carbonaceous materials. **Chemical Engineering Journal**, v. 283, p. 936–947, 2016.

ALVES, L. DE L.; CICHOSKI, A. J.; BARIN, J. S.; RAMPELOTTO, C.; DURANTE, E. C. O ultrassom no amaciamento de carnes. **Ciencia Rural**, v. 43, n. 8, p. 1522–1528, 2013.

ANASTOPOULOS, I.; KYZAS, G. Z. Agricultural peels for dye adsorption: A review of recent literature. **Journal of Molecular Liquids**, v. 200, n. PB, p. 381–389, 2014.

ARLOS, M. J., PARKER, W. J., BICUDO, J. R., LAW, P., HICKS, K. A., FUZZEN, M. L., ... & SERVOS, M. R. Modeling the exposure of wild fish to endocrine active chemicals: Potential linkages of total estrogenicity to field-observed intersex. ***Water Research***, *139*, 187-197, 2018.

BACCAR, R.; SARRÀ, M.; BOUZID, J.; FEKI, M.; BLÁNQUEZ, P. Removal of pharmaceutical compounds by activated carbon prepared from agricultural by-product. **Chemical Engineering Journal**, v. 211–212, n. 2012, p. 310–317, 2012.

BAGOTIA, N; SHARMA, A. K.; KUMAR, S. Review on modified sugarcane bagasse biosorbent for removal of dyes. **Chemosphere**, v. 268, p. 129309, 2021

BERGMANN, C. P.; MACHADO, F. M. (Ed.) **Carbon nanomaterials as adsorbents for environmental and biological applications**. New York: Springer International Publishing, 2015.

CAO, H., ZHANG, W., WANG, C., & LIANG, Y. Sonochemical degradation of poly- and perfluoroalkyl substances–a review. **Ultrasonics Sonochemistry**, *69*, 105245, 2020.

CAZETTA, A. L., PEZOTI, O., BEDIN, K. C., SILVA, T. L., PAESANO JUNIOR, A., ASEFA, T., & ALMEIDA, V. C. Magnetic activated carbon derived from biomass waste by concurrent synthesis: efficient adsorbent for toxic dyes. **ACS Sustainable Chemistry & Engineering**, *4*(3), 1058-1068, 2016.

CHANG, J., ZHANG, E. D., ZHANG, L. B., PENG, J. H., ZHOU, J. W., SRINIVASAKANNAN, C., & YANG, C. J. A comparison of ultrasound-augmented and conventional leaching of silver from sintering dust using acidic thiourea. **Ultrasonics Sonochemistry**, v. 34, p. 222-231, 2017.

CHEN, D; SHARMA, S. K.; MUDHOO, A. (Ed.). **Handbook on applications of ultrasound: sonochemistry for sustainability**. CRC press, 2011.

CIMIRRO, N. F., LIMA, E. C., CUNHA, M. R., DIAS, S. L., THUE, P. S., MAZZOCATO, A. C., Dotto, G.L.; Gelesky, M. A.; PAVAN, F. A. Removal of pharmaceutical compounds from aqueous solution by novel activated carbon synthesized from lovegrass (Poaceae**). Environmental Science and Pollution Research**, *27*(17), 21442-21454, 2020.

COBLEY, A.; MASON, T. J.; PANIWNYK, L., & SAEZ, V. Aspects of ultrasound and materials science. Handbook on Applications of Ultrasound: **Sonochemistry for Sustainability**, 41-73, 2012.

COLMENARES, J. C.; CHATEL, G. (Ed.). **Sonochemistry: from basic principles to innovative applications**. Springer, 2017.

CRINI, G.; LICHTFOUSE, E.; WILSON, L.; MORIN-CRINI, N. Conventional and non-conventional adsorbents for wastewater treatment. **Environmental Chemistry Letters**, v. 17, n. 1, p.195-213, 2019.

CUNHA, M. R., LIMA, E. C., LIMA, D. R., DA SILVA, R. S., THUE, P. S., SELIEM, M. K., SHER, F; DOS REIS, G.S.; LARSSON, S. H. Removal of captopril pharmaceutical from synthetic pharmaceutical-industry wastewaters: Use of activated carbon derived from Butia catarinensis. **Journal of Environmental Chemical Engineering**, *8*(6), 104506, 2020

DĄBROWSKI, A. (2001). **Adsorption—from theory to practice**. Advances in colloid and interface science, *93*(1-3), 135-224.

DE ANDRADE, F. V.; AUGUSTI, R.; DE LIMA, G. M. Ultrasound for the remediation of contaminated waters with persistent organic pollutants: A short review. **Ultrasonics Sonochemistry**, v. 78, p. 105719, 2021.

DOKE, KAILAS MAHADEO; KHAN, EJAZUDDIN M. Adsorption thermodynamics to clean up wastewater; critical review. **Reviews in Environmental Science and Bio/Technology**, v. 12, n. 1, p. 25-44, 2013.

ERTÜRK, M. D.; SAÇAN, M. T. Assessment and modeling of the novel toxicity data set of phenols to Chlorella vulgaris. **Ecotoxicology and Environmental Safety**, v. 90, p. 61–68, 2013.

FREUNDLICH, H. Adsorption in solution Phys. **In: Chem. Soc**. 1906. p. 1361-1368.

GADELHA, J. R.; ROCHA, A. C.; CAMACHO, C.; ELJARRAT, E.; PERIS, A.; AMINOT, Y.; READMAN, J. W.; BOTI, V.; NANNOU, C.; KAPSI, M.; ALBANIS, T.; ROCHA, F.;

MACHADO, A.; BORDALO, A.; VALENTE, L .M. P.; NUNES, M. L.; MARQUES, A.; ALMEIDA, C. M. R. Persistent and emerging pollutants assessment on aquaculture oysters (Crassostrea gigas) from NW Portuguese coast (Ria De Aveiro). **Science of The Total Environment**, v. 666, p. 731-742, 2019.

GEDANKEN, AHARON. Using sonochemistry for the fabrication of nanomaterials. **Ultrasonics sonochemistry**, v. 11, n. 2, p. 47-55, 2004.

GISI, S. DE; LOFRANO, G.; GRASSI, M.; NOTARNICOLA, M. Characteristics and adsorption capacities of low-cost sorbents for wastewater treatment: A review**. Sustainable Materials and Technologies**, v. 9, p. 10–40, 2016.

GOMIDE, R. **Operações unitárias: operações de transferência de massa**. São Paulo: Dag Gráfica e, 1988.

GOSKONDA, SRIDEVI; CATALLO, W. JAMES; JUNK, THOMAS. Sonochemical degradation of aromatic organic pollutants. **Waste Management**, v. 22, n. 3, p. 351-356, 2002.

GUPTA, V. K.; CARROTT, P. J. M.; RIBEIRO CARROTT, M. M. L.; SUHAS. Low-cost adsorbents: growing approach to wastewater treatment—a review. **Critical reviews in environmental science and technology**, v. 39, n. 10, p. 783-842, 2009.

HIREMATH, L., NIPUN, S., SRUTI, O., KALA, N. G., & AISHWARYA, B. M. Sonochemistry: applications in biotechnology. In: **Sonochemical Reactions**. IntechOpen, 2020.

HO, Y. S.; MCKAY, G. A Comparison of chemisorption kinetic models applied to pollutant removal on various sorbents. **Process Safety and Environmental Protection**, v. 76, n. 4, p. 332–340, 1998.

HU, L.; PENG, Y.; WU, F.; PENG, S.; LI, J.; LIU, Z. Tubular activated carbons made from cotton stalk for dynamic adsorption of airborne toluene. **Journal of the Taiwan Institute of Chemical Engineers**, v. 80, p. 399–405, 2017.

HUNG, Y. T., LO, H. H., WANG, L. K., TARICSKA, J. R., & LI, K. H. Powdered activated carbon adsorption. In: **Advanced physicochemical treatment processes**. Humana Press, p. 123-153, 2006.

IBGE, **Diretoria de Pesquisas, Coordenação de Agropecuária, Produção da Extração Vegetal e da Silvicultura**. Disponível em: https://www.ibge.gov.br/estatisticas/economicas/agricultura-e-pecuaria/9105-producao-da-extracao-vegetal-e-da-silvicultura.html?=&t=destaques. Acesso em maio de 2022.

JANNAT, N., AL-MUFTI, R. L., HUSSIEN, A., ABDULLAH, B., & COTGRAVE, A. Utilisation of nutshell wastes in brick, mortar and concrete: A review. **Construction and Building Materials**, *293*, 123546, 2021.

KAMALI, M.; DEWIL, R; APPELS, L.; AMINABHAVI, T.M. Nanostructured materials via green sonochemical routes–Sustainability aspects. **Chemosphere**, v. 276, p. 130146, 2021.

KASPERISKI, F. M.; LIMA, E. C.; UMPIERRES, C. S.; REIS, G. S. DOS; THUE, P. S.; LIMA, D. R.; DIAS, S. L. P.; SAUCIER, C.; COSTA, J. B. DA. Production of porous activated carbons from Caesalpinia ferrea seed pod wastes: Highly efficient removal of captopril from aqueous solutions. **Journal of Cleaner Production**, v. 197, p. 919–929, 2018.

HATAEE, A.; KARIMI, A.; AREFI-OSKOUI, S.; SOLTANI, R. D. C,; HANIFEHPOUR, Y.; SOLTANI, B.; JOO, S. W. Sonochemical synthesis of Pr-doped ZnO nanoparticles for sonocatalytic degradation of Acid Red 17**. Ultrasonics sonochemistry**, 22, 371-381, 2015.

KOTTUPARAMBIL, S.; KIM, Y. J.; CHOI, H.; KIM, M. S.; PARK, A.; PARK, J.; SHIN, W.; HAN, T. A rapid phenol toxicity test based on photosynthesis and movement of the freshwater flagellate, Euglena agilis Carter. **Aquatic Toxicology**, v. 155, p. 9–14, 2014.

KUMAR, KSHITIZ; SRIVASTAV, SHIVMURTI; SHARANAGAT, VIJAY SINGH. Ultrasound assisted extraction (UAE) of bioactive compounds from fruit and vegetable processing by-products: A review. **Ultrasonics Sonochemistry**, v. 70, p. 105325, 2021.

KUMAR, R.; MAGO, G.; BALAN, V.; WYMAN, C. E. Physical and chemical characterizations of corn stover and poplar solids resulting from leading pretreatment technologies. **Bioresource Technology,** v. 100, n. 17, p. 3948–3962, 2009.

KÜMMERER, K. The presence of pharmaceuticals in the environment due to human use - present knowledge and future challenges. **Journal of Environmental Management**, v. 90, n. 8, p. 2354–2366, 2009.

LANGMUIR, I. The adsorption of gases on plane surfaces of glass, mica and platinum. **Journal of the American Chemical Society**, v. 40, n. 9, p. 1361–1403, 1 set. 1918.

LARA-VÁSQUEZ, E. J.; SOLACHE-RIÓS, M.; GUTIÉRREZ-SEGURA, E. Malachite green dye behaviors in the presence of biosorbents from maize (Zea mays L.), their Fe-Cu nanoparticles composites and Fe-Cu nanoparticles. **Journal of Environmental Chemical Engineering**, v. 4, n. 2, p. 1594–1603, 2016.

LEANDRO, R. I. M., ABREU, J. J. D. C., MARTINS, C. D. S., SANTOS, I. S., BIANCHI, M. L., & NOBRE, J. R. C. Elementary, chemical and energy characteristics of Brazil nuts waste (Bertholletia excelsa) in the state of Para. **Floresta e Ambiente**, *26*, 2019

LEITE, A. B., SAUCIER, C., LIMA, E. C., DOS REIS, G. S., UMPIERRES, C. S., MELLO, B. L.,DIAS, S.L.P ; SAMPAIO, C. H. Activated carbons from avocado seed: optimisation and application for removal of several emerging organic compounds**.** **Environmental Science and Pollution Research**, v. 25, n. 8, p. 7647-7661, 2018.

LI, N.; LI, J.; ZHANG, Q.; GAO, S.; QUAN, X.; LIU, P.; XU, C. Effects of endocrine disrupting chemicals in host health: Three-way interactions between environmental 128 exposure, host phenotypic responses, and gut microbiota**. Environmental Pollution, v. 271, 12 p, 2021.**

LI, ZHANFENG *et.al.* Sonochemical fabrication of inorganic nanoparticles for applications in catalysis. **Ultrasonics Sonochemistry**, v. 71, p. 105384, 2021.

LIMA, É. C.; ADEBAYO, M. A.; MACHADO, F. M. Kinetic and equilibrium models of adsorption. In: C.P. BERGMANN, F.M. MACHADO (ed). **Carbon Nanomaterials as Adsorbents for Environmental and Biological Applications**. Springer International Publishing, p. 33–69, 2015.

LIMA, E. C., HOSSEINI-BANDEGHARAEI, A., MORENO-PIRAJÁN, J. C., ANASTOPOULOS, I. A critical review of the estimation of the thermodynamic parameters on adsorption equilibria. Wrong use of equilibrium constant in the Van't Hoof equation for calculation of thermodynamic parameters of adsorption. **Journal of Molecular Liquids**, v. 273, p. 425-434, 2019.

LIMA, É. C., DEHGHANI, M. H., GULERIA, A., SHER, F., KARRI, R. R., DOTTO, G. L., & TRAN, H. N. Adsorption: Fundamental aspects and applications of adsorption for effluent treatment. In: **Green Technologies for the Defluoridation of Water. Elsevier**, p. 41-88, 2021.

LIMA, E.C.; NAUSHAD, M. ; DOS REIS, G.S.; DOTTO; G.L.; PAVAN, F.A.; GULERIA,A.; SELIEM; M.K.; SHER, F. Production of carbon-based adsorbents from lignocellulosic biomass, in **Biomass-Derived Materials for Environmental Applications**. Elsevier, Amsterdam, Netherlands 2022.

MACHADO, F. M., FAGAN, S. B., SILVA, I. Z. D., & ANDRADE, M. J. D. Carbon nanoadsorbents. In **Carbon nanomaterials as adsorbents for environmental and biological applications** (pp. 11-32). Springer, Cha, 2015.

MASON, T.; PETERS, D. An introduction to the uses of power ultrasound in chemistry. **Practical Sonochemistry**, p. 1–48, 2002.

MCELROY, C. R.; CONSTANTINOU, A.; JONES, L. C.; SUMMERTON, L.; CLARK, J. H. Towards. a holistic approach to metrics for the 21st century pharmaceutical industry. **Green Chemistry**, v. 17, n. 5, p. 3111-3121, 2015.

MUTTAKIN, M.; MITRA, S.; THU, K.; ITO, K.; SAHA, B. B. Theoretical framework to evaluate minimum desorption temperature for IUPAC classified adsorption isotherms. **International Journal of Heat and Mass Transfer**, v. 122, p. 795–805, 2018.

NORMAN - NETWORK OF REFERENCE LABORATORIES, RESEARCH CENTRES AND RELATED ORGANISATIONS FOR MONITORING OF EMERGING ENVIRONMENTAL SUBSTANCES. **NORMAN Glossary of Terms**. 2021c. Disponível em: < http://www.norman-network.net/?q=node/9>. Acesso em ago. 2019

NORMAN - NETWORK OF REFERENCE LABORATORIES, RESEARCH CENTRES AND RELATED ORGANISATIONS FOR MONITORING OF EMERGING ENVIRONMENTAL SUBSTANCES. **List of emerging substances** latest update February 2016. 2016. Disponível em: <http://www.norman-network.net/>. Acesso em ago. 2019.

NILSEN, E.; SMALLING, K. L.; AHRENS, L.; GROS, M.; MIGLIORANZA, K. S. B.; PICÓ, Y.; SCHOENFUSS, H. L. Critical review: Grand challenges in assessing the adverse effects of contaminants of emerging concern on aquatic food webs. **Environmental Toxicology and Chemistry**, v. 38, n. 1, p. 46–60, 2019.

OKOLIE, J. A., NANDA, S., DALAI, A. K., & KOZINSKI, J. A. Chemistry and specialty industrial applications of lignocellulosic biomass. **Waste and Biomass Valorization**, *12*(5), 2145-2169, 2021.

PELÁEZ-CID, A. ALICIA; TEUTLI-LEÓN, MM MARGARITA; MONTOYA, V. H. Lignocellulosic precursors used in the elaboration of activated carbon. Lignocellulosic Precursors Used in the Elaboration of Activated Carbon, Lignocellulosic Precursors Used in the Synthesis of Activated Carbon–Characterization Techniques and Applications in the **Wastewater Treatment**, v. 1, p. 1-17, 2012.

PETRECHEN, G. P., ARDUIN, M., & AMBRÓSIO, J. D. Morphological characterization of Brazil nut tree (Bertholletia excelsa) fruit pericarp. **Journal of Renewable Materials**, 7*(7),* 683–692*.92, 2019.* https://doi.org/10.32604/jrm.2019.04588.

PETRICIOLET, ADRIAN (Ed.). **Lignocellulosic Precursors Used in the Synthesis of Activated Carbon-Characterization Techniques and Applications in the Wastewater Treatment**. BoD–Books on Demand, 2012.

PREDIERI, B.; BRUZZI, P.; BIGI, E., CIANCIA, S.; MADEO, S. F.; LUCACCIONI, L.; IUGHETTI, L. Endocrine disrupting chemicals and type 1 diabetes. **International Journal of Molecular Sciences**, *21*(8), 2937, 2020.

DE SOUZA, T. N. V., VIEIRA, M. G. A., DA SILVA, M. G. C., BRASIL, D. D. S. B., & DE CARVALHO, S. M. L. H3PO4-activated carbons produced from açai stones and Brazil nut shells: removal of basic blue 26 dye from aqueous solutions by adsorption. **Environmental Science and Pollution Research**, v. 26, n. 28, p. 28533-28547, 2019.

QIU, H.; LV, L.; PAN, B. C.; ZHANG, Q. J.; ZHANG, W. M.; ZHANG, Q. X. Critical review in adsorption kinetic models. **Journal of Zhejiang University: Science A**, v. 10, n. 5, p. 716– 724, 2009.

RAND, B.; APPLEYARD, S. P.; YARDIM, M. F. (Ed.). **Design and control of structure of advanced carbon materials for enhanced performance**. Springer Science & Business Media, 2012.

RODRIGUEZ-NARVAEZ, O. M., PERALTA-HERNANDEZ, J. M., GOONETILLEKE, A., & BANDALA, E. R. Treatment technologies for emerging contaminants in water: A review. **Chemical Engineering Journal**, *323*, 361-380, 2017.

RUDZINSKI, W.; PLAZINSKI, W. Theoretical description of the kinetics of solute adsorption at heterogeneous solid/solution interfaces. On the possibility of distinguishing between the diffusional and the surface reaction kinetics models. **Applied Surface Science**, v. 253, n. 13 SPEC. ISS., p. 5827–5840, 2007.

RUTHVEN, D. M. **Principles of adsorption and adsorption processes**. John Wiley & Sons, 1984.

SAUCIER, C., KARTHICKEYAN, P., RANJITHKUMAR, V., LIMA, E. C., DOS REIS, G. S., & DE BRUM, I. A. Efficient removal of amoxicillin and paracetamol from aqueous solutions using magnetic activated carbon. Environmental Science and pollution research, v. 24, n. 6, p. 5918-5932, 2017.

ŞAYAN, E.; EDECAN, M. An optimization study using response surface methods on the decolorization of Reactive Blue 19 from aqueous solution by ultrasound**.** **Ultrasonics Sonochemistry**, v. 15, n. 4, p. 530–538, 2008.

SILVA, C. P.; JARIA, G.; OTERO, M.; ESTEVES, V. I.; CALISTO, V. Waste-based alternative adsorbents for the remediation of pharmaceutical contaminated waters: Has a step forward already been taken? **Bioresource Technology**, v. 250, n. December 2017, p. 888– 901, 2018.

SING, K. S.W. Reporting physisorption data for gas/solid systems with special reference to the determination of surface area and porosity (Recommendations 1984). **Pure and Applied Chemistry**, v. 57, n. 4, p. 603-619, 1985.

SIPS, R. On the structure of a catalyst surface. **The Journal of Chemical Physics**, v. 16, n. 5, p. 490–495, 1948.

SOPHIA A., C.; LIMA, E. C. Removal of emerging contaminants from the environment by adsorption. **Ecotoxicology and Environmental Safety**, v. 150, n. December 2017, p. 1–17, 2018.

SOPHIA, C.A. ; LIMA, E.C. ; ALLAUDEEN, N. ; RAJAN, S. Application of graphene based materials for adsorption of pharmaceutical traces from water and wastewater-a review. **Desalination and Water Treatment**, v. 57, n. 57, p. 27573-27586, 2016.

SUSLICK, K. S., CHOE, S. B., CICHOWLAS, A. A., & GRINSTAFF, M. W. Sonochemical synthesis of amorphous iron. **Nature**, *353*(6343), 414-416, 1991.

TAKDASTAN, A.; MAHVI, A. H.; LIMA, E. C.; SHIRMARDI, M.; BABAEI, A. A.; GOUDARZI, G.; NEISI, A.; FARSANI, M. H.; VOSOUGHI, M. Preparation, characterization, and application of activated carbon from low-cost material for the adsorption of tetracycline antibiotic from aqueous solutions. **Water Science and Technology**, v. 74, n. 10, p. 2349–2363, 2016.

Tang WZ (2003) **Physicochemical treatment of hazardous wastes**. CRC Press, US

TAO, Y.; SUN, D. W. Enhancement of Food Processes by Ultrasound: A Review. Critical Reviews in **Food Science and Nutrition**, v. 55, n. 4, p. 570–594, 2015.

TEODOSIU, C.; GILCA, A.-F.; BARJOVEANU, G.; FIORE, S. Emerging pollutants removal through advanced drinking water treatment: A review on processes and environmental performances assessment. **Journal of Cleaner Production**, v. 197, p. 1210–1221, 1 out. 2018.

TORRES, F. G., GONZALES, K. N., TRONCOSO, O. P., CHÁVEZ, J., DE-LA-TORRE, G. E. Sustainable applications of lignocellulosic residues from the production of Brazil nut in the Peruvian Amazon. **Environmental Quality Management**, 2021.

THOMMES, M.; KANEKO, K.; NEIMARK, A. V.; OLIVIER, J. P.; RODRIGUEZ REINOSO, F.; ROUQUEROL, J.; SING, K. S. W. Physisorption of gases, with special reference to the evaluation of surface area and pore size distribution (IUPAC Technical Report). **Pure and Applied Chemistry**, v. 87, n. 9–10, p. 1051–1069, 2015.

THUE, P. S. **Preparation and characterization of microwave–assisted activated carbons from biomass and application for the removal of Emerging Organic Contaminants (EOCs) in aqueous media**. Federal University of Rio Grande do Sul, 2017a.

THUE, P. S.; ADEBAYO, M. A.; LIMA, E. C.; SIELIECHI, J. M.; MACHADO, F. M.; DOTTO, G. L.; VAGHETTI, J. C. P.; DIAS, S. L. P. Preparation, characterization and application of microwave-assisted activated carbons from wood chips for removal of phenol from aqueous solution. **Journal of Molecular Liquids**, v. 223, p. 1067–1080, 2016.

THUE, P. S.; REIS, G. S. DOS; LIMA, E. C.; SIELIECHI, J. M.; DOTTO, G. L.; WAMBA, A. G. N.; DIAS, S. L. P.; PAVAN, F. A. Activated carbon obtained from sapelli wood sawdust by microwave heating for o-cresol adsorption. **Research on Chemical Intermediates**, v. 43, n. 2, p. 1063–1087, 2017b.

THUE, P. S., UMPIERRES, C. S., LIMA, E. C., LIMA, D. R., MACHADO, F. M., DOS REIS, G. S., DA SILVA; R.D; PAVAN, F. A.; TRAN, H. N. Single-step pyrolysis for producing magnetic activated carbon from tucumã (Astrocaryum aculeatum) seed and nickel (II) chloride and zinc (II) chloride. Application for removal of nicotinamide and propanolol. **Journal of Hazardous Materials**, v. 398, p. 122903, 2020.

TRAN, Hai Nguyen et al. Mistakes and inconsistencies regarding adsorption of contaminants from aqueous solutions: a critical review. **Water Research**, v. 120, p. 88-116, 2017.

TRÖGER, R., REN, H., YIN, D., POSTIGO, C., NGUYEN, P. D., BADUEL, C., ... & WIBERG, K. What's in the water?–Target and suspect screening of contaminants of emerging concern in raw water and drinking water from Europe and Asia. **Water Research**, *198*, 117099, 2021.

UMPIERRES, C. S.; PROLA, L. D. T.; ADEBAYO, M. A.; LIMA, E. C.; REIS, G. S. DOS; KUNZLER, D. D. F.; DOTTO, G. L.; ARENAS, L. T.; BENVENUTTI, E. V. Mesoporous Nb2O5/SiO2 material obtained by sol–gel method and applied as adsorbent of crystal violet dye. **Environmental Technology** , v. 38, n. 5, p. 566–578, 2017.

USEPA - UNITED STATES ENVIRONMENTAL PROTECTION AGENCY. Safe Drinking Water Act (SDWA). **Washington/D.C.: USEPA**. Disponível em: < https://www.epa.gov/sdwa>. Acesso em 02 fev. 2021a.

USEPA - UNITED STATES ENVIRONMENTAL PROTECTION AGENCY. CompTox Chemicals Dashboard. **Washington/D.C.: USEPA. 2021b**. Disponível em: < https://comptox.epa.gov/dashboard>. Acesso em fev. 2019.

USGS - UNITED STATES GEOLOGICAL SERVICE. Emerging Contaminants. **Washington/DC: USGS. 2021**. Disponível em: < https://www.usgs.gov/mission-areas/water-resources/science/emerging-contaminants>. Acesso em fev. 2019.

VAGHETTI, J. C. P.; LIMA, E. C.; ROYER, B.; CUNHA, B. M. DA; CARDOSO, N. F.; BRASIL, J. L.; DIAS, S. L. P. Pecan nutshell as biosorbent to remove Cu(II), Mn(II) and Pb(II) from aqueous solutions. **Journal of Hazardous Materials**, v. 162, n. 1, p. 270–280, 2009.

VAJNHANDL, SIMONA; LE MARECHAL, ALENKA MAJCEN. Ultrasound in textile dyeing and the decolouration/mineralization of textile dyes. **Dyes and Pigments**, v. 65, n. 2, p. 89-101, 2005.

WAN, SHU; BI, HENGCHANG; SUN, LITAO. Graphene and carbon-based nanomaterials as highly efficient adsorbents for oils and organic solvents. **Nanotechnology Reviews**, v. 5, n. 1, p. 3-22, 2016.

WANG, X., CHENG, H., YE, G., FAN, J., YAO, F., WANG, Y.,JIAN, Y.;ZHU,W.;HUANG,W.; YE, D. Key factors and primary modification methods of activated carbon and their application in adsorption of carbon-based gases: A review. **Chemosphere**, *287*, 131995, 2022.

WEBER, W. J.; SMITH, E. H. Activated carbon adsorption: The state of the art. Studies in **Environmental Science**, v. 29, n. C, p. 455–492, 1986.

WEN, CHAOTING *et al*. Advances in ultrasound assisted extraction of bioactive compounds from cash crops–A review. **Ultrasonics Sonochemistry**, v. 48, p. 538-549, 2018.

YANG, Ralph T. **Adsorbents: fundamentals and applications**. John Wiley & Sons, 2003.

YAO, Y. Enhancement of mass transfer by ultrasound: Application to adsorbent regeneration and food drying/dehydration. **Ultrasonics Sonochemistry**, v. 31, p. 512–531, 2016.

Zhang, P., Xiang, M., Liu, H., Yang, C., & Deng, S. Novel two-dimensional magnetic titanium carbide for methylene blue removal over a wide pH range: insight into removal performance and mechanism. **ACS Applied Materials & Interfaces**, 11(27), 24027-24036, 2019.

ZHANG, WEINA; HE, WEI; JING, XINLI. Preparation of a stable graphene dispersion with high concentration by ultrasound. **The Journal of Physical Chemistry B**, v. 114, n. 32, p. 10368-10373, 2010.

ZHU, J.; LI, Y.; XU, L.; LIU, Z. Removal of toluene from waste gas by adsorption-desorption process using corncob-based activated carbons as adsorbents. **Ecotoxicology and Environmental Safety**, v. 165, n. 135, p. 115–125, 2018.